Mechanism of Genome Protection by Homologous Recombination Repair

A single molecule DNA-protein interaction study

J. T. Holthausen

Mechanism of Genome Protection by Homologous Recombination Repair

A single molecule DNA-protein interaction study

Mechanisme van genoom bescherming door homologe recombinatie reparatie

Een enkel molecuul DNA-eiwit interactie studie

Proefschrift

**ter verkrijging van de graad van doctor aan de
Erasmus Universiteit Rotterdam
op gezag van de
rector magnificus**

Prof.dr. H.G. Schmidt

**en volgens besluit van het College voor Promoties.
De openbare verdediging zal plaatsvinden op**

Vrijdag 10 Februari 2012 om 13:30 uur

**Jan Thomas Holthausen
geboren te Bergisch Gladbach, Duitsland**

ERASMUS UNIVERSITEIT ROTTERDAM

Promotiecomissie:

Promotoren: Prof.dr. R. Kanaar

                         Prof.dr. C. Wyman

Overige leden: Prof.dr. P. Verrijzer

                         Prof.dr. E. Peterman

                         Prof.dr. T. Sixma

Table of Contents

Aim of the thesis

Changes in our hereditary information are welcome in terms of generating diversity and driving evolution of the species. At the same time the integrity of the genome should not be compromised. As described in chapter 1, a number of compounds react with DNA thereby causing damaging lesions. If those lesions are left unrepaired, they can interfere with replication, transcription and lead to deregulations of their gene products. These in turn can cause diseases and aging. There are DNA repair mechanisms in place that repair DNA lesions and thus maintain and protect genome integrity.

This thesis focuses on the repair of double-stranded DNA breaks by homologous recombination. Chapter 1 explains and discusses homologous recombination. Briefly, at the site of a double-stranded break, DNA is resected to produce an overhang of single-stranded DNA (ssDNA) with and 3' hydroxyl end. Onto this ssDNA the strand exchange protein, RAD51, polymerizes into a right-handed helical filament. This nucleoprotein filament is recombination proficient. That means it can search for homology in duplex DNA, recognize it, melt and invade the duplex DNA at the site of homology, and catalyze strand exchange. These DNA transactions will result in a RAD51 filament on double-stranded DNA (dsDNA), which will then have to disassemble to allow the progression of homologous recombination.

RAD51 is capable of driving strand-exchange all by itself *in vitro*. Further it is essential for cell viability. These two facts should merit RAD51 the title: "Lord of Recombination". However, *in vivo* there are other proteins whose role is to regulate homologous recombination. Among those are recombination mediators, accessory factors or recombination antagonists, that either act on DNA substrates that occur

during recombination and/or interact with proteins driving double-stranded DNA break repair by homologous recombination. Many of these proteins interact with RAD51, or in other ways regulate RAD51 filament assembly. To fully comprehend homologous recombination it is important to understand the underlying mechanisms of RAD51 filament dynamics. In other words: how do RAD51 filaments assemble on ssDNA? How do they search and recognize homology? How do they re-arrange to form on dsDNA after strand exchange? How do they disassemble from dsDNA? These questions need to be addressed first before the effect of recombination mediators and accessory factors can be fully understood.

The work described in this thesis specifically addresses the above questions. Centered on single-molecule techniques, the work described in this thesis supports the development of novel techniques that measure protein-DNA interactions with unprecedented detail. In the thesis the employment of single-molecule assays to reveals new mechanistic data on RAD51-DNA interactions is described. Focused on fluorescent single-molecule assays the work contributes to the understanding of RAD51 assembly on ssDNA and dsDNA (Chapters 3 and 5), as well as RAD51 dissociation from dsDNA (Chapters 3 and 4). By investigating the C-terminal RAD51 interaction domain (CTRD) of recombination mediator BRCA2, whose malfunction is the underlying cause of certain forms of hereditary breast cancer, this work suggests approaches to study the effect of mediator proteins on RAD51 filaments. The thesis contributes to our understanding of the interactions of RAD51 with DNA and thereby lays the foundation for comprehending the regulation of strand exchange by recombination mediator proteins.

Chapter 1:

Introduction

Our genome contains our hereditary information encoded in long DNA polymers. This information needs to be replicated and segregated for cell division, transcribed and translated into proteins, and, in specialized cells, recombined in a controlled fashion to generate genetic diversity. There is a constant threat to the stability of our genome. A plethora of endogenous - e.g. replication errors, free radicals, alkylating agents, spontaneous reactions - and exogenous agents or processes - e.g. UV-light, x-rays, anti-cancer drugs - can modify or damage the DNA, thus interfering with replication and transcription. DNA lesions comprise abasic sites, 8 oxo-guanine, UV-photoproducts, pyrimidine dimers, base mismatches, insertions, deletions, intra- and interstrand cross-links, single- and double-stranded DNA breaks. DNA repair mechanisms have evolved that maintain the genome by repair of the arising DNA lesions. The variety of pathways includes base excision repair, nucleotide excision repair, transcription-coupled repair, mismatch repair, and cross-link repair. Double-stranded DNA breaks can be repaired by either non-homologous end joining or homologous recombination (*1-20*). This thesis will discuss core elements of the repair of double-stranded DNA breaks by homologous recombination.

Double-stranded DNA breaks

Double-strand DNA breaks are especially toxic lesions as they can not only introduce mutations in single genes, but cause translocations and loss of heterozygosity. If left unrepaired, double-strand breaks can result in cell dysfunction and subsequent cell death that lead to senescence phenotypes or cancers (*1*). Defects in homologous recombination have been particularly associated with familial breast cancer and ovarian cancers due to the involvement of breast cancer-susceptibility gene BRCA2 (*21, 22*). A well-known exogenous source for double-stranded DNA breaks are x-rays (short wavelength electromagnetic radiation). The

energy transfer from the radiation can sever the DNA backbone. When this happens in close proximity a double-stranded DNA break arises. However, breaking one DNA strand can also result in a one-ended DSB. This can happen when a single-stranded break is not repaired and that region is then replicated (*23, 24*). Most double-stranded DNA breaks presumably arise not directly, but indirectly from exogenous and endogenous agents as a result of other lesions interfering with replication.

DNA Replication

Eukaryotic DNA replication is a highly ordered process. Tight regulation of the process is important as our genome may only be replicated once per cell cycle, and, unlike in bacteria, the human genome contains many origins of replication on its multiple chromosomes. Regulatory mechanisms are in place that license and then fire an origin of replication in concert with chromosome condensation state and cell cycle progression (*25, 26*). To initiate replication the DNA needs to be unwound by helicases and a polymerase loaded. Briefly, the two DNA strands are separated to form a branched DNA structure into which the replication protein complex assembles. This is called a replication fork. There are different polymerases associated with a replication complex that have different qualities. Pol α initially associates as it has a unique DNA primase activity which it uses to generate short RNA/DNA hybrid primers on each of the DNA strands. As the DNA strands are anti-parallel and DNA synthesis is unidirectional in 5' to 3', the leading strand will be replicated continuously, while the lagging strand will be replicated discontinuously by generation of Okazaki fragments – about 200 nucleotides long stretches of DNA. After initial priming by Pol α, a switch to the more processive and proofreading polymerases δ and/or ε occurs. This switch is coordinated

by a set of proteins including RFC, RPA and PCNA (*27-29*). While polymerases δ and ε perform non-redundant functions, neither is able to bypass protein complexes bound to DNA or DNA lesions that distort DNA, link the strands, are too bulky to enter the polymerase's active site or have severed DNA backbones. These lesions will cause the replication fork to stall and/or collapse. It has been estimated that in an *Escherichia coli* (*E. coli*) cell about 15 - 20 % of the replication forks stall or collapse (*24*).

Stalled replication forks are fragile structures and prone to more damage. There are two main possibilities to overcome fork stalling. The quick solution is translesion synthesis. Briefly, the polymerase in the replication fork is replaced by one that can replicate over the damaged site (*30, 31*). Most commonly Y-family polymerases η, ι and κ are associated with translesion synthesis. Their active sites are large enough to accommodate some irregular DNA structures, but as they lack proofreading activity, they will frequently incorporate incorrect nucleotides on both templates (*32, 33*). These arising mutations need to be repaired by other repair pathways and putatively a larger number of them can arise. That is why translesion synthesis is referred to as a damage tolerant system.

That replication forks stall implies that a lesion was not yet repaired when the replication complex encountered it. Many repair pathways function through protein mediated structure-specific lesion recognition. While that might require the collapse or reversal of the replication fork, alternatively many of these lesions can be bypassed by homologous recombination. Homologous recombination is not limited by structure-specificity. On the other hand one can argue that single-stranded DNA is the structure required for homologous recombination, but is present at many lesions or can be generated by end resection, discussed below. At a replication fork there can be both, single-stranded DNA stretches and

double-stranded DNA breaks. Therefore, homologous recombination can repair replication forks in different ways, e.g. by fork reversal, strand switch or fork cleavage. Many ways to repair replication forks will bypass the lesion error-free, but not remove the lesion itself.

Replication fork repair

One way to repair forks emerges as the replicative polymerases stall, but the helicase continues to unwind the DNA past the lesion, and DNA synthesis continues on the other strand. This would result in the production of a single-stranded gap containing the lesion. The ssDNA can serve as a template for a strand switch with its homologous strand. The homologous DNA can be that of the sister chromatid. DNA synthesis can then proceed with the displaced strand as a template. This repair will result in the formation of Holliday junctions. Their resolution, discussed below, will yield error-free bypass. Alternatively, this gap could be filled in by translesion synthesis and replicative helicases (not shown). That would most likely result in the incorporation of an incorrect nucleotide.

Instead of strand switching, fork reversal together with re-annealing of the nascent strands will result in a four-way DNA junction called chicken foot. When the replisome unwinds DNA positive supercoils can be introduced in front of the fork. Upon replisome dissociation the energy stored in the DNA can drive fork reversal (*34*). In a chicken foot the lesion is back in duplex DNA and can be repaired by pathways recognizing the specific structure of that lesion. Alternatively, if DNA synthesis continued opposite the lesion, the longer nascent strand can serve as a template for the shorter one. Resolving the chicken foot by branch migration will result in error-free bypass of the lesion and a DNA

structure from which replication can resume directly. *In vitro* branch migration is promoted by RecQ helicases (*35*).

Further, a chicken foot structure could be cut by site-specific endonucleases. In general cleavage of stalled forks by structure-specific endonucleases, e.g. Mus81/Eme1, can generate one-ended double-stranded DNA breaks (*36, 37*). In addition a double-stranded DNA break arises when the replication fork encounters a single-stranded break and most lesions that affect only one DNA strand. Replication fork stalling is used in experiments with polymerase inhibitors or nucleotide pool depletion to generate double-stranded DNA breaks and evaluate repair. The emergence of a (one-ended) double-stranded DNA break will trigger homologous recombination.

Homologous Recombination

As derived from work on model organisms the *Homo sapiens* homologous recombination pathway can be separated into three major steps: pre-synapsis, the generation of a recombination proficient DNA end; synapsis, homology search and formation of a joint molecule between the previously generated end and an intact double-stranded DNA (dsDNA) template; post-synapsis, the repair of the broken strands and the resolution of the resulting DNA structure.
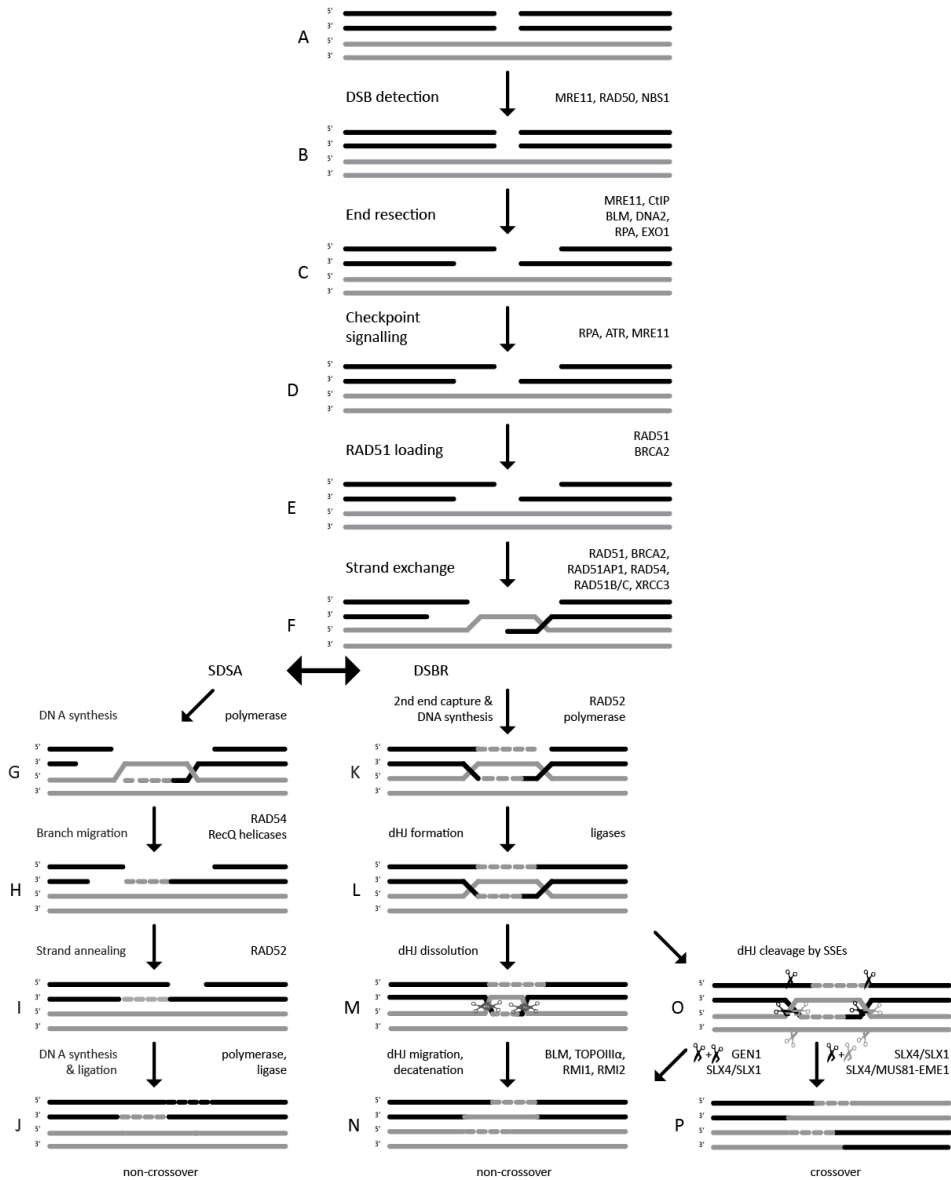
Figure 1 shows a schematic representation of the DNA transaction during double-strand break repair by homologous recombination. Left of the arrows is a description of the step, to its right names of proteins involved in that step. Names of divergent sub-pathways are in italics. Occurrence of a double-stranded DNA break (A) is detected by the MRN complex (B), upon which the DNA ends are resected to produce 3' ssDNA tails (C). Resection takes place by initial resection of MRE11 and CtIP, followed by more

processive resection by complexes containing BLM helicase and DNA2 or EXO1 nucleases. The ssDNA, quickly covered by RPA, is a substrate that triggers the checkpoint signaling cascade (D). RAD51 replaces RPA with help of BRCA2 and forms a filament on the ssDNA (E). The recombination proficient end executes homology search and strand exchange (F). This step can be aided by various recombination mediators including RAD51AP1, RAD54, RAD51B/C and RAD51C-XRCC3. The invading strand primes DNA synthesis that recovers the information at the site of the break (G/K). Depending on the extent of resection, how much DNA has been newly synthesized, and the direction of branch migration, the pathway diverges into either synthesis-dependent strand annealing (SDSA) or double-strand break repair (DSBR). In synthesis-dependent strand annealing branch migration resolves the joint molecule (H). The newly synthesized ssDNA end can be annealed to the other resected ssDNA end (I). Gap-filling DNA synthesis and ligation complete this pathway to produce non-crossover products exclusively (J). In double-strand break repair second end-capture followed by ligation forms two Holliday junctions (L). The double Holliday junctions can be resolved differently by dissolution or cleavage by structure-specific endonucleases (SSEs). Dissolution comprises the convergence of the double Holliday junctions by BLM helicase and the decatenation of the DNA strand by topoisomerase IIIα (M). Ligation of the resulting DNA ends gives non-crossover products (N). Cleavage by structure-specific endonucleases can occur at different places of the Holliday junction. Symmetrical cleavage of the continuous strands of the Holliday junctions, by Holliday junction resolvase GEN1 or the SLX4/SLX1 complex (O), will yield non-crossover products (N). Asymmetrical cleavage or diverse cleavage of the two Holliday junctions, by SLX4/SLX1 or SLX/MUS81-EME1 (O) produces crossover products (P).

Pre-synapsis

Homologous recombination as a mechanism for double-strand break repair, depicted in Figure 1, needs a double-stranded DNA break to initiate. Early proteins to localize to double-stranded DNA breaks are MRE11, RAD50, and NBS1 (MRN complex) (*38*). These are involved in the detection of the double-stranded DNA break and the tethering of the broken DNA ends (*39, 40*). The next step is the generation of a single-stranded DNA (ssDNA) overhang with hydroxyl end by nucleolytic processing. Although MRE11 has exonucleolytic activity (with wrong 3' to 5' polarity) there are many putative nucleases that perform this job in biochemical assays (*41-43*). The Sae2 related CtIP interacts with the

MRN complex and promotes double-stranded DNA break resection (*44*). CtIP is activated by cyclin-dependent kinase (CDK), which confers a regulation mechanism and restricts resection, and subsequently homologous recombination, to S and G2 phase of the cell cycle (*45, 46*). After CtIP/MRE11 mediated initial resection, a nuclease with 5' to 3' polarity together with a helicase, likely of the RecQ family, can provide processive end-resection to generate a hydroxyl single-stranded DNA tail (*35, 47*). There are two examples of complexes mediating end resection. The first comprises the Bloom helicase (BLM) together with the DNA2 helicase/nuclease. MRE11 recruits BLM to the break site, which in turn specifically interacts with DNA2 to resect DNA in an ATP-dependent process. Replication protein A (RPA) interactions promote the 5' to 3' resection polarity of DNA2. The other complex comprises the MRN complex together with BLM and exonuclease 1 (EXO1). BLM enhances EXO1 affinity for DNA ends and MRE11 stimulates its processivity (*48, 49*).

The generated single-stranded DNA end is quickly covered by RPA, which recruits ATR to the site of the double-stranded DNA break. ATR triggers checkpoint signaling by the protein kinase CHK1 (*40, 44, 46*). The correlation of DNA damage and checkpoint signaling and their cell-cylce dependence has been recently reviewed in Warmerdam *et al*. (*50*). More comprehensive information can be found in the doctoral thesis of D. Warmerdam (*51*).

Synapsis

Synapsis – the coming together – of the resected ssDNA and its homologous duplex DNA is mediated by RAD51. The recombinase needs to polymerize into a helical filament on the single-stranded DNA overhang while displacing RPA. As described below and in this thesis,

formation of a nucleoprotein filament is subdivided into nucleation and extension. Nucleation is defined as the initial, stable binding of a RAD51 protomer. The subsequent binding of RAD51 to the nucleation seed is referred to as extension. RAD51 filament assembly is considered a rate-limiting step for homologous recombination and is a tightly regulated step. It can be enhanced by recombination mediators like RAD52 or BRCA2, discussed in more detail below, or antagonized e.g. by RecQ helicase mediated filament disassembly (*52-65*).

The RAD51-ssDNA nucleoprotein filament performs synapsis, the core-process of homologous recombination. It searches the double-stranded DNA template, which mainly confers to the sister-chromatid and not the homologous chromosome, for homology. Once the matching DNA sequence is found RAD51 is able to catalyze strand invasion, leading to the formation of a joint molecule, and strand exchange. A joint molecule has a stable intermediate DNA structure called displacement loop (D-loop). This structure is reminiscent of a stalled replication fork and a similar RAD51 mediated activity has been implicated in replication fork restart and lesion bypass (described above).

Post-synapsis

After strand exchange the timing of the events is less well understood. Essentially, the invading strand primes DNA extension by polymerases. In order to prime extension from the invading strand the RAD51 recombinase filament needs to disassemble or be removed from the DNA. This is discussed in more detail in Chapter 2. There are different kinds of DNA structures that can arise from a RAD51 mediated recombination event and their resolution can result in either crossover or non-crossover products (*66-68*). If there are two dsDNA ends

available then the two main pathways for recombination, depicted in Figure 1 of Chapter 1, are synthesis-dependent strand annealing and double-strand break repair.

DNA synthesis in synthesis-dependent strand annealing, primed from the invading strand, is required to span the site of the break. Subsequent branch migration towards the newly synthesized DNA dissolves the joint molecule. The newly synthesized ssDNA can then be annealed to the single-stranded overhang of the other DNA end. Annealing of RPA-coated ssDNA is promoted by RAD52 (*54, 69*). Branch migration can also cause the capture of the second DNA end, which will result in the formation of two four-stranded DNA structures. Second–end capture is promoted by the RAD52 single-strand annealing function. The captured second-end primes gap-filling DNA synthesis to produce a single-stranded DNA overhang that could be annealed to the extended invading strand after branch migration. I.e. this structure can still be resolved by synthesis-dependent strand annealing. The shorter the double-strand break resection, the more likely second-end capture will occur, and conversely processive resection will favor synthesis-dependent strand annealing, which will exclusively result in non-crossover products (*70*).

When the DNA nicks surrounding each of the four-branched DNA structures are ligated the branches become double Holliday junctions. They cannot be resolved by mere branch migration, but require processing by endonucleases. Currently, there are two main scenarios on how double Holliday junctions can be resolved, recently reviewed in Svendsen *et al.* and Bernstein *et al.* (*47, 71*). One comprises the combined action of a branch-migrating helicase and a topoisomerase that will decatenate the junction. This approach, called dissolution, will result in non-crossover products exclusively. The other approach involves Holliday junction resolvases, which are structure-specific

endonucleases. They incise the Holliday junctions such that they produce directly ligatable crossover and non-crossover products (*71*).

Holliday junciton dissolution

Dissolution is described by Holliday junction migration by helicases of the RecQ family and strand passage activity of topoisomerases. Most prominent, and associated with cancer risk, are the Bloom (BLM) and Werner (WRN) helicases (*47, 70*). They cannot only unwind a variety of structures that might occur during recombination, like 3' tailed duplexes, bubble structures, D-loops, and forked duplexes, but specifically and processively migrate Holliday junctions in an ATP-dependent manner (*62, 72-74*). However, for the non-crossover dissolution of double Holliday juncitons BLM exhibits an exclusive function (*75, 76*). BLM activity can cause the Holliday junctions to converge, upon which a topoisomerase III can untangle the branched strands. BLM associates with the α isoform of topoismerase III, TOPOIIIα, This association is bridged by RMI1 binding and the dissolution activity further stimulated by RMI2. The dissolution complex comprising BLM, TOPOIIIα, RMI1 and RMI2, has also been referred to as "resolvasome" (*77-83*). In this scenario BLM actually promotes recombination as it drives double Holliday junction dissolution. Above BLM was mentioned to have an anti-recombination function in disruption of (inactive) RAD51 filaments as well (*84*).

Structure-specific endonuclease cleavage of Holliday junctions

The other scenario to resolve Holliday junctions requires endonucleases that specifically recognize branched DNA structures, like 3' or 5' flaps, and D-loops as a precursor to Holliday junctions. While the

focus here is on Holliday junctions that arise during recombinational repair, many of the above structures are also present at stalled replication forks.

Holliday junctions, though often depicted as a regular cross, need to be conceived as an x-like structure with two continuous/non-crossing strands. A bona-fide Holliday junction resolvase is expected to dimerize onto the junction and introduce symmetrical nicks, one in each of the continuous strands. Such cuts can be directly ligated and will result in non-crossover products exclusively. Only recently a human Holliday junction resolvase, GEN1, has been identified. The protein belongs to the Rad2/XPG family, i.e. it is monomeric in solution and should not accommodate Holliday junctions in its active site. However, GEN1 has evolved to do so and, as is characteristic for Holliday junction resolvases, dimerizes onto the Holliday junction to introduce symmetrical nicks on the continuous strands. GEN1 preferentially cleaves 5' flaps, Holliday junctions and replication forks containing such a structure. It can be conceived that the 5' flap cleaving is mediated by monomeric, while Holliday junction cleavage is mediated by dimeric GEN1 (*85, 86*).

The SLX4-endonuclease complex is another resolvase for Holliday junctions. As conceived partially from model organisms, SLX4 serves as a scaffold that can associate different structure-specific endonucleases, as well as other proteins involved in DNA repair and telomere maintenance. A scaffold whose activity might be regulated by cell-cycle proteins, like polo-like kinase 1 (PLK1), presents itself as a putative control mechanism for homologous recombination and restricts it to cell cycle phases. In the context of Holliday junctions, SLX4 interactions with the endonucleases SLX1 and MUS81-EME1 are relevant (*71, 87-90*). The SLX4/SLX1 complex nicks static and mobile Holliday junctions. Cleavage of Holliday junctions can result in both, crossover and non-crossover

products. Cleavage of mobile Holliday junctions, like with GEN1, presumable results in non-crossover products (*71, 88, 89*).

While SLX4/SLX1 cleavage allows non-crossover product formation, the SLX4/MUS81-EME1 complex forms crossover products. This feature is inherent to the asymmetrical nick and counter-nick introduced by the MUS81-EME1 that leaves gaps and flaps after Holliday junction cleavage (*91-93*). Indeed MUS81-EME1 preferentially cleaves 3' flap structures and nicked Holliday junctions. Both structures are abundant at stalled replication forks, but can also promote the formation of crossover products from recombination intermediates. Therefore, MUS81-EME1 has been linked to meiotic recombination. However, MUS81-EME1 mutants lack strong phenotypes, except in *Saccharomyces pombe*, correlating it to an essential function like double-strand break repair or chromosome segregation in meiotic recombination (*94-96*). MUS81-EME1 is more likely to play a role in replication fork restart. Its structure-specificity makes it suitable to generate double-stranded DNA breaks at stalled replication forks, especially important for interstrand cross-link repair (*36, 37*).

As described above, one-ended double-strand breaks can result indirectly from a variety of lesions. Their emergence triggers recombinational repair, which is especially suited to bypass lesions and restart replication forks. It can be conceived that the resolution of the resulting DNA structures occurs via synthesis-dependent strand annealing. However, a Holliday junction can be generated that will then need to be cleaved as described above. Cleavage of a single Holliday junction should result in non-crossover products. All forms of recombination require the formation of a recombinase filament onto single-stranded DNA. The assembly and disassembly of this core-structure of recombination is the center of this thesis and therefore will be addressed in more detail.

RAD51 nucleoprotein filament

The importance of the recombinase in mammalian cells can easily be noticed since removal infers embryonic lethality in mice as well as vertebrate cells (*97, 98*). Decades of research have been spent trying to elucidate the role of recombinases in homologous recombination as well as in understanding the underlying mechanisms. Most advances have first been achieved in *Escherichia coli*, which now serve as a paradigm for the comparison of homologous recombination in other organisms. Early research focused on genetic and biochemical experiments that, apart from showing the necessity of RAD51 for vertebrate organisms to be viable, also resulted in an extensive biochemical characterization of the recombinase. RAD51's ability to hydrolyze ATP is increased in the presence of DNA, especially single-stranded DNA (ssDNA), and in contrast to RecA is not affected by high salt concentrations (*99*). Further characterization of nucleotide binding and exchange showed the inhibitory effect of ADP or non-hydrolysable ATP-γS on ATP hydrolysis and indicates that not ATP binding but ADP release might be the rate limiting step in the RAD51 ATP hydrolysis cycle (*100*). Since the recombinase has ATPase activity, DNA binding studies were carried out with a variety of nucleotide co-factors. IAsys Biosensor studies (IAB) and gel shift experiments show that RAD51 binds ssDNA and dsDNA with and without nucleotide cofactors, but, unlike with RecA, there are two different forms of RAD51-DNA complexes in the gel shift experiments, which are modulated by the presence of saturating nucleotide concentrations (*101*). In the same study gel-filtration experiments showed that nucleotide binding by RAD51 reduces its tendency to aggregate and instead elute with an average molecular mass (100-250 kDa) corresponding to 3-8 RAD51 monomers, potentially hexameric to octameric rings (*101-103*). Although it exists as octamers in solution RAD51 could not be shown to bind DNA as octameric rings (unpublished data Kowalczykowski, S. C.) (*104*).

It is evident that ATPase activity must have an important role for the recombinase function and this was addressed by generating RAD51 Walker domain mutants (K133R and K133A), which have greatly attenuated ATPase activity. In vivo studies show that heterozygote mutant cell lines are viable but display different behavior in processes where homologous recombination is involved (*86, 105-108*). Biochemical studies with non-hydrolysable ATP analogs revealed that there are differences in RAD51-DNA interactions in presence of ATP or ADP. RAD51 with ATP could protect DNA from endonuclease cleavage, including unwound plasmid DNA in presence of topoisomerases (*109*). RecA filaments even protected ssDNA bound by it from methylation (*110*). Further, assays for homologous DNA pairing and D-loop formation (see above) not only showed that ATP is required, but that non-hydrolysable forms of ATP, or the ATPase deficient RAD51K133R mutant, yield much more product (unpublished data) (*109*). Other studies in this context, where ATP hydrolysis by RAD51 was suppressed, using Ca^{2+} instead of Mg^{2+}, show that the active pre-synaptic filament is formed with ATP-bound RAD51 (*111*).

Crystal structure and electron microscopy

A major drawback of these studies is that, although they identify components required for the reaction, they cannot address all aspects of the underlying mechanisms. These assays are dependent on DNA structures as read-out. They do not address the putative structure of the recombinase due to oligomerization or DNA-interaction. From model organisms it was expected that ATP binding to RAD51 has an allosteric effect. To address this, crystal structures of archeal and bacterial homologues of RAD51 were used together with electron microscopy (EM). Helical reconstruction of EM pictures (*112*) revealed that RAD51, in presence of ATP and aluminum fluoride, forms a one-start right-handed helical structure on DNA, referred to as a filament. This helical filament on dsDNA is composed of 6.4 RAD51 monomers per turn and

has an average pitch of 99 Å. This implies that the dsDNA, around which the RAD51 filament is wrapped, is stretched with respect to B-DNA from ~10 bp to ~19 bp per turn, which equals a rise from 3.4 Å to 5.1 Å per base-pair (*113*). The bottom line is that the DNA inside the RAD51-DNA nucleoprotein filament is stretched by 50% over the regular B-DNA length. Since these helix parameters are conserved among five recombinases representing the three kingdoms of life it was assumed that they are derived from the intrinsic features of the DNA in that there is a direct relationship between pitch and DNA twist. Data supporting this notion is the fact that RecA bind faster to stretched DNA than B-DNA (*114*). In chapter 5 of this thesis we show that RAD51 filament formation is accelerated in a DNA tension dependent manner. It appears that RecA like proteins stabilize a pre-existing conformation between two DNA molecules

As higher resolution crystal structures became available it was understood that RAD51 shared an evolutionary conserved Walker ATPase core domain with recombinases *ec*RecA / *mv*RadA / *sc*Rad51, but unlike RecA has an additional N-terminal domain. In an extended filament the Walker A domain of one monomer interacts with the Walker B domain of the adjacent one and ATP is bound in this interface. In addition to this interface additional contacts between the N-terminal of one and the ATPase core domain of the adjacent monomer were detected (*115, 116*). Work with archeal RadA and yeast Rad51 showed that multiple contacts of the N-terminus with the monomer core are required for ATPase activity and monomer rotation (*102*). In EM reconstructions of extended RAD51 filaments lobes became visible, that were not present in compressed, ADP bound, filaments (*104*). Super-imposition of the RAD51 crystal structure suggests that these lobes are the RAD51 N-terminus and the appearance could be due to an allosteric change upon ATP binding. Crystallography and EM reconstruction have

given a good understanding of the structure of the RAD51 nucleoprotein filament.

RAD51 filament assembly

   Although crystallography and EM are among the strongest techniques to address structural conformations, they fail to describe the conformational dynamics of recombinase proteins and their DNA substrates. Especially the assembly of the pre-synaptic filament, the re-arrangements during strand exchange and the filament disassembly thereafter need to be addressed. Other techniques need to be applied to investigate the mode of filament dynamics. Single-molecule analyses provide additional information.

Scanning force microscopy

   To address RAD51 filament assembly scanning force and fluorescent microscopy, as well as magnetic tweezers have been employed. Scanning force microscopy (SFM) is a method that, unlike EM, does not require fixatives or harsh conditions. Reactions can be analyzed at nanometer resolution by deposition on mica as they are. SFM studies allow visualizing transient RAD51-DNA complexes, and exposed the irregularity of RAD51 filaments on ssDNA and dsDNA in conditions that allowed ATP hydrolysis. Suppression of ATP hydrolysis was necessary to observe regular, extended nucleoprotein filaments. ATPase activity was suppressed by the use of non-hydrolysable ATP analogs (ATPγS or AMP-PNP), replacing Mg^{2+} with Ca^{2+} or the RAD51 K133R mutant. But even these filaments had a limited persistence length and many kinks resulting from little gaps. This implied that the DNA is not completely covered and indicated dynamic rearrangements. In combination with an

assay for joint molecule formation a correlation of regular, extended RAD51-DNA complexes to increased ability to form joint molecules could be shown (*117*). This data is in accordance with other publications, that show that nucleotide co-factor binding, but not hydrolysis is necessary for (pre-) synaptic stages of homologous recombination (*109, 111, 118*).

Magnetic tweezers

To address the dynamics of filament assembly and understand the mechanism behind it, real-time measurements and observation of the assembly process were needed. In magnetic tweezers studies RAD51 filament assembly was measured as extension of the DNA substrate. From Monte Carlo simulations kinetic parameters of the reaction were deduced (*119, 120*). These simulations were based on data obtained from the crystallography work (max. 50% extension) and DNA binding studies indicating that one RAD51 monomer binds 3 nucleotides or basepairs (*113, 121, 122*). The model suggests that RAD51 filament formation consists of two separable steps: nucleation and extension. In this model the RAD51 protomer or binding unit for nucleation is considered to be a pentamer. The ratio between nucleation and extension is 1:220 ± 16 for ssDNA and 1:246 ± 18 for dsDNA respectively. The simulations give a nucleation rate of $(3.9 \pm 0.3) \times 10^{-4}$ pentamers s^{-1} nt^{-1} and a growth rate per filament of 0.085 ± 0.006 pentamers s^{-1} for ssDNA. On dsDNA the nucleation rate is $(4.3 \pm 0.3) \times 10^{-4}$ pentamers s^{-1} bp^{-1} and the growth rate is 0.106 ± 0.008 pentamers s^{-1} (*120*). These values imply that with respect to RecA filaments nucleation for RAD51 plays a much more important role than extension. Increased nucleation along the DNA would result in a larger number of patches. Since it is assumed that the RAD51 protomer is a pentamer, it would cover at least 15 nucleotides. Because of this, and assuming that RAD51 filaments do not slide along DNA, there can be gaps of up to 14 nucleotides within

the filament (*123*). Proposing that RAD51 can seed nucleation sites with opposite polarity it is unlikely that conformational rearrangements can result in a transition into a continuous filament (*104*). These assumptions are in congruence with the incomplete DNA extension measured in the force microscopy and the contour and persistence length measurements in SFM (*108, 117, 120, 124*) and fluorescence microscopy studies (*125*).

Fluorescence microscopy

In addition to SFM and magnetic tweezers also fluorescent microscopy was employed. Here one can observe the fluorescently labeled protein instead of DNA, but at lower resolution. Fluorescent studies were mostly limited to dsDNA substrates. One series of experiments using RAD51 labeled in different colors in limiting concentrations (added to dsDNA one after the other) showed that RAD51 forms multiple filament patches along DNA with limited extensions (*126*). These dual color "Harlequin" filaments also made evident that there is no exchange of RAD51 monomers within or at the edge of formed filament patches, since there was no mixing of the color signals. Other studies on dsDNA confirmed that nucleation rates are RAD51 concentration dependent. The rate of filament formation was measured as extension of dsDNA by RAD51 binding (*127*) and/or comparing the length of filaments assembled from fluorescently labeled protein to the initial dsDNA length (*128*). Nucleation rates could also be slowed down by increasing salt concentrations, thus allowing counting of nucleation sites and rates (*128*). The nucleation rate measured on dsDNA at 100 nM NaCl was 2.7×10^{-7} nucleation events $s^{-1}\,bp^{-1}$.

In Chapter 5 of this thesis we show in unprecedented detail the nucleation and extension of fluorescently labeled RAD51 onto dsDNA

and, for the first time, on ssDNA. Briefly, the experiments reveal a previously undetected preference of RAD51 binding to ssDNA, protein and salt concentration dependent nucleation and extension rates on both DNA substrates, and DNA tension dependent nucleation and extension rates on dsDNA. In the buffer conditions most similar to those in the tweezers or the above described fluorescent microscopy study; we showed a nucleation rate of 2×10^{-7} nucleation events s^{-1} bp^{-1} on dsDNA. The rate for ssDNA was $1.6 \times 10^{-5} \pm 2.3 \times 10^{-6}$ nucleation events s^{-1} nt^{-1}. Furthermore our study allowed quantifying RAD51 within the nucleation clusters. The data revealed that nucleation occurs in a distribution of cluster sizes that seem to be dependent on protein concentration. These studies together give a good understanding of how the RAD51 nucleoprotein is assembled in vitro.

Filament structure in strand exchange

The dsDNA inside a recombinase nucleoprotein filament is extended up to 150% of its B-form length. This is a feature conserved in nucleoprotein filaments of any of the three kingdoms of life (*112*). This conservation implies an essential role of DNA overstretching in recombinase mediated strand exchange. Another important consideration is that the DNA is not stretched homogenously, but between basepair triplets that themselves maintain the stacking conformation of B-form DNA (*121, 122*). One possible scenario for the relevance of overstretched DNA, discussed below, is to promote intrinsic RAD51 disassembly from dsDNA (*129*). However, recombinase readily dissociates from ssDNA as well. Single-stranded DNA does not have a defined conformation like B-form DNA. Thus ssDNA cannot be overstretched and no energy stored in it, when a filament forms on it. This notion is supported by the tension-independent nucleation rates on ssDNA revealed in chapter 5 of this thesis. Nonetheless, it is conceivable

that the ssDNA within a RAD51 filament is in a conformation that corresponds to the overstretched dsDNA. Based on RAD51 nucleation rates it has been proposed that filament patches are restricted in their length (*119, 120*). Because of naked DNA between the patches, which act as hinges, the filament is more flexible compared to continuous filaments. One idea is that several filament patches can probe duplex DNA at the same time. Simultaneous or not, this implies the engagement of a limited size filament with duplex DNA in search for homology. This is in accordance with magnetic tweezers data addressing the extent of DNA unwinding during homology search (*130*).

Taking the above consideration into account, the following scenario for homology search and strand exchange can be conceived: The ssDNA-RAD51 has a conformation such that nucleotide triplets are exposed in the major groove of the filament. When a filament patch engages duplex DNA in search for homology, a set of nucleotide triplets of the duplex can flip out and bind the one in the nucleoprotein filament. If the adjacent triplet is to bind, the duplex DNA needs stretching (reduction in twist). For that to happen, an energy barrier needs to be overcome. This step likely provides a mechanism that quickly reverts filament interactions at sites of heterology. Only exact pairing of a triplet set might stabilize the interaction enough to account for the DNA overstretching. Two things will occur when subsequent nucleotide triplets base-pair. The homologous DNA will be displaced and the DNA downstream of the invasion site will negatively supercoil. Up to this point the generated joint is referred to as paranemic. Successive triplet pairing and DNA unwinding can be (transiently) stabilized by binding of the displaced strand to the secondary binding site in the minor groove of the filament. This stabilization could provide the capacity of RAD51 to tolerate up to three mismatches (*131*). Any mismatch within a triplet destabilizes the interaction of the nucleoprotein filament with the duplex DNA. It appears that RAD51 can tolerate one mismatching triplet.

If the region of heterology is larger, the filament will not pair. The structure resulting from successive triplet binding is a three-strand complex that has the RAD51 filament only around the invading single-strand DNA. Evidence for this recombination intermediate comes from DNA methylation studies of joint molecules (*110*).

In the canonical model, also presented in this thesis, a transition needs to occur that will result in a nucleoprotein filament around the duplex DNA formed between invading and complementary template strand. That transition also will produce a plectonemic joint, where the joint heteroduplex DNA assumes a helical structure again. One way to achieve this is the disassembly and subsequent rapid assembly of the nucleoprotein filament. However, accumulation of plectonemic DNA joints is promoted by the suppression of RAD51 ATPase activity or by use of ATPase deficient mutants. As ATPase is suppressed, it is difficult to conceive how such extensive rearrangements, which result in the transition of the ssDNA-RAD51 nucleoprotein filament to a dsDNA-RAD51 filament, can occur. Another way to envision the transition relies on the negative supercoiling that was introduced into the duplex DNA. The energy stored in the negatively coiled DNA could result in twisting of the invading and complementary strand, so that both are paired in a helical conformation at the major groove. The displaced strand simultaneously wrapping around the minor groove. This structure already can be referred to as plectonemic joint. At this point, RAD51 disassembly can only result in heteroduplex formation with reversion to B-form DNA. However, this implies that the duplex DNA is only formed upon recombinase dissociation from DNA. The complex as described would still inhibit access of polymerase to the invading end. At present it is not possible to distinguish RAD51 filaments on ssDNA or dsDNA engaged in strand exchange *in vivo*. Anyways, RAD51 ATPase is not fully suppressed *in vivo*, and the necessary rearrangement that will allow the complementary strand to enter into the primary DNA binding site within

the filament, can take place. It is most likely that a recombinase filament wrapped around double-stranded DNA is the final product of strand exchange. The presented scenario is only an example how strand exchange can be envisioned mechanistically. In any case, the nucleoprotein filament needs to disassembly for successful repair by recombination.

RAD51 filament disassembly

After successful strand exchange, the RAD51 filament is wound around double-stranded DNA. As described above the filament inhibits the access of polymerases to the end of the invading strand. Therefore, the dissociation of RAD51 from dsDNA has been investigated in detail by an ensemble of single-molecule studies as well. In magnetic tweezers studies filament disassembly was measured as DNA length reduction over time. Since the assembly studies showed tightly associated filament segments (*126*), a model where RAD51 dissociates only from filament (patch) ends was postulated. The Monte Carlo simulations used to fit and retrieve kinetics data from the experiments considered this model. They yielded a dissociation rate from dsDNA of 0.021 ± 0.001 monomers per filament patch end s^{-1} (*119, 120*). This data is in accordance with data obtained from fluorescent microscopy measuring the dissociation of fluorescently labeled protein from dsDNA, which were also fit with exponential dissociation traces (*108, 126, 132*). That the dissociation data from dsDNA could be best fit with an exponential equation implies that dissociation takes place at many places at the same time, and is governed by a single kinetic step. That dissociation occurs throughout the filament is explained by its discontinuity. A model, based on nucleation and extension rates obtained from the magnetic tweezers experiments, predicts an average filament patch length of 30 ± 24 (mean ± SD, n = 408) RAD51 monomers in presence of Mg^{2+} and ATP, and 21 ±

15 (mean ± SD, n = 578) RAD51 monomers in presence of Ca^{2+} and ATP (*120*). Data obtained from experiments with ssDNA needed to be fit with a double exponential equation, indicating that there are two different rates of dissociation. A possible explanation is that there are two different events affecting the shortening of DNA: an initial fast step at a rate of 0.35 ± 0.08 monomers s^{-1} and a slow step at a rate of 0.036 ± 0.004 monomers s^{-1}. The interpretation is that the fast rate could be due to an allosteric change in the filament structure, e.g. due to ATP hydrolysis, and the slow rate is the actual dissociation of the RAD51 monomers from ssDNA. This idea is derived from the crystallography studies mentioned above, that show a reduction of the filament pitch in an ADP bound state. Further, fluorescent microscopy studies showed a similar behavior. An extended filament, assembled in the presence of Mg^{2+} and ATP, shrank rapidly at a rate of 0.79 ± 0.04 monomers min^{-1} when moved into a buffer containing only Mg^{2+} (*128*). Surprisingly the fast shrinking of these filaments yielded an end-to-end length that corresponds to B-DNA length. The interpretation is similar in that ATP hydrolysis results in a quick initial shrinkage into a compressed ADP-bound filament with only residual ATP bound. Indeed it was possible to assemble non-extended filaments of the same contour length in presence of ADP and Mg^{2+}. Changing the buffer used in these experiments to a buffer similar to the one used by Modesti *et al.* did not allow to capture these filaments during disassembly, nor allow assembly of ADP filaments (*126*). The differences between the experimental conditions of these studies are addressed in Chapter 4 of this thesis.

Another study addressed the correlation of ATP hydrolysis and RAD51 dissociation from dsDNA in more detail. Combining fluorescence microscopy with force measurements by dual optical traps allows to quantitatively asses protein, labeled with single fluorescent tag, while measuring and manipulating tension on DNA molecules (*125*). The data obtained showed that RAD51 dissociation takes place in bursts and that

the driving force behind it is the tension that was build up in the DNA by the extension through the active RAD51 filament. The observed burst-wise disassembly can be explained by assuming that RAD51 dissociates only from patch ends, that random ATP hydrolysis occurs along the nucleoprotein filament, and by hypothesizing that RAD51 monomers stay on the DNA as long as the final monomer in a patch does not hydrolyze ATP. Once the terminal monomer in a RAD51 patch hydrolyses ATP, it and all adjacent monomers that have already hydrolyzed ATP will dissociate. Further it was shown, that tension on the DNA slows down dissociation and can even inhibit it at a tension of 48 ± 3 pN. Therefore the rate-limiting step in RAD51 dissociation can be the monomer dissociation at high tension or the ATP hydrolysis at low tension (*129*). The study further showed that the pause length between bursts was determined by the ATP hydrolysis rate derived from biochemical studies (*99*). Another peculiarity was that ATP hydrolysis continued during high tension. Thus it was possible to measure the intrinsic monomer dissociation rate of RAD51 upon tension release: $0.51 \pm 0.14\ \text{s}^{-1}$ (*129*). An increase in ATP concentration in the reaction buffer did not change the burst-wise dissociation, indicating that ATP renewal occurs very slowly or not at all, and that ADP release is slower than dissociation. This would be consistent with the notion that ADP release is the rate-limiting step of the RAD51 ATP-hydrolysis cycle (*99, 100, 133*). Tension as the driving force behind RAD51 monomer dissociation from dsDNA is consistent with the idea that an extended filament on dsDNA exists in vivo and that the extension of DNA by the filament is necessary for it to perform strand invasion and joint molecule formation.

Recombination mediators

Although RAD51 can perform all DNA transaction necessary for homologous recombination *in vitro*, the core steps of recombination are aided and presumably tightly controlled by recombination mediators and accessory factors *in vivo* (*134-136*). Here we will discuss breast cancer-susceptibility gene BRCA2 in detail.

Breast cancer susceptibility gene (BRCA2)

The tumor suppressor BRCA2 has been associated to breast, ovarian and other cancers based on its role in homologous recombination as a recombinase regulator. Lack of BRCA2 leads to the accumulation of chromosomal breaks, translocations and exchanges, that can give rise to cancers (*22, 52, 61, 137-143*). BRCA2 consists of 8 BRC domains, three OB-folds with a tower domain, and a C-terminal region spanning exon 27 that contains a region designated as C-terminal RAD51 binding domain (CTRD). The BRC domains bind to monomeric RAD51 with different affinities at the RAD51 monomer : monomer interface (*144-146*). At super stoichiometric amounts to RAD51, the BRC4 peptide can disrupt RAD51 filaments, while at sub stoichiometric amounts it will bind to the nucleoprotein filament (*145, 147, 148*). The CTRD binds multimeric RAD51 modulated by CDK mediated phosphorylation (*132, 147-149*). The OB-folds confer ssDNA binding and the tower domain possibly dsDNA binding. This leads to speculations that BRCA2, like its *Ustilago maydis* orhtologue Brh2, specifically binds to ss-dsDNA junctions (*150, 151*). Work with fragments of BRCA2 implied a role in directing RAD51 nucleation away from dsDNA onto ssDNA (*57, 58, 60, 152*). Recently, the purification of full length BRCA2 has supported and extended the initial findings.

Full-length BRCA2 binds about 4-6 RAD51 in solution, independent of the associated nucleotide co-factor (*54, 153*). As described above and in this thesis, that is sufficient to nucleate RAD51 filaments. BRCA2 efficiently binds ssDNA whether RAD51 is bound or not. A preference for either 5' or 3' tailed DNA substrates was only detectable at high salt concentrations (*54*). Thus BRCA2 promotes RAD51 nucleation on any single-stranded DNA substrate, i.e. single-stranded gaps as efficiently as ssDNA tails of both polarities. In *E. coli* and *Ustilago maydis* filaments are seeded with 5'-3' polarity by RecBCD or junction-specific by Brh2, respectively (*150, 154*). Based on these findings 5' end invasion as a mechanism for lesion bypass of replication forks cannot be excluded (*155*). Further this suggests that BRCA2 functions in single-strand gap repair as well. In prokaryotes two distinct complexes mediate recombinase filament formation, RecFOR and RecBCD for daughter-strand gap repair and double-strand break repair, respectively (*154, 156*). Succinctly BRCA2 promotes RAD51 filament formation on ssDNA without junction-specificity and with both polarities.

Importantly, BRCA2 stimulates RAD51 mediated strand exchange in the presence of RPA (*54, 153*). Interestingly, it does so without interacting with either RPA or RAD52. This is different from yeast Rad52, which needs the single-stranded DNA binding protein interaction to replace it with recombinase (*157*). Further distinction of BRCA2 stems from its inability to anneal RPA coated ssDNA, like its *U. maydis* and *Caenorhabditis elegans* orthologues (*53, 158*). It seems that in human BRCA2 and RAD52 have evolved to separate RPA displacement by RAD51 and RPA-covered ssDNA annealing, respectively. This means that RAD52 functions in second-end capture, single-strand annealing and synthesis-dependent strand annealing. There is no redundancy between these and the BRCA2 function. Instead BRCA2 in human overcomes the rate-limiting step of RAD51 nucleation onto RPA-coated ssDNA by preventing assembly onto dsDNA, promoting assembly onto ssDNA, and putatively

stabilizing the recombinase filament by suppressing RAD51 ATPase (*54, 153*). It is conceivable how BRCA2 can reduce ssDNA-dependent ATP hydrolysis in an *in vitro* assay. As RAD51 needs to dimerize to hydrolyze ATP and BRC binding occupies the domain, a BRCA2 concentration dependent decrease in ATP hydrolysis would be expected as less RAD51 remains available to multimerize. How BRCA2 is associated to or if it remains associated to a RAD51 filament still needs to be elucidated.

In cells BRCA2 interacts with DSS1 (*139, 159, 160*). Addition of DSS1 further stimulates BRCA2 mediated RAD51 replacement of RPA on ssDNA (*153*). However, how DSS1 stimulates BRCA2 function in the in vitro assay remains unclear. Another protein to interact with BRCA2 is PALB2. The interaction lies within the N-terminus of BRCA2 and is relevant for BRCA2 localization and its checkpoint functions (*161, 162*). Failure of PALB2 to interact with BRCA2 contributes to familial breast cancer and can cause Fanconia aneamia (FA) (*163-166*).

The CTRD of BRCA2 has been less intensively studied than the BRC repeats. Biochemical studies with CTRD peptides suggested that the domain stabilizes RAD51 filaments (*145, 147, 148*). This notion was further supported by studies that link the state of CTRD binding affinity for RAD51 to persistence of RAD51 foci and delayed mitotic entry in avian cells (*167*). Chapter three describes an approach to complement the biochemical studies that showed the stabilizing effect of CTRD on RAD51 filament disassembly. Employing an ensemble of single-molecule studies showed that CTRD does not reduce intrinsic RAD51 dissociation from dsDNA, but at high concentration rather entangles RAD51 filaments. Further CTRD reduces RAD51 filament formation on dsDNA in a concentration dependent manner.

A recent study suggests that the CTRD modulates BRCA2 function. Biochemical experiments with incomplete BRCA2 peptides have shown

that the BRCA2 CTRD is dispensable to promote strand exchange (*57, 59*). This infers that the CTRD is not necessary for RAD51 loading onto RPA-coated ssDNA and subsequently not for double-strand break repair. However, C-terminal truncations of BRCA2 show increased chromosomal instability conferring increased carcinogenesis and hematopoietic dysfunction (*138, 140, 168*). The study proposes a new role for BRCA2 in nascent strand protection at stalled replication forks that is dependent on the ability of BRCA2 to interact with RAD51 via its CTRD (*169*).

   Briefly, it was shown that nascent DNA strands are degraded by MRE11. This degradation was dependent on the presence of the CTRD and its ability to bind RAD51. CTRD binding to RAD51 is modulated by CDK-dependent phosphorylation. In the presence of stalled replication forks CHK1 is activated in the check-point signaling cascade. The kinase inhibits CDK activity and loss of RAD51 binding by CTRD phosphorylation. Degradation of the nascent strands can also lead to strand uncoupling. Either degradation and or fork uncoupling causes a reduction in replication fork restart and hence an increase in genomic aberrations. However, reduced replication fork restart did not affect cell viability. The data suggested that the CTRD interacts with the RAD51 filament and stabilizes it. Conversely, it was shown that overexpression of RAD51 K133R can compensate for the loss of CTRD (*169*). The underlying idea is that RAD51 K133R does not hydrolyze ATP and hence not disassemble by itself. Ergo, interaction of the filament with CTRD is supposed to have a similar effect. However, as discussed above also the BRC repeats reduce RAD51 ATPase and are proposed to stabilize filaments (*57, 145, 147*). Hence this should be a redundant function between BRC repeats and CTRD and not solely depend on the presence of the CTRD. Nevertheless, it is evident that CDK dependent phosphorylation of BRCA2 CTRD can modulate its function to protect replication forks from nucleolytic degradation. This BRCA2 function is separate from its

function in double-strand break repair derived from RAD51 loading onto RPA-coated ssDNA.

RAD51 associated protein 1 (RAD51AP1)

Cells with reduced RAD51AP1 expression exhibit sensitivity to double-strand break inducing agents that could be attributed to reduced recombination efficiency (*170, 171*). That reduction of recombination efficiency is expected to stem from RAD51AP1 interaction with RAD51. Biochemical assays showed that RAD51AP1 stimulates the RAD51-mediated formation of joint molecules. When RAD51-coated ssDNA invades duplex DNA, a branched structure is created. RAD51AP1 bound such branched DNA structures most efficiently. Work with truncation mutants revealed that the ability to bind RAD51 and branched DNA structures reside in the C-terminus and N-terminus of RAD51AP1, respectively. The highest stimulation of RAD51 D-loop formation was achieved when RAD51AP1 bound both, RAD51 and branched DNA. Therefore RAD51AP1 functions as a recombination mediator during the synaptic stage of recombination (*170, 171*). Similarly, RAD51AP1 was shown to specifically interact with DMC1 and also promote DMC1 mediated joint molecule formation. A function in meiotic recombination is supported by the localization of RAD51AP1 with DMC1 to meiotic chromatin (*172*).

RAD54

Another protein supposed to affect RAD51 disassembly is RAD54, which was shown to be able to remove RAD51 from circular and linear dsDNA (*173*). The experiments suggested that species-specific interactions between RAD51 and RAD54 are required for removal of

RAD51 from dsDNA. In the used conditions RAD51 appeared to be stuck on dsDNA after ATP hydrolysis much like it was observed in fluorescence microscopy experiments addressing RAD51 dissociation from dsDNA (*128*). Other studies suggest that the conformation of the RAD51 nucleoprotein filament directs the mode of RAD54 action. Here a RAD51 filament, stabilized by suppression of ATP hydrolysis, would direct RAD54 branch migration activity towards extension of a D-loop structure, thus away from the RAD51 filament (*174, 175*). This notion is supported by data showing that RAD54 increases the rate and extend of heteroduplex extension (*176, 177*), and that dsDNA partially covered with RAD51 most efficiently stimulates RAD54 ATPase activity, which directly correlates with translocation/branch migration activity (*178*). This data is not contradictory to RAD54 helping in the removal of RAD51 in the ADP-bound filament, but supposes a mechanism that can bias towards the double-strand break repair pathway of homologous recombination, leading to the formation of double Holliday junctions and resolution by junction-specific endonucleases as opposed to non-crossover products yielding synthesis-dependent strand annealing (*66, 174, 179*). On the other hand RAD54 mediated branch migration could also promote synthesis-dependent strand annealing. RAD54 has also been proposed and biochemically shown to be involved in earlier steps of homologous recombination (*180*).

RAD51 paralogues

In vertebrates there are five RAD51 paralogues. RAD51B, RAD51C and RAD51D were identified based on their similarity to RAD51 (*181-183*). XRCC2 and XRCC3 were found in complementation studies with mitomycin C (*184, 185*). Mutations in the paralogues have been associated with increased carcinogenesis (*186-189*). RAD51C has

recently been implicated with the Fanconi Anemia like syndrome and ATR/CHK2 meditated checkpoint signaling (*188, 190, 191*).

DT40 chicken cells lacking any of the five paralogues present a homologous recombination defective phenotype, i.e. chromosome aberrations, defective repair and reduced gene targeting. That deficiency can be compensated by overexpression of human RAD51. Therefore it was concluded that all five RAD51 paralogues have RAD51 mediator function in homologous recombination (*192, 193*).

The paralogues interact with each other and with RAD51 forming diverse complexes (*194-200*). RAD51C-XRCC3 promotes joint molecule formation and strand exchange (*201*). Additional, XRCC3 has been associated with a late role in recombination (*194*). In accordance the RAD51C-XRCC3 complex was found to mediate Holliday junction resolvase and branch migration activity (*202*). However this function of the RAD51-XRCC3 complex seems to be associated to meiotic crossover resolution before chromosome segregation (*203*).

Another paralogue complex is RAD51B-RAD51C. Its mediator function has been associated to the promotion of RAD51 mediated joint molecule formation between circular ssDNA and linear dsDNA (*198*). It can partially alleviate the RPA imposed inhibition of joint molecule formation (*118*). This mediator function seems to stem from ATP-dependent ssDNA binding of RAD51B-RAD51C, and the dsDNA melting promoted by RAD51C (*204*).

Regulation of homologous recombination

Homologous recombination can be regulated by a plethora of mediator or accessory factors, either by interacting with homologous recombination proteins or by interacting with DNA structures arising during homologous recombination, or both. As evident form the details on homologous recombination and the recombination mediators described above, the arising DNA structures and their intermediates might play an even more pivotal role in regulation of recombination. The paragraph on replication fork repair can be summarized in different DNA transactions that culminate in the incident of a DNA structure that can be recognized by proteins of homologous recombination: the double-strand break. DNA end recognition and resection are both control steps that regulate progression of homologous recombination and bias the choice between non-homologous end-joining and homologous recombination. The DNA resection provides the platform for RPA-binding and consequently checkpoint signaling. The RAD51 filament needs to assemble onto the RPA-covered ssDNA, if double-strand break repair by homologous recombination is to take place – a bottleneck in the repair pathway. The filament itself can be described as meta-stable, as RAD51 constantly associates to DNA-bound protein patches and simultaneously dissociates from DNA after ATP hydrolysis. This balance between association and dissociation itself is a control step for the progression of strand exchange. It can easily be tilted by proteins promoting assembly or by those disrupting filaments. BRCA2, as described above, has a fundamental role in promoting the assembly of RAD51 filaments on RPA-covered single-strand DNA. On the contrary helicases like BLM can disrupt RAD51 filaments.

During homology search and strand exchange many metastable intermediate DNA structures arise, some of which can be trapped – like the D-loop, a branched DNA structure. Proteins binding to the arising

DNA structures are potential recombination mediators as the stabilization of the DNA intermediates could promote the progression of strand exchange or limit the reversal of the arising DNA structures to a previous intermediate. Apart from stabilizing intermediate DNA structures, structure-specific binding of proteins could also cause displacement of other recombination mediators or accessory factors in order to regulate progression of homologous recombination, or block the progression. The mediator protein RAD51AP1, described in detail above, specifically binds D-loops which, together with its RAD51 binding activity, enhance D-loop formation. A great number of other proteins interact with the branched DNA structures that arise during strand exchange, e.g. RAD54 and BLM. One of the most prominent branched DNA structures arising during homologous recombination are the Holliday junctions. Their resolution by protein complexes evolving around BLM helicase and by structure-specific endonucleases has been described above. Although Holliday junctions only occur after strand exchange their resolution still poses a regulatory step in homologous recombination. On the other hand there are distinct sub-pathways available after strand exchange. As depicted in Figure 1, synthesis-dependent strand annealing does not involve the formation of Holliday junctions. The extent of DNA resection prior to filament assembly can affect via which sub-pathway breaks are repaired. In that sense the extent of resection, and thus the proteins resecting, have a regulatory role in double-strand break repair. The plethora a potential recombination mediators and accessory factors highlights the importance of regulation of strand exchange in homologous recombination. To fully comprehend how regulatory proteins work, one must first analyze the intrinsic behavior of the strand-exchange protein RAD51. This thesis is a contribution to the understanding of RAD51 filament assembly on and disassembly from DNA.

References

1.	J. H. Hoeijmakers, Nature 411, 366 (May 17, 2001).
2.	D. C. van Gent, M. van der Burg, Oncogene 26, 7731 (Dec 10, 2007).
3.	T. Helleday, J. Lo, D. C. van Gent, B. P. Engelward, DNA Repair (Amst) 6, 923 (Jul 1, 2007).
4.	M. Hammel et al., J Biol Chem 285, 1414 (Jan 8, 2010).
5.	E. Weterings, D. J. Chen, J Cell Biol 179, 183 (Oct 22, 2007).
6.	E. Rass, A. Grabarz, P. Bertrand, B. S. Lopez, Cancer Radiother, (Jul 5, 2011).
7.	S. Ozturk, N. Demir, Histol Histopathol 26, 505 (Apr, 2011).
8.	J. Essers, W. Vermeulen, A. B. Houtsmuller, Curr Opin Cell Biol 18, 240 (Jun, 2006).
9.	B. Pascucci, M. D'Errico, E. Parlanti, S. Giovannini, E. Dogliotti, Biochemistry (Mosc) 76, 4 (Jan, 2011).
10.	G. Xu, M. Herzig, V. Rotrekl, C. A. Walter, Mech Ageing Dev 129, 366 (Jul-Aug, 2008).
11.	K. H. Almeida, R. W. Sobol, DNA Repair (Amst) 6, 695 (Jun 1, 2007).
12.	W. Vermeulen, DNA Repair (Amst) 10, 760 (Jul 15, 2011).
13.	A. F. Fagbemi, B. Orelli, O. D. Scharer, DNA Repair (Amst) 10, 722 (Jul 15, 2011).
14.	T. Nouspikel, Cell Mol Life Sci 66, 994 (Mar, 2009).
15.	P. C. Hanawalt, G. Spivak, Nat Rev Mol Cell Biol 9, 958 (Dec, 2008).
16.	S. Tornaletti, Cell Mol Life Sci 66, 1010 (Mar, 2009).
17.	P. Hsieh, K. Yamane, Mech Ageing Dev 129, 391 (Jul-Aug, 2008).
18.	K. Fukui, J Nucleic Acids 2010, (2010).
19.	P. Modrich, J Biol Chem 281, 30305 (Oct 13, 2006).
20.	J. Jiricny, Nat Rev Mol Cell Biol 7, 335 (May, 2006).
21.	P. Sung, L. Krejci, S. Van Komen, M. G. Sehorn, J Biol Chem 278, 42729 (Oct 31, 2003).
22.	A. R. Venkitaraman, Annu Rev Pathol 4, 461 (2009).
23.	C. Wyman, R. Kanaar, Annu Rev Genet 40, 363 (2006).
24.	M. M. Cox et al., Nature 404, 37 (Mar 2, 2000).
25.	D. Remus et al., Cell 139, 719 (Nov 13, 2009).
26.	D. Remus, J. F. Diffley, Curr Opin Cell Biol 21, 771 (Dec, 2009).
27.	Z. O. Jonsson, U. Hubscher, Bioessays 19, 967 (Nov, 1997).
28.	G. Maga, M. Stucki, S. Spadari, U. Hubscher, Journal of molecular biology 295, 791 (Jan 28, 2000).
29.	M. Stucki, I. Stagljar, Z. O. Jonsson, U. Hubscher, Prog Nucleic Acid Res Mol Biol 65, 261 (2001).
30.	V. Pages, R. P. Fuchs, Oncogene 21, 8957 (Dec 16, 2002).
31.	A. R. Lehmann, Mutat Res 509, 23 (Nov 30, 2002).
32.	T. A. Kunkel, Y. I. Pavlov, K. Bebenek, DNA repair 2, 135 (Feb 3, 2003).
33.	W. Yang, Curr Opin Struct Biol 13, 23 (Feb, 2003).
34.	L. Postow, N. J. Crisona, B. J. Peter, C. D. Hardy, N. R. Cozzarelli, Proceedings of the National Academy of Sciences of the United States of America 98, 8219 (Jul 17, 2001).
35.	I. D. Hickson, Nat Rev Cancer 3, 169 (Mar, 2003).
36.	K. Hanada et al., Nature structural & molecular biology 14, 1096 (Nov, 2007).
37.	K. Hanada et al., The EMBO journal 25, 4921 (Oct 18, 2006).
38.	M. Lisby, J. H. Barlow, R. C. Burgess, R. Rothstein, Cell 118, 699 (Sep 17, 2004).
39.	M. de Jager et al., Molecular cell 8, 1129 (Nov, 2001).
40.	D. D'Amours, S. P. Jackson, Nat Rev Mol Cell Biol 3, 317 (May, 2002).
41.	T. T. Paull, M. Gellert, Molecular cell 1, 969 (Jun, 1998).
42.	R. S. Williams et al., Cell 135, 97 (Oct 3, 2008).
43.	Y. Wang et al., Genes & development 14, 927 (Apr 15, 2000).
44.	A. A. Sartori et al., Nature 450, 509 (Nov 22, 2007).
45.	P. Huertas, F. Cortes-Ledesma, A. A. Sartori, A. Aguilera, S. P. Jackson, Nature 455, 689 (Oct 2, 2008).
46.	P. Huertas, S. P. Jackson, The Journal of biological chemistry 284, 9558 (Apr 3, 2009).
47.	K. A. Bernstein, S. Gangloff, R. Rothstein, Annual review of genetics 44, 393 (2010).
48.	A. V. Nimonkar et al., Genes & development 25, 350 (Feb 15, 2011).
49.	A. V. Nimonkar, A. Z. Ozsoy, J. Genschel, P. Modrich, S. C. Kowalczykowski, Proceedings of the National Academy of Sciences of the United States of America 105, 16906 (Nov 4, 2008).
50.	D. O. Warmerdam, R. Kanaar, Mutat Res 704, 2 (Apr-Jun, 2010).
51.	D. O. Warmerdam, (Spetermber 24th, 2010, 2010).
52.	J. San Filippo, P. Sung, H. Klein, Annu Rev Biochem 77, 229 (2008).
53.	M. I. Petalcorin, J. Sandall, D. B. Wigley, S. J. Boulton, J Mol Biol 361, 231 (Aug 11, 2006).
54.	R. B. Jensen, A. Carreira, S. C. Kowalczykowski, Nature, (Aug 22, 2010).
55.	F. E. Benson, P. Baumann, S. C. West, Nature 391, 401 (Jan 22, 1998).
56.	P. Baumann, S. C. West, J Mol Biol 291, 363 (Aug 13, 1999).

57.   A. Carreira et al., Cell 136, 1032 (Mar 20, 2009).
58.   A. Carreira, S. C. Kowalczykowski, Cell Cycle 8, 3445 (Nov 1, 2009).
59.   M. K. Shivji et al., Nucleic acids research 34, 4000 (2006).
60.   M. K. Shivji et al., Proc Natl Acad Sci U S A 106, 13254 (Aug 11, 2009).
61.   M. K. Shivji, A. R. Venkitaraman, DNA repair 3, 835 (Aug-Sep, 2004).
62.   C. Z. Bachrati, R. H. Borts, I. D. Hickson, Nucleic acids research 34, 2269 (2006).
63.   B. Pardo, B. Gomez-Gonzalez, A. Aguilera, Cell Mol Life Sci 66, 1039 (Mar, 2009).
64.   Y. Hu et al., Genes & development 21, 3073 (Dec 1, 2007).
65.   D. V. Bugreev, X. Yu, E. H. Egelman, A. V. Mazin, Genes & development 21, 3085 (Dec 1, 2007).
66.   F. Paques, J. E. Haber, Microbiol Mol Biol Rev 63, 349 (Jun, 1999).
67.   J. W. Szostak, T. L. Orr-Weaver, R. J. Rothstein, F. W. Stahl, Cell 33, 25 (May, 1983).
68.   M. A. Resnick, J Theor Biol 59, 97 (Jun, 1976).
69.   T. Sugiyama, J. H. New, S. C. Kowalczykowski, Proc Natl Acad Sci U S A 95, 6049 (May 26, 1998).
70.   W. K. Chu, I. D. Hickson, Nat Rev Cancer 9, 644 (Sep, 2009).
71.   J. M. Svendsen, J. W. Harper, Genes Dev 24, 521 (Mar 15, 2010).
72.   A. J. van Brabant et al., Biochemistry 39, 14617 (Nov 28, 2000).
73.   P. Mohaghegh, J. K. Karow, R. M. Brosh, Jr., V. A. Bohr, I. D. Hickson, Nucleic acids research 29, 2843 (Jul 1, 2001).
74.   D. K. Orren, S. Theodore, A. Machwe, Biochemistry 41, 13483 (Nov 19, 2002).
75.   L. Wu et al., The EMBO journal 24, 2679 (Jul 20, 2005).
76.   L. Wu, I. D. Hickson, Nature 426, 870 (Dec 18, 2003).
77.   S. Raynard et al., The Journal of biological chemistry 283, 15701 (Jun 6, 2008).
78.   S. Raynard, W. Bussen, P. Sung, The Journal of biological chemistry 281, 13861 (May 19, 2006).
79.   L. Wu et al., Proceedings of the National Academy of Sciences of the United States of America 103, 4068 (Mar 14, 2006).
80.   L. Wu, I. D. Hickson, Nucleic acids research 30, 4823 (Nov 15, 2002).
81.   F. B. Johnson et al., Cancer Res 60, 1162 (Mar 1, 2000).
82.   T. R. Singh et al., Genes & development 22, 2856 (Oct 15, 2008).
83.   D. Xu et al., Genes & development 22, 2843 (Oct 15, 2008).
84.   D. V. Bugreev, O. M. Mazina, A. V. Mazin, The Journal of biological chemistry 284, 26349 (Sep 25, 2009).
85.   S. C. Ip et al., Nature 456, 357 (Nov 20, 2008).
86.   U. Rass et al., Genes Dev 24, 1559 (Jul 15, 2010).
87.   S. L. Andersen et al., Molecular cell 35, 128 (Jul 10, 2009).
88.   S. Fekairi et al., Cell 138, 78 (Jul 10, 2009).
89.   I. M. Munoz et al., Molecular cell 35, 116 (Jul 10, 2009).
90.   T. T. Saito, J. L. Youds, S. J. Boulton, M. P. Colaiacovo, PLoS Genet 5, e1000735 (Nov, 2009).
91.   A. Ciccia, A. Constantinou, S. C. West, The Journal of biological chemistry 278, 25172 (Jul 4, 2003).
92.   P. H. Gaillard, E. Noguchi, P. Shanahan, P. Russell, Molecular cell 12, 747 (Sep, 2003).
93.   K. T. Ehmsen, W. D. Heyer, Nucleic acids research 36, 2182 (Apr, 2008).
94.   H. Interthal, W. D. Heyer, Mol Gen Genet 263, 812 (Jun, 2000).
95.   G. R. Smith, M. N. Boddy, P. Shanahan, P. Russell, Genetics 165, 2289 (Dec, 2003).
96.   M. N. Boddy et al., Cell 107, 537 (Nov 16, 2001).
97.   E. Sonoda et al., EMBO J 17, 598 (Jan 15, 1998).
98.   T. Tsuzuki et al., Proc Natl Acad Sci U S A 93, 6236 (Jun 25, 1996).
99.   G. Tombline, R. Fishel, J Biol Chem 277, 14417 (Apr 26, 2002).
100.   G. Tombline, K. S. Shim, R. Fishel, J Biol Chem 277, 14426 (Apr 26, 2002).
101.   G. Tombline, C. D. Heinen, K. S. Shim, R. Fishel, J Biol Chem 277, 14434 (Apr 26, 2002).
102.   V. E. Galkin et al., Structure 14, 983 (Jun, 2006).
103.   T. Kinebuchi et al., Molecular cell 14, 363 (May 7, 2004).
104.   S. Yang, X. Yu, E. M. Seitz, S. C. Kowalczykowski, E. H. Egelman, J Mol Biol 314, 1077 (Dec 14, 2001).
105.   A. L. Forget, M. S. Loftus, D. A. McGrew, B. T. Bennett, K. L. Knight, Biochemistry 46, 3566 (Mar 20, 2007).
106.   A. Ruksc, E. C. Birmingham, M. D. Baker, DNA Repair (Amst) 6, 1876 (Dec 1, 2007).
107.   J. M. Stark et al., J Biol Chem 277, 20185 (Jun 7, 2002).
108.   H. Sanchez, R. Kanaar, C. Wyman, Ultramicroscopy 110, 844 (Jun, 2010).
109.   P. Chi, S. Van Komen, M. G. Sehorn, S. Sigurdsson, P. Sung, DNA Repair (Amst) 5, 381 (Mar 7, 2006).
110.   K. Adzuma, Genes Dev 6, 1679 (Sep, 1992).
111.   D. V. Bugreev, A. V. Mazin, Proc Natl Acad Sci U S A 101, 9988 (Jul 6, 2004).
112.   E. H. Egelman, Ultramicroscopy 85, 225 (Dec, 2000).
113.   E. H. Egelman, J Mol Biol 309, 539 (Jun 8, 2001).
114.   J. F. Leger, J. Robert, L. Bourdieu, D. Chatenay, J. F. Marko, Proc Natl Acad Sci U S A 95, 12295 (Oct 13, 1998).
115.   Y. Wu, Y. He, I. A. Moya, X. Qian, Y. Luo, Molecular cell 15, 423 (Aug 13, 2004).
116.   A. B. Conway et al., Nat Struct Mol Biol 11, 791 (Aug, 2004).
117.   D. Ristic et al., Nucleic Acids Res 33, 3292 (2005).

118.	S. Sigurdsson, K. Trujillo, B. Song, S. Stratton, P. Sung, J Biol Chem 276, 8798 (Mar 23, 2001).
119.	T. van der Heijden, C. Dekker, Biophys J 95, 4560 (Nov 15, 2008).
120.	T. van der Heijden et al., Nucleic Acids Res 35, 5646 (2007).
121.	A. Reymer, K. Frykholm, K. Morimatsu, M. Takahashi, B. Norden, Proc Natl Acad Sci U S A 106, 13248 (Aug 11, 2009).
122.	Z. Chen, H. Yang, N. P. Pavletich, Nature 453, 489 (May 22, 2008).
123.	K. Adzuma, J Biol Chem 273, 31565 (Nov 20, 1998).
124.	M. T. van Loenhout, T. van der Heijden, R. Kanaar, C. Wyman, C. Dekker, Nucleic Acids Res, (May 8, 2009).
125.	J. Mameren et al., Biophys J 91, L78 (Oct 15, 2006).
126.	M. Modesti et al., Structure 15, 599 (May, 2007).
127.	T. K. Prasad, C. C. Yeykal, E. C. Greene, J Mol Biol 363, 713 (Oct 27, 2006).
128.	J. Hilario, I. Amitani, R. J. Baskin, S. C. Kowalczykowski, Proc Natl Acad Sci U S A 106, 361 (Jan 13, 2009).
129.	J. van Mameren et al., Nature, (Dec 7, 2008).
130.	T. van der Heijden et al., Molecular cell 30, 530 (May 23, 2008).
131.	D. Ristic, R. Kanaar, C. Wyman, Nucleic acids research 39, 155 (Jan 1, 2011).
132.	J. T. Holthausen et al., Nucleic acids research, (May 16, 2011).
133.	K. S. Shim et al., DNA Repair (Amst) 5, 704 (Jun 10, 2006).
134.	C. Wyman, R. Kanaar, Curr Biol 14, R629 (Aug 10, 2004).
135.	J. T. Holthausen, C. Wyman, R. Kanaar, DNA repair 9, 1264 (Dec 10, 2010).
136.	R. Kanaar, C. Wyman, R. Rothstein, The EMBO journal 27, 581 (Feb 20, 2008).
137.	T. Thorslund, S. C. West, Oncogene 26, 7720 (Dec 10, 2007).
138.	G. Donoho et al., Genes Chromosomes Cancer 36, 317 (Apr, 2003).
139.	M. Kojic, H. Yang, C. F. Kostrub, N. P. Pavletich, W. K. Holloman, Molecular cell 12, 1043 (Oct, 2003).
140.	K. A. McAllister et al., Cancer Res 62, 990 (Feb 15, 2002).
141.	M. E. Moynahan, M. Jasin, Nat Rev Mol Cell Biol 11, 196 (Mar, 2010).
142.	M. E. Moynahan, A. J. Pierce, M. Jasin, Molecular cell 7, 263 (Feb, 2001).
143.	P. L. Welcsh, K. N. Owens, M. C. King, Trends Genet 16, 69 (Feb, 2000).
144.	T. Thorslund, F. Esashi, S. C. West, Embo J 26, 2915 (Jun 20, 2007).
145.	V. E. Galkin et al., Proc Natl Acad Sci U S A 102, 8537 (Jun 14, 2005).
146.	L. Pellegrini et al., Nature 420, 287 (Nov 21, 2002).
147.	F. Esashi, V. E. Galkin, X. Yu, E. H. Egelman, S. C. West, Nat Struct Mol Biol 14, 468 (Jun, 2007).
148.	O. R. Davies, L. Pellegrini, Nat Struct Mol Biol 14, 475 (Jun, 2007).
149.	F. Esashi et al., Nature 434, 598 (Mar 31, 2005).
150.	H. Yang, Q. Li, J. Fan, W. K. Holloman, N. P. Pavletich, Nature 433, 653 (Feb 10, 2005).
151.	H. Yang et al., Science 297, 1837 (Sep 13, 2002).
152.	J. San Filippo et al., The Journal of biological chemistry 281, 11649 (Apr 28, 2006).
153.	J. Liu, T. Doty, B. Gibson, W. D. Heyer, Nat Struct Mol Biol, (Aug 22, 2010).
154.	M. M. Cox, Critical reviews in biochemistry and molecular biology 42, 41 (Jan-Feb, 2007).
155.	N. Mazloum, W. K. Holloman, Molecular cell 36, 620 (Nov 25, 2009).
156.	K. Morimatsu, S. C. Kowalczykowski, Molecular cell 11, 1337 (May, 2003).
157.	T. Sugiyama, S. C. Kowalczykowski, J Biol Chem 277, 31663 (Aug 30, 2002).
158.	N. Mazloum, Q. Zhou, W. K. Holloman, Biochemistry 46, 7163 (Jun 19, 2007).
159.	N. J. Marston et al., Molecular and cellular biology 19, 4633 (Jul, 1999).
160.	K. Gudmundsdottir, C. J. Lord, E. Witt, A. N. Tutt, A. Ashworth, EMBO Rep 5, 989 (Oct, 2004).
161.	B. Xia et al., Molecular cell 22, 719 (Jun 23, 2006).
162.	M. Tischkowitz et al., Proceedings of the National Academy of Sciences of the United States of America 104, 6788 (Apr 17, 2007).
163.	B. Xia et al., Nat Genet 39, 159 (Feb, 2007).
164.	H. Erkko et al., Nature 446, 316 (Mar 15, 2007).
165.	S. Reid et al., Nat Genet 39, 162 (Feb, 2007).
166.	N. Rahman et al., Nat Genet 39, 165 (Feb, 2007).
167.	N. Ayoub et al., Curr Biol 19, 1075 (Jul 14, 2009).
168.	S. Navarro et al., Mol Ther 14, 525 (Oct, 2006).
169.	K. Schlacher et al., Cell 145, 529 (May 13, 2011).
170.	M. Modesti et al., Molecular cell 28, 468 (Nov 9, 2007).
171.	C. Wiese et al., Molecular cell 28, 482 (Nov 9, 2007).
172.	E. Dray et al., Proceedings of the National Academy of Sciences of the United States of America 108, 3560 (Mar 1, 2011).
173.	J. A. Solinger, K. Kiianitsa, W. D. Heyer, Molecular cell 10, 1175 (Nov, 2002).
174.	M. J. Rossi, A. V. Mazin, J Biol Chem 283, 24698 (Sep 5, 2008).
175.	D. V. Bugreev, F. Hanaoka, A. V. Mazin, Nat Struct Mol Biol 14, 746 (Aug, 2007).
176.	J. A. Solinger, W. D. Heyer, Proc Natl Acad Sci U S A 98, 8447 (Jul 17, 2001).
177.	J. A. Solinger, G. Lutz, T. Sugiyama, S. C. Kowalczykowski, W. D. Heyer, J Mol Biol 307, 1207 (Apr 13, 2001).

178. K. Kiianitsa, J. A. Solinger, W. D. Heyer, J Biol Chem 277, 46205 (Nov 29, 2002).
179. O. M. Mazina, A. V. Mazin, T. Nakagawa, R. D. Kolodner, S. C. Kowalczykowski, Cell 117, 47 (Apr 2, 2004).
180. T. L. Tan, R. Kanaar, C. Wyman, DNA Repair (Amst) 2, 787 (Jul 16, 2003).
181. J. S. Albala et al., Genomics 46, 476 (Dec 15, 1997).
182. M. K. Dosanjh et al., Nucleic acids research 26, 1179 (Mar 1, 1998).
183. D. L. Pittman, L. R. Weinberg, J. C. Schimenti, Genomics 49, 103 (Apr 1, 1998).
184. N. J. Jones, R. Cox, J. Thacker, Mutat Res 183, 279 (May, 1987).
185. N. Liu et al., Molecular cell 1, 783 (May, 1998).
186. L. M. Pelttari et al., Hum Mol Genet, (Jun 9, 2011).
187. J. Johnson, S. Healey, K. K. Khanna, G. Chenevix-Trench, Breast Cancer Res Treat, (Apr 28, 2011).
188. F. Vaz et al., Nat Genet 42, 406 (May, 2010).
189. A. Slupianek, S. K. Jozwiakowski, E. Gurdek, T. Skorski, Leukemia 23, 2308 (Dec, 2009).
190. M. Katsura et al., Nucleic acids research 37, 3959 (Jul, 2009).
191. S. Badie et al., J Cell Biol 185, 587 (May 18, 2009).
192. M. Takata et al., Molecular and cellular biology 20, 6476 (Sep, 2000).
193. M. Takata et al., Molecular and cellular biology 21, 2858 (Apr, 2001).
194. M. A. Brenneman, B. M. Wagener, C. A. Miller, C. Allen, J. A. Nickoloff, Molecular cell 10, 387 (Aug, 2002).
195. H. Kurumizaka et al., Nucleic acids research 31, 4041 (Jul 15, 2003).
196. J. Y. Masson, A. Z. Stasiak, A. Stasiak, F. E. Benson, S. C. West, Proceedings of the National Academy of Sciences of the United States of America 98, 8440 (Jul 17, 2001).
197. D. Schild, Y. C. Lio, D. W. Collins, T. Tsomondo, D. J. Chen, The Journal of biological chemistry 275, 16443 (Jun 2, 2000).
198. S. Sigurdsson et al., Genes & development 15, 3308 (Dec 15, 2001).
199. Y. Yonetani et al., Nucleic acids research 33, 4544 (2005).
200. C. Rajesh, A. M. Gruver, V. Basrur, D. L. Pittman, Proteomics 9, 4071 (Aug, 2009).
201. H. Kurumizaka et al., Proceedings of the National Academy of Sciences of the United States of America 98, 5538 (May 8, 2001).
202. Y. Liu, J. Y. Masson, R. Shah, P. O'Regan, S. C. West, Science 303, 243 (Jan 9, 2004).
203. Y. Liu, M. Tarsounas, P. O'Regan, S. C. West, The Journal of biological chemistry 282, 1973 (Jan 19, 2007).
204. Y. C. Lio, A. V. Mazin, S. C. Kowalczykowski, D. J. Chen, The Journal of biological chemistry 278, 2469 (Jan 24, 2003).

Chapter 2:

Regulation of DNA strand exchange in homologous recombination

J. Thomas Holthausen[1], Claire Wyman[1,2] and Roland Kanaar[1,2]

[1]Department of Cell Biology & Genetics, Cancer Genomics Center, [2]Department of Radiation Oncology, Erasmus Medical Center, PO Box 2040, 3000 CA Rotterdam, The Netherlands

Abstract

Homologous recombination, the exchange of DNA strands between homologous DNA molecules, is involved in repair of many structural diverse DNA lesions. This versatility stems from multiple ways in which homologous DNA strands can be rearranged. At the core of homologous recombination are recombinase proteins such as RecA and RAD51 that mediate homology recognition and DNA strand exchange through formation of a dynamic nucleoprotein filament. Four stages in the life cycle of nucleoprotein filaments are filament nucleation, filament growth, homologous DNA pairing and strand exchange, and filament dissociation. Progression through this cycle requires a sequence of recombinase-DNA and recombinase protein-protein interactions coupled to ATP binding and hydrolysis. The function of recombinases is controlled by accessory proteins that allow coordination of strand exchange with other steps of homologous recombination and that tailor to the needs of specific aberrant DNA structures undergoing recombination. Accessory proteins are also able to reverse filament formation thereby guarding against inappropriate DNA rearrangements. The dynamic instability of the recombinase-DNA interactions allows both positive and negative action of accessory proteins thereby ensuring that genome maintenance by homologous recombination is not only flexible and versatile, but also accurate.

Introduction

Evolution, the fundamental process that drives biological diversity, demands changes in genomic DNA, the carrier of genetic information. In this light the inherent instability of DNA, a molecule subject to spontaneous hydrolysis reactions and attack from chemicals or radiation, is an advantage. Alterations in the chemical structure of DNA can induce mutations that fuel evolution. However, at the level of the individual, a certain degree of genome stability is required to guard against diseases, including cancer. DNA repair reactions that can restore the structure and function of damaged DNA provide a balance between evolution and development of disease (*1, 2*). We focus on one such repair reaction; homologous recombination, the exchange of DNA strands between homologous DNA molecules.

Due to the chemical complexity of DNA numerous structurally diverse lesions can occur. It is therefore not surprising that multiple DNA repair reactions have evolved (*1, 2*). Decades of genetic and biochemical experiments resulted in the classification of distinct repair pathways and the outline of their mechanisms are emerging. Many DNA repair pathways function by pinpointing the offending covalent chemical adduct modifying DNA through a structure-specific DNA binding protein or protein complex. This recognition event triggers a series of subsequent lesion-processing reactions that eventually restore DNA structure to effect repair. Examples of such pathways include base excision repair, nucleotide excision repair and mismatch repair, which are initiated by recognition of the damaged or incorrect deoxynucleotide, followed by its excision and reinsertion of the correct nucleotide(s) using the complementary DNA strand as a template. The advantage of structure recognition to initiate repair is high specificity, but this also inherently limits the diversity of lesions that can be repaired through each pathway. Homologous recombination does not have this limitation since it does not directly recognize DNA lesions. Instead, the process is initiated on the single-stranded form of DNA, which does not

need to contain lesions itself, although it could have arisen as a response to DNA lesions (*3-5*). This indirect DNA damage recognition mode and the multiple ways to rearrange homologous DNA strands allows great flexibility in applying homologous recombination to repair many structural diverse DNA lesions or alternative DNA structures, including single-strand gaps, double-strand breaks (DSBs) (Fig. 1), interstrand crosslinks and stalled/collapsed replication forks (*6-9*).

The multiple applications of homologous recombination in DNA repair imply that this process is subject to multiple control mechanisms (*10*). In addition, homologous recombination is only a repair mechanism if the DNA rearrangements catalyzed contribute to DNA genomic stability rather than instability. The exchange of base-paired partners between a DNA segment in need of repair and an undamaged duplex partner of homologous sequence is at the core of DNA repair by homologous recombination (*11, 12*). Control of homologous recombination repair is focused on controlling this strand exchange step. Notably this reaction is absolutely required for error-free repair of damage involving both strands of duplex DNA. To provide context for this central reaction and its control, we briefly describe seminal events during a complete homologous recombination event leading to the repair of a DSB (Fig. 1).

DNA double-strand break repair by homologous recombination

A DSB occurs when covalent bonds in the phosphodiester backbone in both strands of duplex DNA are severed in close proximity. The first order of business is then to keep the break ends, as well as the sister chromatids, nearby so the intact sister chromatid can serve as the repair template for the broken one. In eukaryotes these steps require proteins of the SMC family; the MRN (in vertebrates or MRX in yeast) and cohesin complexes

(*15, 16*). Next, a key intermediate DNA substrate of homologous recombination is generated; single-stranded DNA with a 3' end (Fig. 1C). This requires the action of nucleases, often aided by DNA helicases. In prokaryotes, such as *Escherichia coli*, the nuclease and helicase functions are provided by the RecBCD complex (*17*). More players appear to influence this step in eukaryotes. In yeast, the MRX complex, in cooperation with Sae2, is important for initiating DNA resection (*18*).
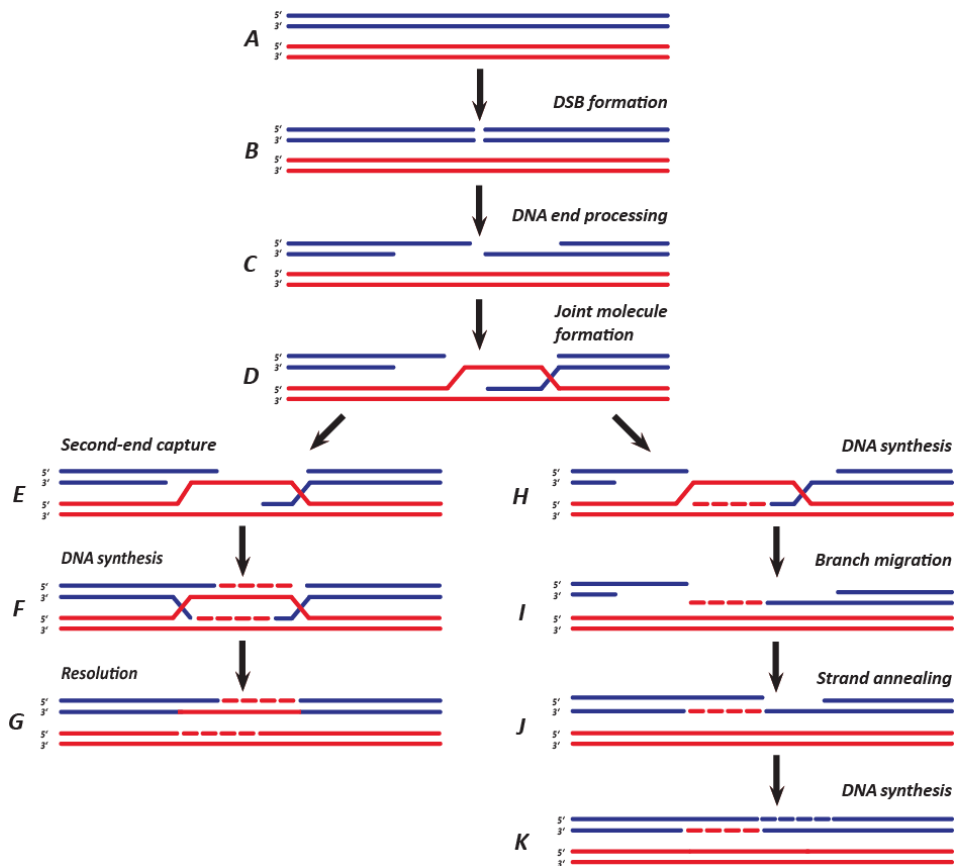
Fig 1. Schematic representation of amodel for DSB-initiated homologous recombination. (A) Two duplex DNAs, representing homologous sister chromatids, are indicated by parallel blue and red lines. This cartoon focuses on the DNA events during

recombination and therefore participating proteins are omitted. Upon DSB formation (B), the ends are nucleolytically processed to result in 3' single-stranded tails (C). (D) Recombinase proteins assembled in a nucleoprotein filament on the single-stranded DNA mediate joint molecule formation between the processed broken DNA and the homologous duplex repair template via homology recognition and DNA strand exchange. Downstream of joint molecule formation, two subpathways of homologous recombination are indicated: DSBR (*13*) and SDSA (*14*). (E) In the DSBR pathway the second DNA end is engaged and upon DNA synthesis, the recombining molecules are joined via Holliday junctions (F). (G) Resolution of the junctions by structure-specific endonucleases releases two repaired duplex DNAs. (H) Upon DNA synthesis in the SDSA pathway the joint molecule is dissolved (I) and the newly synthesized DNA strand anneals with the processed second DNA end (J). Repair DNA synthesis completes repair (K).

Then more extensive single-stranded DNA is generated through the action of the Sgs1 helicase in cooperation with the Dna2 nuclease, or the Exo1 5'-3' exonuclease (*19*). All these steps are a prelude to the molecular events that define homologous recombination; recognition of homologous DNA sequence to generate a joint molecule between single-stranded DNA and its duplex repair template followed by DNA strand exchange, *i.e.*, switching base-paired partners between these DNAs (Fig. 1D).

The core reactions of homologous recombination, homology recognition and strand exchange, are mediated by recombinase proteins such as RecA in prokaryotes and by Rad51 in eukaryotes, including yeasts and mammals (*20*). The DNA rearrangement events that define homologous recombination are catalyzed by RecA and Rad51 assembled into protein filaments on single-stranded DNA. These nucleoprotein filaments are molecular machines promoting specific DNA rearrangement reactions through their sequential assembly, rearrangement and disassembly. The core of the recombination process is controlled by accessory/mediator proteins that modulate the dynamic interaction of recombinase proteins in nucleoprotein filaments (*21*). Subsequent steps in homologous recombination can include the

engagements of the second DNA end, DNA branch migration, and eventual resolution of repaired DNA strands (Fig. 1E-G). Multiple sub-pathways exist to achieve this, including gene conversion (with or without associated crossover) and synthesis dependent strand annealing (SDSA) (*13, 14, 22*).

Upon joint molecule formation, a critical common step in the homologous recombination pathways is the hand off of the 3' end of the incoming DNA molecule to a DNA polymerase, such that recombination will result in two restored duplex DNAs. At this stage of the reaction the partner DNA molecules are physically joined via branched DNA structures, which upon ligation can be converted into so-called Holliday junctions (Fig. 1F). There appear to be a plethora of structure-specific endonucleases that can resolve these structures resulting in the completion of DNA repair by homologous recombination. Enzymes such as the *E. coli* RuvABC complex and the eukaryotic Gen1 protein incise Holliday junctions producing directly ligatable crossover and non-crossover products (*23*). Alternatively, a DNA helicase, BLM, in combination with a type I topoisomerase, can resolve Holliday junctions exclusively in a non-crossover mode (*24*). Branched DNA intermediates in homologous recombination can also be acted upon by evolutionary-conserved structure-specific endonucleases, including Mus81/Eme1 and Slx1/Slx4 (*23, 25*). Since homologous recombination contributes to the repair of many different DNA lesions and obstructed replication forks, each of which might involve subtly differently (protein covered) branched DNA intermediates, the variety of structure-specific endonucleases involved is not surprising.

The recombinase nucleoprotein filament: Structure, variation and dynamics

Homologous recombination is important in many different DNA repair events because joint molecule formation and strand exchange can be used

to rescue a wide variety of aberrant DNA structures. These recombinases proteins, RecA and RAD51, accomplish this stunning feat as helical protein filaments bound to the DNAs being acted on. While polymerized around single-stranded DNA in a right-handed filament, they recognize homologous duplex DNA and switch base-paired partners such that the incoming single-strand is now base paired with its complement in the double-stranded DNA partner molecule (Fig. 3) (*26*). We view this process as driven by the assembly of recombinase filaments on single-stranded DNA, rearrangement of recombinase filaments and DNA partners in a complex involving both the single-stranded DNA and partner homologous double-stranded DNA and finally disassembly of recombinase filaments from the product double-stranded DNA. Here, we review these events from work describing four stages of recombinase action that can be distinguished during homologous recombination; filament nucleation, filament growth, homologous DNA pairing and strand exchange, and filament dissociation. Strand exchange is catalyzed by this sequence of recombinase-DNA and recombinase protein-protein interactions coupled to ATP binding and hydrolysis. The intervention of different mediator proteins is needed to coordinate strand exchange with the other steps of homologous recombination repair and to tailor the process to the needs of specific aberrant DNA structures.

The recombinase nucleoprotein filament, the catalytic core of homologous recombination, has been extensively studied and its description reflects the tools available for analysis. Initially, electron microscopic (EM) images showed that RecA and Rad51 form extensive right-handed helical filaments around DNA that are highly symmetrical and regular (*27*). However, it is difficult to envision how a regular and static nucleoprotein filament can go through the transitions required for recombination, which involve interaction with single-stranded DNA at initiation, three DNA strands during strand exchange and double-stranded DNA near completion of recombination. Not surprisingly, subsequent analyses of three-dimensional reconstructions from EM images and comparison with higher resolution

crystal structures revealed structural variation among nucleoprotein filaments (*28-30*). Most notably filament pitch varied considerably and could be correlated to status of bound nucleotide cofactor. Scanning force microscopy (SFM) images revealed irregular structure and provided the prelude to more recent insight into the dynamic nature of the nucleoprotein filaments (*31*). The ability to quantitatively determine dynamic interactions of recombinase proteins with DNA arrived with the development of tools to manipulate, observe and detect changes in single DNA molecules in real-time (*12*). The kinetic details obtained from following recombinase nucleoprotein filament dynamics at different stages reveal steps likely to be influenced by mediator proteins that modify and optimize strand exchange for different circumstances.

Recombinase filament nucleation

Nucleation, the initial association of recombinase protomers with DNA, lays the foundation for nucleoprotein filament formation and therefore represents an important control step. Nucleation determines, at least in part, the location on DNA where recombination can occur. New quantitative insight into nucleation came from experiments following single DNA molecules, either measuring the real-time changes in DNA length as recombinase proteins bind using magnetic tweezers (*32*), by observing binding with fluorescent versions of the recombinase (*33, 34*) or by real-time changes in FRET signal that occur when recombinase binding to DNA spatially separates donor and acceptor fluorophores (*35, 36*).
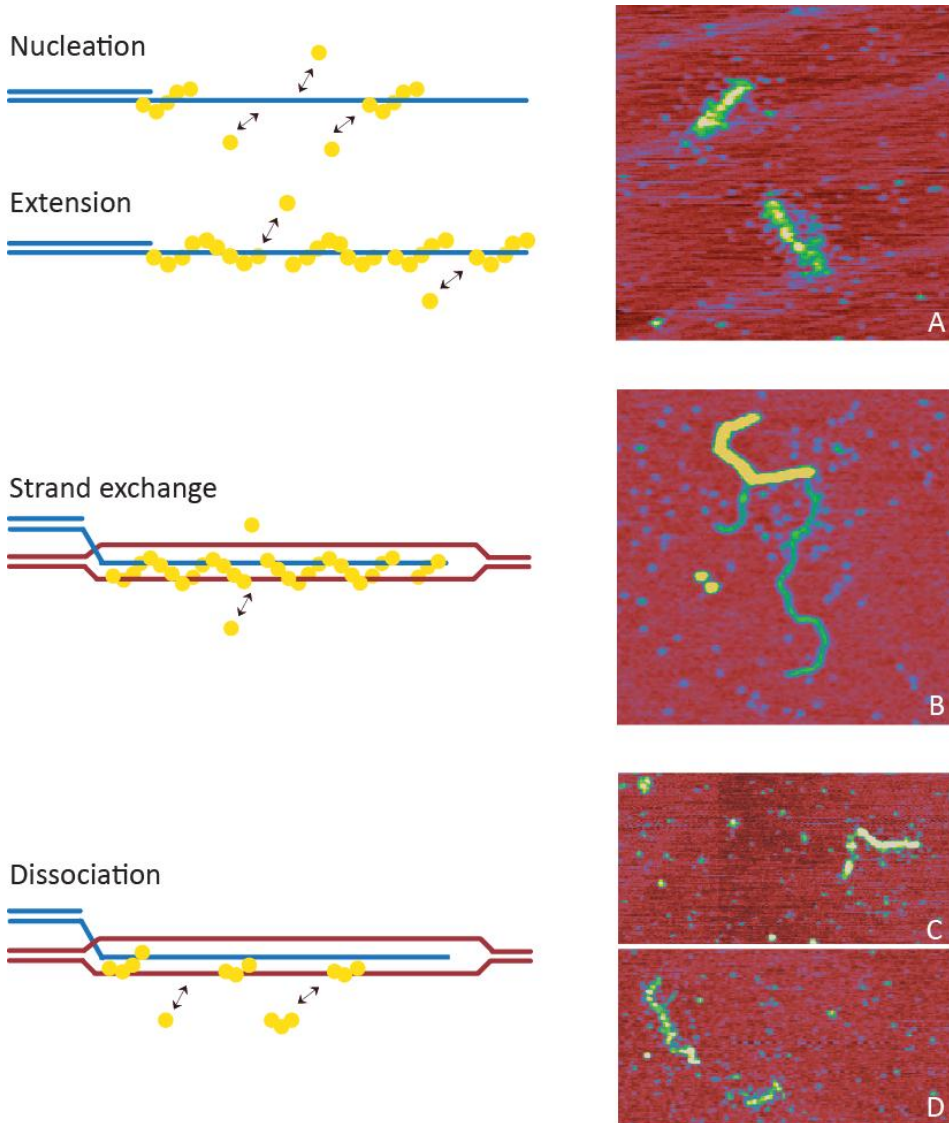
Fig. 2. Recombinase nucleoprotein filament dynamics during homologous recombination. In the panels on the left, the interaction of recombinase protomers with different DNA substrates is indicated during recombinase filament nucleation, extension, strand exchange and dissociation. The reversible interaction (indicated by the double headed arrows) of recombinase protomers (shown in yellow) with DNA (red and blue lines) allows mediator proteins to influence all stages shown as discussed in detail in the text. The events shown are nucleation of clusters of recombinase protomers on single-stranded DNA, recombinase filament growth, joint molecule

formation with homologous duplex DNA into a structure in which base pairs are switched between complementary strands, and dissociation of recombinase protomers from double-stranded DNA upon ATP hydrolysis such that downstream steps in homologous recombination can proceed. Panels A–D on the right display SFM images of human RAD51–DNA complexes at the stage indicated by the left-hand panels. (A) Snap shot of a reaction mixture (ATP/Mg^{2+} conditions) containing assembling RAD51 filaments on 810-nucleotide single-stranded DNA molecules. The image is ~1 μm ×1 μm. The color from red to yellow represents height from 0 to 3 nm. (B) Image of a joint molecule with pairing of a 3' single-strand tailed DNA molecule (240 nucleotides and 500 base pairs) and the homologous region of a 3-kb linear double-stranded DNA molecule formed under conditions of suppressed ATP hydrolysis (ATP/Ca^{2+}). The image is ~ 1μm × 1μm. The color from red to yellow represents height from 0 to 5 nm. (C and D) An early (C) and later (D) snap shot of a reaction mixture (ATP/Mg^{2+} conditions) containing RAD51 filaments disassembling from 1.8-kb double-stranded DNA molecules. The images are ~ 0.5 μm × 1 μm. The color from red to yellow represents height from 0 to 3 nm.

   RecA and RAD51 generally exhibit multiple nucleation events along a DNA molecule in a stochastic manner, although RecA shows a slight bias towards AT-rich regions (*33*). However, the proteins differ strongly in nucleation rate. RAD51 nucleates on DNA up to 1000-fold faster than RecA, which implies that RAD51 filament growth is dominated by nucleation at the expense of filament extension. As absolute rates of nucleation depend on reaction conditions this comparisons is for roughly equivalent conditions or those that promote efficient strand exchange activity *in vitro*. Nucleation requires binding of 4 to 5 recombinase proteins (*32*). Although nucleation does not require ATP hydrolysis, it is influenced by ATP binding, which is not surprising since nucleation rather than dissociation requires a stable interaction with DNA. The ATP cofactor binds at the monomer-monomer interface of recombinases in nucleoprotein filaments and stabilizes protein-protein interactions. Therefore, most studies were done in conditions suppressing ATP hydrolysis (Ca^{2+}-ATP) (*37*) or with the non-hydrolysable ATP analogs, ATP-γ-S and AMP-PNP. This also allows studying filament formation separate from the influence of dissociation. The joint molecule formation and strand exchange steps of homologous recombination require ATP

binding but not hydrolysis. In fact suppressing ATP hydrolysis increases the efficiency of these reactions putatively by stabilizing the protein-DNA complexes formed as products.

Since recombinase nucleation is a critical step in homologous recombination this step is likely subject to regulation. It is not surprising that nucleation is sensitive to environmental conditions. Observations of fluorescent protein showed that nucleation rates for RecA as well as RAD51 on double-stranded DNA are dependent on monovalent salt concentration, as expected for protein-DNA interactions largely involving ionic interactions with the DNA backbone. At higher salt concentrations nucleation onto double-stranded DNA is reduced (*33, 34*). This comprises a biologically relevant putative control step since mediator proteins could locally mimic high salt conditions by inhibiting binding to double-stranded DNA and thereby bias filament formation towards single-stranded DNA. While RecA already preferentially binds single-stranded DNA over double-stranded DNA, RAD51 does not show such a bias. This may indicate that RAD51-mediated recombination utilizes mediators to control loading onto the proper DNA substrate.

Control of recombinase loading must also account for activity needed at specific DNA structures, such as double-strand/single-strand transitions. In the case of human RAD51, the breast cancer-susceptibility gene 2 protein (BRCA2) is expected to direct RAD51 filament nucleation to the single-stranded DNA at the double- to single-stranded junction resulting from resection of a DSB. Structural work on BRCA2 predicts RPA-like OB-folds and a tower-domain imparting single- and double-stranded DNA binding properties, respectively, and potentially junction-binding specificity (*38*). Furthermore, BRCA2 contains domains that specifically bind monomeric (BRC domains) or multimeric (TR2, exon 27 C-terminal domain) forms of RAD51 (*39-41*). Experiments with peptide fragments of human BRCA2 show inhibition of RAD51 filament formation on double-stranded DNA and

enhanced strand exchange activity (*42*). The most compelling evidence though is derived from work on *Ustilago maydis* Brh2, which specifically directs *U. maydis* Rad51 filament nucleation to double-stranded/single-stranded DNA junctions promoting filament formation on single-stranded DNA (*43*). Several studies have shown that the BRC repeats interact with RAD51 at the same place as the monomer-monomer interface (*44*), thus preventing filament formation on double-stranded DNA (*40, 42, 45*). However, for single-stranded DNA binding by RAD51 such antagonizing effect by BRC4 was not observed. Hence it was postulated that the BRC repeats within BRCA2 direct RAD51 filament formation towards single-stranded DNA (*42*).

For RecA the protein complex that generates the DNA substrate, a single-stranded 3'-overhang, also facilitates recombinase loading. At DNA ends this is accomplished by the RecBCD helicase/nuclease. The current model involves RecBCD unwinding DNA from an end until it encounters a specific sequence, called a χ-site, which modifies the nuclease activity resulting in production of a single-stranded DNA with a 3' end. Interaction between the RecB subunit and RecA facilitate loading of RecA onto the newly generated single-stranded DNA to from the nucleoprotein filament (*46, 47*).

Depending on the particular substrate onto which a recombinase is to be loaded, different nucleation effectors can be required. While RecBCD requires a DSB, the RecFOR pathway promotes homologous recombination repair of single-strand gaps, present at stalled or collapsed replication forks. RecFOR acts by modulating RecA binding to single-strand binding protein (SSB)-coated DNA. Specifically, RecF is implicated in directing RecA loading to the edges of the gaps (*10*). Indeed, loading of recombinases on single-stranded DNA *in vivo* is potentially problematic, since single-stranded DNA is bound by high affinity single-strand DNA binding proteins that can interfere with filament formation. The RecBCD pathway avoids this problem by loading RecA directly onto the single-stranded DNA as it is generated. In the

RecFOR pathway RecF facilitates RecA loading but the mechanism is not yet clear. Human RAD51 has to compete with RPA, the human equivalent of *E. coli* SSB, for the single-stranded DNA. As described above displacement of RPA could be mediated by junction specific seeding of a RAD51 filament (*43*). For yeast, Rad52 can promote exchange of RPA for Rad51. Substoichiometric amounts of Rad52 suffice to alleviate the inhibitory effect of RPA on homologous pairing and strand exchange reactions. This mediator activity is dependent on interactions between Rad51 and Rad52 (*48*). For the human proteins, although not yet demonstrated experimentally, BRCA2 has also been suggested to serve this function.

Nucleoprotein filament extension

Formation of a functional nucleoprotein filament requires more extensive coverage of single-stranded DNA than a single nucleation event can achieve. Filament extension formally involves binding of additional recombinase proteins adjacent to nucleated patches on DNA. The biophysical properties observed during filament extension, as additional protomers extensively cover DNA, differ for RecA and RAD51 due to their very different nucleation rates. The absolute rates are influenced by conditions but can be compared between the proteins at roughly equivalent conditions or those that promote efficient strand exchange reactions *in vitro*. While RecA nucleation is relatively infrequent and thus rate limiting, filament growth by extension is a rapid process. This high cooperativity for RecA extension results in long, continuous filaments. For RAD51 nucleation dominates such that extension is limited by the adjacent nucleation. Since nucleation is random along the DNA and every RAD51 monomer covers three nucleotides or base pairs, RAD51 filaments are not continuous, but contain gaps of bare DNA too small for an additional RAD51 protomer to bind (*32-34, 49, 50*). Under conditions of active ATP hydrolysis the average patch size is estimated to be about 30 or 35 monomers for double-stranded and single-stranded DNA, respectively.

Thus, due to differences in intrinsic rates of nucleation and extension RAD51 nucleoprotein filaments assembled *in vitro* differ from their RecA equivalents in flexibility since the bare DNA gaps in RAD51 nucleoprotein filaments can act as flexible hinges (*31*). Increased flexibility of nucleoprotein filaments might be advantageous during subsequent steps of recombination as we discuss in the section 'Homologous pairing and strand exchange'.

Currently single molecule experiments are revealing additional details of filament extension. Observations of fluorescent RecA suggest that filaments on double-strand DNA are extended by units of two to seven monomers (*33*), which encompasses the four to five monomers suggested for RAD51 based on magnetic-tweezers experiments (*32*). Another single molecule approach, using RecA, measured differences in FRET intensity, which reports on the distance of DNA-bound acceptor and donor fluorophores that change upon RecA binding. In these experiments RecA filaments extended from double-stranded DNA over a double-stranded/single-stranded DNA junction onto single-stranded DNA. Modeling of the data suggests that RecA filaments extend one monomer at the time (*35*). However, following RecA filament behavior in magnetic tweezers indicated that DNA-bound RecA monomers rearrange, a possibility that was not included in the modeling of RecA filament elongation from the FRET data (*51*). Elongation of a RecA filament over the DNA junction however did provide a mechanism to displace SSB from single-stranded DNA. The FRET studies revealed that SSB can migrate along single-stranded DNA and be displaced by an elongating filament. Diffusing SSB could melt out secondary structures in the single-stranded DNA and transiently facilitate filament extension (*35*). It is likely that a RecA filament seeded by RecBCD could displace SSB in the same fashion. In the RecFOR pathway SSB is likely displaced by RecA due to RecO and RecR interactions rather than diffusional migration of SSB.

The RecA FRET studies showed that addition of RecA can occur at both ends of a filament. However, binding of RecA took place with different rates at the respective ends. A ten-fold difference in apparent dissociation constant favored extension at the 3' end of the RecA filament (*36*). In conditions allowing ATP hydrolysis filament growth is affected by concurrent dissociation. The FRET studies revealed that the dissociation rates for both termini were similar. So the net growth of a RecA filament is modulated by a difference in binding affinities. In this way ATP hydrolysis can contribute to rearrangements within the filaments. While previous studies argued that sliding of recombinase proteins does not occur, dissociation of proteins at a 5' end which may remain bound to single-stranded DNA and re-establishes protein-protein contacts to an adjacent 3' end provides a plausible mechanism (*49, 52*). Given that a RecA monomer is reported to bind from three to seven nucleotides of single-stranded DNA depending on bound nucleotide, a change in the number of nucleotides bound in the ATP hydrolysis cycle could result in protein changing position along DNA (*53*). This also infers that extension can occur by monomers since that is currently believed to be the unit for dissociation. Such rearrangements will lead to reduction of gaps within a nucleoprotein filament and potentially one continuous filament, *i.e.* more recombinase on a given DNA molecule. Thus the maximum extension of the DNA length by recombinase would increase in conditions of active ATP hydrolysis. Indeed this was observed in magnetic tweezers experiments after switching assembly conditions from suppressed to active ATP hydrolysis (*51*). If the adjacent 3' filament end was not available, for instance due to capping by the RecA mediator RecX, this would result in a net disassembly as observed in experiments with RecA and substoichiometric concentrations of RecX.

For RAD51 such rearrangements, or rather the extent thereof, are unlikely to happen. The relatively high nucleation rate of RAD51 leads to filaments with more gaps and more ends to disassemble thus less stable filaments. Growth profiles of RAD51 filaments with suppressed ATP

hydrolysis are similar on single-stranded DNA and double-stranded DNA. In the presence of ATP hydrolysis there is a difference. RAD51 assembly onto single-stranded DNA is greatly affected by dissociation such that the growth profiles differ (*32*). This implies that the RAD51 filament on single-stranded DNA is a very dynamic structure and indeed it can hardly be visualized (without fixation) as a defined structure by SFM or EM (*31*). The dynamic nature of recombinase filaments in ATP hydrolysis permitting environments is likely to play an important role in later steps of strand exchange reactions.

Homologous pairing and strand exchange

The ability to address mechanistic questions is strongly influenced by technical advances and sensitivity of measurements. As discussed above, single molecule experimental setups allowed new mechanistic questions to be addressed. Magnetic tweezers were also applied to answer questions about homologous pairing and stand exchange. Interestingly, while a signature strand exchange by RecA was observed in real time, no signals were detected of homologous paring, a necessary preceding step. Based on the detection limits of the instrument this suggests that initial homologous paring interactions involve less than 16 base pairs lasting less than one second. Strand exchange was detected as a real-time change in length of a tethered double-stranded target DNA upon interaction of a single-strand RecA nucleoprotein complex. The experiments revealed that, under the employed experimental conditions, the active synaptic region involved in strand exchange was independent of the length of DNA exchanged and remained a constant 80 base pairs (*54*).

As pointed out above differences in intrinsic nucleation rates between RecA and RAD51 result in nucleoprotein filaments with distinct biophysical characteristics; continuous and relatively stiff for RecA versus interrupted and flexible for RAD51. During homology search flexible filaments can allow

multiple sites of interaction between filament segments and the homologous target DNA, while stiffer continuous filaments would be limited in that respect. Additionally, the bare single-stranded DNA in filaments can act as a swivel to relieve potential topological constrains arising during recombination between helical filaments and target DNA. Mediator proteins in the cell might increase the flexibility of RecA filaments *in vivo*. For example, RecX bound in the major groove of a filament as a cap thereby blocking further addition of RecA (*10, 55, 56*). This could introduce gaps in RecA filaments and thereby increase flexibility in the nucleoprotein filament. Mediators such as RecX might not be required for homologous recombination in general but instead could assist RecA-mediated recombination in specific subpathways, such as during recombination-assisted stalled replication fork restart.

In general, differences in DNA/chromatin organization in bacterial and eukaryotic cells may require recombinase nucleoprotein filaments with different biophysical properties. The target DNA substrate in bacteria might retain a certain degree of flexibility itself such that efficient homology search and subsequent strand exchange can occur with stiffer recombinase nucleoprotein filaments. In eukaryotes the situation is different since target DNA is arranged in chromatin. Recent studies suggest that DSBs in heterochromatin can be repaired by homologous recombination (*57, 58*). In that context the DNA is wrapped around histones in a highly ordered structure. Hence an increased flexibility of the RAD51 nucleoprotein filament would be required to efficiently probe DNA wrapped around histones.

The size of recombinase filament patches might influence their ability to bypass heterology. The shorter they are the less probable that they can stabilize longer stretches of mis-paired bases. In agreement with this hypothesis the longer stiffer RecA filaments are able to bypass larger heterologous stretches (*59-61*), while Rad51 is very inefficient in bypassing

heterologous regions of more than several nucleotides (*60*). In diploid eukaryotes it might be important to have a less promiscuous DNA strand exchange machinery to reduced loss of heterozygosity. Crystal structures reveal that RecA-single-stranded DNA complexes have three nucleotides bound per monomer arranged in approximate B-form DNA structure, with DNA stretching occurring between the triplets (*14*). Therefore, it is likely that the nucleoprotein filament probes target duplex DNA in units of three nucleotides. RAD51 filaments apparently allow for one such unit to mis-match. Further mis-matches would be expected to destabilize the interactions and stall plectonemic joint formation to favor continued homology search. The size of filament patches may not only be important for the flexibility of the nucleoprotein filament but also for its accuracy in homologous pairing.

During strand exchange and subsequent repair reactions DNA structures arise that can be stabilized by structure-specific binding of proteins, *e.g.* RAD51AP1 (*62, 63*). Each of these DNA structure-protein interactions can serve as control points in recombination through stabilization or destabilization of an intermediate. This could promote recombination or limit the extent of recombination as needed. For instance, some proteins specifically favor the formation and stability of Holliday junctions. Additionally, yeast Srs2 helicase promotes SDSA likely by remodeling DNA intermediates of strand exchange in favor of this process. By similar remodeling of strand exchange intermediates, human RAD54 is implicated in both directing repair toward formation of double Holliday junctions or toward SDSA (*64*).

Recombinase dissociation from DNA

Dissociation of recombinase from nucleoprotein filaments is an intrinsic property dependent on ATP hydrolysis (*49*). *In vitro* ATP binding, but not

hydrolysis, is required for the formation of nucleoprotein filaments, formation of joint molecules, and strand exchange (*37, 65, 66*). Nonetheless dissociation occurs even during filament assembly, especially on single-stranded DNA. This filament formation as a balance between protein association with and disassociation from DNA can result in inefficient formation of filaments on single-stranded DNA *in vitro* and explain why the above mentioned reactions are more efficient in conditions where the ATPase activity is attenuated. One can argue that mediator proteins act *in vivo* to temporarily suppress recombinase ATPase activity at sites of DNA repair or stabilize filaments in a different way. A bacterial candidate for such an activity is DinI, which stabilizes RecA filaments while not directly affecting ATPase activity (*67*). This activity of DinI might counteract RecA dissociation from filaments formed on correct DNA substrates in need or recombinational repair, *i.e.* at a DSB. Recruitment of proteins such as DinI to sites of DNA damage but not to sites on DNA where homologous recombination would be deleterious would constitute a control point taking advantage of nucleoprotein dynamics, which favor disassembly without the need for other proteins.

Direct observation and quantification of fluorescent variants of RAD51 show intrinsic dissociation behavior that can be interpreted in terms of ATP hydrolysis (*49, 68*). RAD51 filaments disassemble from an end in a stochastic manner with bursts of varying numbers of monomers separated by pauses of varying time. This is explained by ATP hydrolysis randomly taking place at any position within the nucleoprotein filament but dissociation only occurring when the terminal monomer hydrolyses ATP. Internal RAD51 monomers that have hydrolyzed ATP are kept in place through protein-protein interactions in the filament. Upon hydrolysis of ATP by a terminal RAD51 monomer the interface with the only neighbor is broken. This breaks the structure that stabilized stretched DNA across the monomer interface and the released energy stored in DNA by the filament would drive the dissociation of the RAD51 monomers. Monomers would dissociate from the

end of a patch until the point where ATP is still bound (*68*). While RAD51 is able to dissociate from double-stranded DNA by itself the dissociation rate is dependent on ATP hydrolysis and slower from double-stranded than from single-stranded DNA. Thus, RAD51 dissociation might be too slow for efficient subsequent reactions *in vivo* or persist at the wrong placed posing a threat for unwanted recombination events. Hence, it has been postulated that other proteins act on recombinase filaments to promote their disruption.

Elevated levels or inappropriate recombination can lead to undesired recombination events resulting in genetic instability. Thus the activity of recombinase filaments to form joint molecules and accomplish strand exchange needs to be carefully controlled and properly targeted. For this purpose there are a variety of remodeling enzymes that antagonize the activities of recombinase nucleoprotein filaments. Globally a variety of helicases can disrupt toxic recombinase filaments. Their redundant activities may reflect the importance of this task but in some cases reveal specificity for certain repair pathways. At persisting stalled replication forks in *E. coli* the RecFOR-loaded RecA can activate the SOS response, which will lead to expression of a set of proteins including UvrD (*69*). This helicase is implicated in rescuing replication by fork reversal, a process blocked by the presence of RecA filament or RecA-created DNA structures. UvrD can clearly antagonize homologous recombination *in vivo.* One putative mechanism is the active removal of the RecA filament by ATP-dependent translocation of UvrD along the DNA, thus allowing reversal of replication forks and repair by repair pathways other than recombination (*69, 70*). *In vitro* many helicases or translocating proteins can disassemble recombinase filaments.

The helicase associated with Rad51 disassembly in yeast is Srs2. It has an important function in controlling inappropriate recombination. Where Rad52 promotes displacement of RPA by Rad51 filaments, Srs2 antagonizes this activity. Thus Rad51 filament formation is controlled by the interplay

between Rad52 promoted assembly and Srs2 promoted disassembly (*71-73*). Srs2 acts upon Rad51 filaments in a more specific manner than UvrD disruption of RecA filaments. The Srs2 helicase activity can push protein off of DNA but it also specifically enhances Rad51 disassembly. Extensive studies with truncation mutants of Srs2 reveal that specific interactions between Srs2 and Rad51 stimulate ATP hydrolysis by Rad51 promoting its intrinsic dissociation from DNA (*71*).

While DNA translocating enzymes can have anti-recombination function, such as UvrD and Srs2 discussed above, they can also promote recombination. For example, the Rad54 protein requires double-strand DNA to activate its ATPase activity and thereby trigger its translocation activity. Rad54 can thus remove Rad51 from double-stranded DNA, which is either the product of strand exchange or an inappropriate substrate for filament formation (*64*). Rad54-mediated removal of Rad51 from the double-stranded DNA product of recombination actually stimulates recombinational repair because it allows DNA transactions downstream of strand exchange to occur that might otherwise be blocked by bound Rad51. Promoting Rad51 dissociation by Rad54 requires species-specific interactions between the proteins (*74*). The detailed studies on intrinsic RAD51 dissociation, described above, suggest a mechanism for RAD54 catalyzed recombinase filament disassembly (*34, 64*). RAD51 filament stability crucially depends on the nucleotide state of the terminus protein in a filament. When a terminal RAD51 monomer is in the ATP-bound state it functions as a sort of cap that inhibits disassembly. Within a filament, RAD51 monomers appear to be locked on the DNA by their neighbors, independent of nucleotide state (*68*). Rad54 can interact at filament ends (*75*). The prediction is that protein-protein interactions between RAD54 and the terminal RAD51 would stimulate ATP hydrolysis here and thus RAD51 disassembly from DNA. As a result, RAD54 would accelerate disassembly by substantially decreasing the duration of pauses that occur during unaided RAD51 nucleoprotein filament disassembly.

Conclusion

Regulating DNA strand exchange, the salient step of homologous recombination, is obligatory to both actively prevent genome instability and promote genome stability. Modulation at any of the component steps in DNA strand exchange; nucleation of recombinase proteins on DNA, nucleoprotein filament growth, strand exchange, and recombinase dissociation from DNA, provide rich regulatory possibilities and allows controlling recombination to fit different repair requirements. The key to this regulation, essentially providing quality control for homologous recombination, lies in the dynamic instability of the recombinase nucleoprotein filament. The recombinase nucleoprotein filament is not a straightjacket in which homologous pairing and DNA strand exchange take place with machine-like precision. Instead, it is a meta-stable entity undergoing constant association of recombinase molecules with DNA and ATP hydrolysis mediated dissociation from DNA. This dynamic instability of interacting molecular partners allows constructive and destructive processes to occur in competition. The relative success of concurrent structural build-up and tear down tips the balance controlling inappropriate as well as appropriate reaction steps. Quality control or progression down specific homologous recombination subpathways can then be established by factors that slightly shift the equilibrium to eventually favor appropriate events.

Tight regulation of filament formation itself is an obvious control step early in the reaction. Indeed, the first obstacle to forming a recombinase nucleoprotein filament is the presence of high affinity single-stranded DNA-binding proteins that need to be displaced. Mediator proteins, such as Rad52 in yeast, promote RPA displacement by Rad51, after which single-stranded DNA binding proteins actually promote later steps leading to efficient strand exchange reactions (*48*). Thus, a single protein can antagonize filament formation and yet promote strand exchange. This paradox is also evident in studies of BRCA2, where high concentrations of

BRC peptide inhibit recombinase filament formation, while lower concentrations can stabilize filaments (*40, 45*). Even after a nucleoprotein filament has formed on single-stranded DNA, completing homologous recombination is not inevitable because mediators actively dissociated recombinase filaments on single-stranded DNA, such as Srs2 in yeast. Recombination is subject to a balance between positive and negative mediators, in this case Rad52 and Srs2. This theme is present throughout the steps of homologous recombination; intermediate structures arise and can disassemble, either by the effect of mediator proteins or intrinsically. Progression to subsequent steps of recombination requires appropriate stabilization of these intermediates. For instance, the intermediate DNA (branched) structures of strand exchange are also intrinsically metastable and can be stabilized or destabilized by structure-specific DNA proteins, such as RAD51AP1 (*62*).

The influence of recombination mediators on nucleoprotein filaments assembly, stability, and interactions with partner DNA as well as recombination mediator effects of DNA structures emerging during progression of recombination, ensures that genome maintenance by homologous recombination is not only a flexible process, engaged in repair of multiple structurally diverse lesions, but also an accurate process.

Acknowledgments

References

1. R. Hakem, *The EMBO journal* **27**, 589 (Feb 20, 2008).
2. J. H. Hoeijmakers, *Nature* **411**, 366 (May 17, 2001).
3. M. E. Moynahan, M. Jasin, *Nat Rev Mol Cell Biol* **11**, 196 (Mar, 2010).
4. J. San Filippo, P. Sung, H. Klein, *Annu Rev Biochem* **77**, 229 (2008).
5. C. Wyman, R. Kanaar, *Annu Rev Genet* **40**, 363 (2006).
6. J. Atkinson, P. McGlynn, *Nucleic acids research* **37**, 3475 (Jun, 2009).
7. S. Lambert, B. Froget, A. M. Carr, *DNA repair* **6**, 1042 (Jul 1, 2007).
8. D. Branzei, M. Foiani, *DNA repair* **6**, 994 (Jul 1, 2007).
9. R. C. Heller, K. J. Marians, *Nat Rev Mol Cell Biol* **7**, 932 (Dec, 2006).
10. M. M. Cox, *Critical reviews in biochemistry and molecular biology* **42**, 41 (Jan-Feb, 2007).
11. C. Wyman, R. Kanaar, *Curr Biol* **14**, R629 (Aug 10, 2004).
12. J. Hilario, S. C. Kowalczykowski, *Current opinion in chemical biology* **14**, 15 (Feb, 2010).
13. J. W. Szostak, T. L. Orr-Weaver, R. J. Rothstein, F. W. Stahl, *Cell* **33**, 25 (May, 1983).
14. M. A. Resnick, *J Theor Biol* **59**, 97 (Jun, 1976).
15. E. Kinoshita, E. van der Linden, H. Sanchez, C. Wyman, *Chromosome Res* **17**, 277 (2009).
16. K. M. Feeney, C. W. Wasson, J. L. Parish, *Biochem J* **428**, 147 (2010).
17. J. T. Yeeles, M. S. Dillingham, *DNA repair* **9**, 276 (Mar 2, 2010).
18. E. P. Mimitou, L. S. Symington, *DNA repair* **8**, 983 (Sep 2, 2009).
19. E. P. Mimitou, L. S. Symington, *Trends Biochem Sci* **34**, 264 (May, 2009).
20. S. C. West, *Nat Rev Mol Cell Biol* **4**, 435 (Jun, 2003).
21. P. Sung, H. Klein, *Nat Rev Mol Cell Biol* **7**, 739 (Oct, 2006).
22. F. Paques, J. E. Haber, *Microbiol Mol Biol Rev* **63**, 349 (Jun, 1999).
23. J. M. Svendsen, J. W. Harper, *Genes & development* **24**, 521 (Mar 15, 2010).
24. L. Wu, I. D. Hickson, *Annu Rev Genet* **40**, 279 (2006).
25. W. D. Heyer, *Curr Biol* **14**, R56 (Jan 20, 2004).
26. C. Wyman, *Structure* **14**, 949 (Jun, 2006).
27. X. Yu, M. S. VanLoock, S. Yang, J. T. Reese, E. H. Egelman, *Curr Protein Pept Sci* **5**, 73 (Apr, 2004).
28. V. E. Galkin *et al.*, *Structure* **14**, 983 (Jun, 2006).
29. M. S. VanLoock *et al.*, *Structure* **11**, 187 (Feb, 2003).
30. X. Yu, S. A. Jacobs, S. C. West, T. Ogawa, E. H. Egelman, *Proc Natl Acad Sci U S A* **98**, 8419 (Jul 17, 2001).
31. D. Ristic *et al.*, *Nucleic acids research* **33**, 3292 (2005).
32. T. van der Heijden *et al.*, *Nucleic acids research* **35**, 5646 (2007).
33. R. Galletto, I. Amitani, R. J. Baskin, S. C. Kowalczykowski, *Nature* **443**, 875 (Oct 19, 2006).
34. J. Hilario, I. Amitani, R. J. Baskin, S. C. Kowalczykowski, *Proceedings of the National Academy of Sciences of the United States of America* **106**, 361 (Jan 13, 2009).
35. C. Joo *et al.*, *Cell* **126**, 515 (Aug 11, 2006).
36. R. Roy, A. G. Kozlov, T. M. Lohman, T. Ha, *Nature* **461**, 1092 (Oct 22, 2009).
37. D. V. Bugreev, A. V. Mazin, *Proceedings of the National Academy of Sciences of the United States of America* **101**, 9988 (Jul 6, 2004).
38. H. Yang *et al.*, *Science* **297**, 1837 (Sep 13, 2002).
39. T. Thorslund, F. Esashi, S. C. West, *The EMBO journal* **26**, 2915 (Jun 20, 2007).
40. V. E. Galkin *et al.*, *Proceedings of the National Academy of Sciences of the United States of America* **102**, 8537 (Jun 14, 2005).
41. O. R. Davies, L. Pellegrini, *Nat Struct Mol Biol* **14**, 475 (Jun, 2007).
42. A. Carreira *et al.*, *Cell* **136**, 1032 (Mar 20, 2009).
43. H. Yang, Q. Li, J. Fan, W. K. Holloman, N. P. Pavletich, *Nature* **433**, 653 (Feb 10, 2005).
44. L. Pellegrini *et al.*, *Nature* **420**, 287 (Nov 21, 2002).
45. F. Esashi, V. E. Galkin, X. Yu, E. H. Egelman, S. C. West, *Nat Struct Mol Biol* **14**, 468 (Jun, 2007).
46. S. K. Amundsen, G. R. Smith, *Genetics* **175**, 41 (Jan, 2007).

47.   M. S. Dillingham, S. C. Kowalczykowski, *Microbiol Mol Biol Rev* **72**, 642 (Dec, 2008).
48.   T. Sugiyama, S. C. Kowalczykowski, *The Journal of biological chemistry* **277**, 31663 (Aug 30, 2002).
49.   M. Modesti *et al.*, *Structure* **15**, 599 (May, 2007).
50.   J. K. De Zutter, K. L. Knight, *Journal of molecular biology* **293**, 769 (Nov 5, 1999).
51.   M. T. van Loenhout, T. van der Heijden, R. Kanaar, C. Wyman, C. Dekker, *Nucleic acids research*, (May 8, 2009).
52.   T. K. Prasad, C. C. Yeykal, E. C. Greene, *Journal of molecular biology* **363**, 713 (Oct 27, 2006).
53.   S. C. Kowalczykowski, *Annu Rev Biophys Biophys Chem* **20**, 539 (1991).
54.   T. van der Heijden *et al.*, *Molecular cell* **30**, 530 (May 23, 2008).
55.   S. Ragone, J. D. Maman, N. Furnham, L. Pellegrini, *The EMBO journal* **27**, 2259 (Aug 20, 2008).
56.   J. C. Drees, S. L. Lusetti, S. Chitteni-Pattu, R. B. Inman, M. M. Cox, *Molecular cell* **15**, 789 (Sep 10, 2004).
57.   A. A. Goodarzi *et al.*, *Molecular cell* **31**, 167 (Jul 25, 2008).
58.   A. T. Noon *et al.*, *Nat Cell Biol* **12**, 177 (Feb, 2010).
59.   D. E. Adams, S. C. West, *Journal of molecular biology* **263**, 582 (Nov 8, 1996).
60.   V. F. Holmes, K. R. Benjamin, N. J. Crisona, N. R. Cozzarelli, *Nucleic acids research* **29**, 5052 (Dec 15, 2001).
61.   K. J. MacFarland, Q. Shan, R. B. Inman, M. M. Cox, *The Journal of biological chemistry* **272**, 17675 (Jul 11, 1997).
62.   M. Modesti *et al.*, *Molecular cell* **28**, 468 (Nov 9, 2007).
63.   C. Wiese *et al.*, *Molecular cell* **28**, 482 (Nov 9, 2007).
64.   A. V. Mazin, O. M. Mazina, D. V. Bugreev, M. J. Rossi, *DNA repair* **9**, 286 (Mar 2, 2010).
65.   P. Chi, S. Van Komen, M. G. Sehorn, S. Sigurdsson, P. Sung, *DNA repair* **5**, 381 (Mar 7, 2006).
66.   S. Sigurdsson, K. Trujillo, B. Song, S. Stratton, P. Sung, *The Journal of biological chemistry* **276**, 8798 (Mar 23, 2001).
67.   S. L. Lusetti, O. N. Voloshin, R. B. Inman, R. D. Camerini-Otero, M. M. Cox, *The Journal of biological chemistry* **279**, 30037 (Jul 16, 2004).
68.   J. van Mameren *et al.*, *Nature* **457**, 745 (Feb 5, 2009).
69.   R. Lestini, B. Michel, *THE EMBO journal* **26**, 3804 (Aug 22, 2007).
70.   X. Veaute *et al.*, *The EMBO journal* **24**, 180 (Jan 12, 2005).
71.   E. Antony *et al.*, *Molecular cell* **35**, 105 (Jul 10, 2009).
72.   S. Colavito *et al.*, *Nucleic acids research* **37**, 6754 (Nov, 2009).
73.   C. Seong, S. Colavito, Y. Kwon, P. Sung, L. Krejci, *The Journal of biological chemistry* **284**, 24363 (Sep 4, 2009).
74.   X. Li, W. D. Heyer, *Nucleic acids research* **37**, 638 (Feb, 2009).
75.   K. Kiianitsa, J. A. Solinger, W. D. Heyer, *Proceedings of the National Academy of Sciences of the United States of America* **103**, 9767 (Jun 27, 2006).

Chapter 3:

Effect of the BRCA2 CTRD domain on RAD51 filaments analyzed by an ensemble of single molecule techniques

J.T. Holthausen[1], M.T.J. van Loenhout[4], H. Sanchez[1], D. Ristic[1], S. van Rossum-Fikkert[1], M. Modesti[1,3], C. Dekker[4], R. Kanaar[1,2], and C. Wyman[1,2]

[1]Department of Genetics and Department of [4]Radiation Oncology, Cancer Genomics Center, Erasmus Medical Center, P.O. Box 2040, 3000 CA Rotterdam, The Netherlands
[3]Centre National de la Recherche Scientifique, Unité Propre de Recherche 3081, Laboratory of Genome Instability and Carcinogenesis conventionné par l'Université d'Aix-Marseille 2, 13402 Marseille Cedex 20, France
[4]Kavli Institute of Nanoscience, Delft University of Technology, Lorentzweg 1, 2628 CJ Delft, The Netherlands

Abstract

Homologous recombination is essential for the preservation of genome stability, thereby preventing cancer. The recombination protein RAD51 drives DNA strand exchange, which requires the assembly, rearrangement and disassembly of a RAD51 filament on DNA, coupled to ATP binding and hydrolysis. This process is facilitated and controlled by recombination mediators and accessory factors. Here, we have employed a range of single molecule techniques to determine the influence of the C-terminal RAD51 interaction domain (CTRD) of the breast cancer tumor suppressor BRCA2 on intrinsic aspects of RAD51-DNA interactions. We show that at high concentration the CTRD entangles RAD51 filaments and reduces RAD51 filament formation in a concentration dependent manner. It does not affect the rate of filament disassembly measured as the loss of fluorescent signal due to intrinsic RAD51 protein dissociation from dsDNA. We conclude that, outside the context of the full-length protein, the CTRD does not reduce RAD51 dissociation kinetics, but instead hinders filament formation on double-stranded DNA. The CTRDs mode of action is most likely sequestration of multiple RAD51 molecules thereby rendering them inactive for filament formation on double-stranded DNA.

Introduction

Double-stranded DNA breaks (DSBs) are severe lesions that can result in chromosomal rearrangements leading to cellular senescence or the onset and progression of cancers (*1, 2*). In S and G2 phases of the cell cycle, homologous recombination (HR) provides a pathway for the faithful repair of such lesions (*3*). HR can be divided in three steps: pre-synapsis, synapsis and post-synapsis (*4*). Pre-synapsis consist of the recognition of a DSB, and the resection of one strand leaving tailed DNA that is bound by RAD51 to form a nucleoprotein filament (*5, 6*). During synapsis this nucleoprotein filament interacts with the intact sister chromatid (homology search), and strand invasion occurs at the site of homology resulting in joint molecule formation and strand exchange. Post-synapsis is defined as the events leading to the recovery of lost information by polymerase-mediated DNA resynthesis and the resolution of branched DNA structures resulting in two intact chromatids (*7, 8*).

Biochemical assays have defined RAD51 recombinase as the catalyst of synapsis. It forms a helical filament on single-stranded DNA (ssDNA) that can drive the DNA transactions required for HR *in vitro*. The RAD51 nucleoprotein filament will invade a homologous double-stranded DNA (dsDNA) and form a joint molecule. To catalyze strand exchange the RAD51 nucleoprotein filament undergoes dynamic rearrangements that result in DNA strands exchanging base-paired partners leading to the formation of a filament on heteroduplex DNA – one strand being the invading ssDNA while the other is the complementary strand of the template DNA. The next step in repairing a DNA break requires the invading strand to prime DNA extension by a polymerase. This stage requires RAD51 removal from the heteroduplex DNA (*9-11*), and these dissociation reactions have been addressed in previous single molecule studies (*12-15*).

The actions of RAD51 are facilitated by recombination mediators and controlled by accessory factors (16-17). One such mediator is the BRCA2 protein which is essential for efficient HR in mammalian cells (*16-18*). The role that BRCA2 plays in maintaining genome stability has been attributed to its ability to interact directly with RAD51 (*19, 20*). Biochemical studies with BRCA2 peptides have defined interactions with RAD51 via a series of eight BRC repeats and a C-terminal domain, designated CTRD (C-terminal RAD51 interaction domain; previously referred to as TR2 (*21, 22*)). This domain contains a cyclin-dependent kinase phosphorylation site that modulates RAD51 binding (*21, 23*). The BRC domains, best characterized by BRC4, which has the highest affinity for RAD51, interact with RAD51 at the polymerization domain and can thereby disrupt RAD51 filaments at concentrations equal to or higher than the RAD51 concentration (*22-25*). The CTRD of BRCA2 interacts with multimeric RAD51 and can inhibit the destabilization of RAD51 filaments caused by the BRC repeats (*22, 24, 25*). In avian cells the CTRD of BRCA2 influences the persistence of RAD51 in local nuclear accumulations in a manner consistent with stabilizing RAD51 filaments (*26*). To determine whether the CTRD of BRCA2 might provide an effect opposite to the BRC repeats, by helping to stabilize RAD51 filaments on dsDNA, we used an array of single-molecule techniques together with ensemble studies. First we visualized the effect of the CTRD on RAD51 dissociation from dsDNA. We observed individual filaments formed with fluorescent RAD51 and quantified their disassembly in time by fluorescent microscopy in a microfluidic flow system (*12*). We then analyzed the effect of the CTRD on RAD51 nucleoprotein filament structure by optical fluorescence microscopy, by scanning force microscopy imaging (*27*), and a combination of both techniques (*28*). We then analyzed the effect of the CTRD on RAD51 filament assembly on dsDNA, following the extension of individual dsDNA molecules by RAD51 binding, in magnetic tweezers (*13, 29*).

Results

The initial aim was to measure the dissociation kinetics of RAD51 in the absence and presence of the CTRD of BRCA2 to determine whether the CTRD played a role in filament stabilization.

Filament dissociation

RAD51 filaments were formed by incubating Alexa Fluor 488 labeled protein with 48-kb lambda phage dsDNA molecules in the presence of ATP and $CaCl_2$, conditions that stabilize RAD51 nucleoprotein filaments (*12, 27, 32*). The lambda phage dsDNA molecules were biotinylated at one end in order to tether the nucleoprotein filaments on the neutravidin-coated surface of a flow cell, where they were extended by buffer flow and observed in a fluorescent microscope. ATPase dependent dissociation of RAD51 from dsDNA was measured as a loss of fluorescent signal over time, corrected for background. Control traces in Ca^{2+}/ATP buffer in absence or presence of a synthetic CTRD peptide (Figure 1 hollow circle and triangle, respectively) showed that the RAD51 complex was stable over time and that the CTRD did not affect the photostability of the fluorophore. Switching buffer to one containing ATP and $MgCl_2$ triggered RAD51 dissociation from dsDNA (*12, 14*). Stabilization of RAD51 filaments by the CTRD was expected to slow the kinetics for RAD51 dissociation (*23*). As a reference, RAD51 filaments were assembled in absence of the CTRD and RAD51 filament disassembly was measured over time (Figure 1, solid circles). When the CTRD was added at a ratio of RAD51:CTRD = 15:1 to pre-formed filaments, there was no detectable effect of the CTRD on RAD51 dissociation from dsDNA (Figure 1, solid triangles). The dissociation data overlap which showed that the rate is the same and implies that there is no difference in the way dissociation takes place. A phosphorylated

CTRD peptide (P-CTRD), which does not interact with RAD51, also did not affect the rate of RAD51 dissociation significantly (Figure 1, crosses).
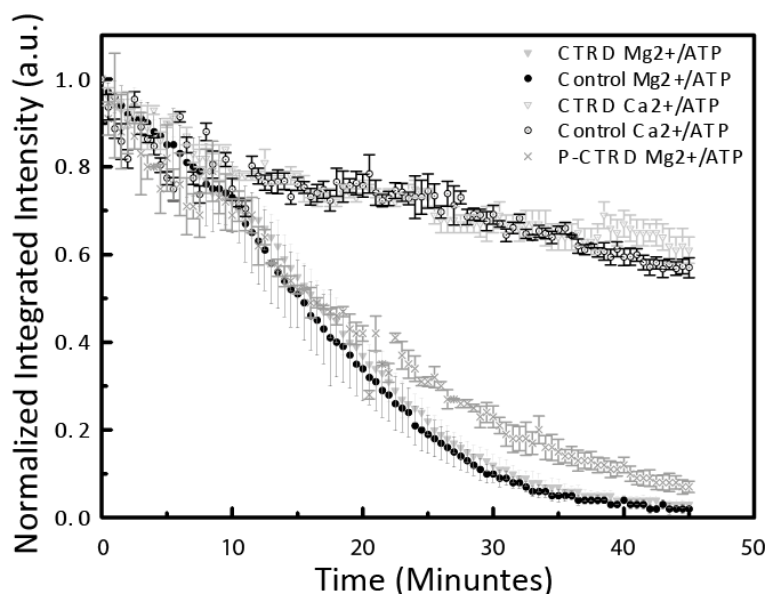
Figure 1. The effect of the CTRD on RAD51 disassembly from individual dsDNA molecules in a flow cell. RAD51 disassembly from dsDNA was measured as loss of fluorescence signal. The CTRD did not significantly influence the dissociation rate when ATP hydrolysis was triggered by Mg2+/ATP. The Ca2+/ATP control filaments were also not affected by the presence of the CTRD. The non-interacting P-CTRD also did not influence the dissociation rate significantly. The error bars represent the standard error.

Confirming CTRD interaction with RAD51-DNA complexes

To demonstrate that the CTRD peptide can interact with RAD51-dsDNA complexes under our reaction conditions, we employed electrophoretic mobility shift assays (EMSA). Using conditions identical to those in the flow cell before switching to Mg^{2+}/ATP buffer (i.e. ATPase suppressing Ca^{2+}/ATP buffer) complex formation between RAD51-dsDNA

and the CTRD was assessed using agarose gels (Figure 2). In the flow cell experiment the ratio RAD51:CTRD was ~ 15:1. Therefore the amount of the CTRD was varied in a range encompassing the ratio in the flow cell. A higher amount of RAD51 was needed to fully shift the short dsDNA (see Figure S1) and therefore the CTRD concentrations were adjusted to keep the ratios of RAD51:CTRD similar. The CTRD concentrations used gave RAD51:CTRD ratios of 22:1 (45 nM CTRD), 11:1 (91 nM CTRD) and 7:1 (137 nM CTRD). Figure 2 shows a representative gel where titration of the CTRD had a minor effect on dsDNA migration in the controls (lanes 2-4), but showed clear interaction with the RAD51-dsDNA complexes by "super-shifting" them in a concentration dependent manner (lanes 6-8). To show specificity, the EMSA assay was also performed with P-CTRD, which includes a phopsphate group at the cyclin-dependent kinase phosphorylation site (S3291E), that does not interact with RAD51 (21).This non-interacting P-CTRD failed to form ternary complexes with the RAD51-dsDNA complex (Figure S2). The assays confirm that the CTRD interacts with RAD51-dsDNA complexes at a similar ratio of RAD51:CTRD and in the same buffer conditions that were used in the flow cell.
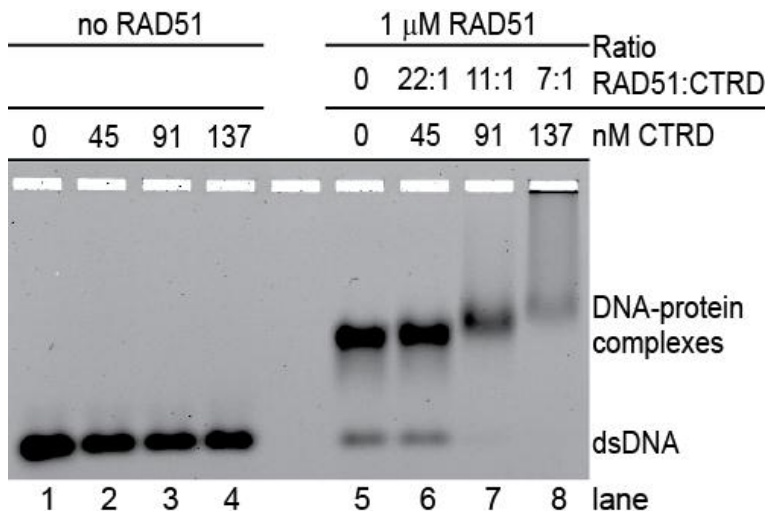
Figure 2. CTRD interaction with RAD51 filaments. Electrophoretic mobility shift assays (EMSA) were preformed with fluorescently end-labeled dsDNA and RAD51 (1 μM), CTRD or a combination of both using agarose gels to separate unbound from bound DNA. Reaction mixtures contained the indicated concentrations of the CTRD. Interaction of the CTRD with the RAD51–dsDNA complexes is evident in lanes 6–8 as 'super-shifting' of the complex in a CTRD concentration dependent manner.

CTRD-induced entanglement of RAD51-DNA complexes

Previous biochemical assays indicate that the BRCA2 CTRD stabilizes RAD51 filaments (*23*). These experiments, however, utilized excess of the CTRD with respect to RAD51. To approach a comparable ratio of RAD51:CTRD, we increased the CTRD concentration 10-fold with respect to the conditions used for the experiments shown in Figure 1. However, distinctly separated, flow-stretched filaments were not observed, even at a RAD51:CTRD ratio of 1.5:1. Instead round, bright fluorescent signals were observed that presumably represented CTRD-induced entanglement of RAD51-dsDNA complexes (data not shown). A portion of these RAD51/CTRD-dsDNA complexes was deposited for imaging using combined fluorescence and scanning force microscopy (SFM). Fluorescence detection allows locating and identifying the labeled RAD51 and SFM provides nm resolution structural information of the protein-DNA complexes (Figure 3). The fluorescent image (Figure 3A) shows an overlay of a representative complex of RAD51 protein and fluorescent polystyrene beads. The polystyrene beads serve to align the combined fluorescent picture (Figure 3A) with the topographic image (Figure 3B) obtained by SFM (*28*). Analysis of the SFM image (Figure 3F) revealed that it was indeed an entanglement of (partial) RAD51 filaments since the height of the structure corresponded to single RAD51 filaments on dsDNA, while unbound dsDNA was also observed (compare Figure 3, panel F with E and H, respectively; see Figure 3D for height

traces of the corresponding cross sections). Entanglement was due to the presence of the CTRD because in a control experiment using the same concentration of non-interacting P-CTRD no aggregation was observed (Figure 3C). Instead regular RAD51 filaments on dsDNA could be seen (compare Figure 3G with 3E, corresponding height traces in Figure 3D). In flow cell experiments without CTRD about 15 ± 6 filaments on average could be seen in a 40 μm by 40 μm field (n = 95). However, at CTRD concentrations above 45 nM about 1.5 ± 0.7 intense, round fluorescent signals were observed in the same size field (n = 9). Since the same amount of DNA and RAD51 were used in both filament formation reactions this suggests that one such aggregate consists on average of approximately 10 filaments.
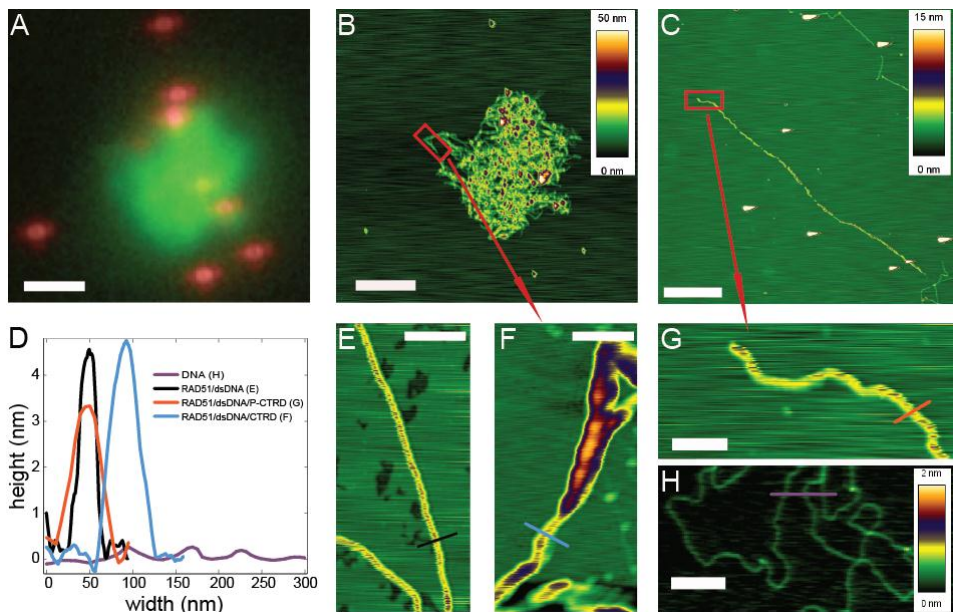
Figure 3. CTRD-induced RAD51 filament entanglement. Fluorescent (A) and SFM (B, C, E) images of RAD51 filaments on phage λ dsDNA. Filaments were either assembled in the presence of 45 nM CTRD (A, B, F), 45 nM of phosphorylated control peptide P-CTRD (C and G) or without peptide (E). (A) Image of combined fluorescence signals from RAD51 and fluorosphere markers. The bright green object in the center of the image in panel A was scanned for nanometer topography. (B) The topographic image reveals

entangled RAD51 filaments. (F) A higher resolution picture of the red boxed area in panel B shows stretches of single filament (cyan cross section) and partial filaments revealing DNA stretches not bound by RAD51. (D) Plot of height and width of the cross sections taken in scan F (blue trace) and G (red trace) comparing them to control depositions of RAD51 filaments in absence of peptide (panel E, black trace) and dsDNA alone (panel H, magenta trace). Images A–C are 10 μm by 10 μm, the white bar is 2 μm. Images E–H are 1 μm by 0.5 μm, the white bar 0.2 μm. The height in the topography scans is indicated with color as shown by the scale bars to the right of each image. The height scale in panels E–G corresponds to the one in panel C.

Filaments formed in the presence of CTRD are qualitatively distinct

In the RAD51 dissociation experiments in the flow cell (such as plotted in Figure 1) the CTRD was added after RAD51 filament formation and incubated for an additional 15 minutes at 37 ºC. Examples of such filaments are shown in the upper left picture in figure 4 (Figure 4A). These filaments appear similar as filaments with RAD51 alone (*12*); the fluorescence covers most of the DNA contour with some gaps. In previous experiments the CTRD influenced filaments when pre-incubated with RAD51 for 15 minutes at 37 ºC before addition of DNA (*21, 23*). Therefore we prepared filaments after pre-incubation of the CTRD with RAD51. Strikingly, RAD51 filaments were distinct from the filaments formed in the absence of the CTRD (compare Figure 4B to 4A). The filaments formed after pre-incubation appeared to be less complete, consisting of shorter filament patches covering less DNA (Figure 4B). Thus a change in the order of addition revealed that a pre-incubation of the CTRD with RAD51 is interfering with extensive filament formation. The presence of the CTRD during filament formation results in incomplete, "patchy" filaments, which could not be analyzed reliably in dissociation experiments. Therefore we decided to analyze these filaments using SFM.
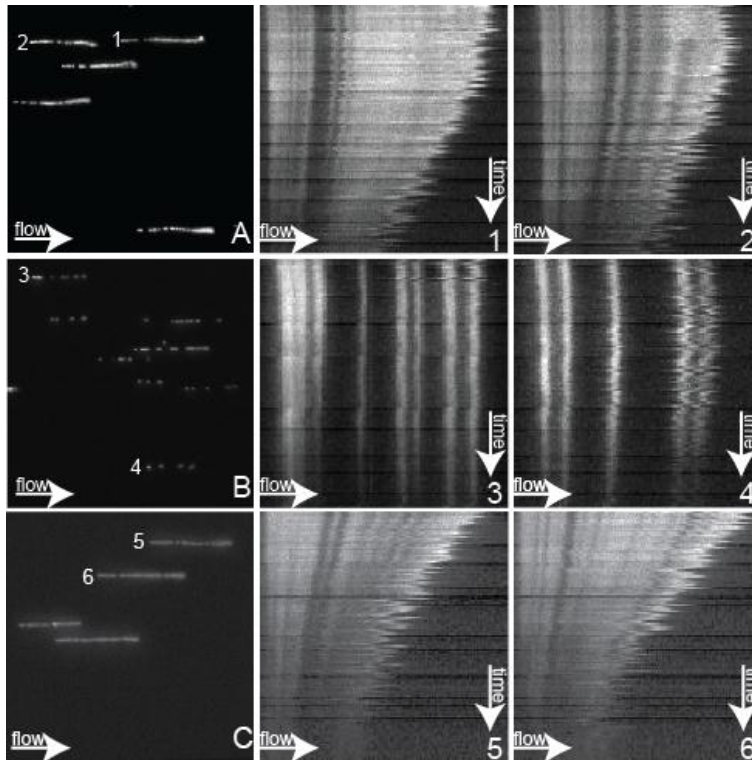
Figure 4. Appearance of RAD51 filaments in flow cell experiments. RAD51 nucleoprotein filaments (A–C) and their corresponding kymographs showing disassembly over time after ATP hydrolysis has been triggered (A 1/2, B 3/4, C 5/6). Fluorescent signal was acquired as described previously for flow cell experiments (12). The images on the left (A–C) show 40 μm by 40 μm images of RAD51 filaments on dsDNA inside the flow cell before ATP hydrolysis was triggered. Adjacent to images A, B and C are the example kymographs of the filaments numbered accordingly. The kymographs are pictures horizontally displaying a filament, with its anchor point on the left, and vertically displaying disassembly of RAD51 over time. Each pixel line towards the bottom of the kymograph represents a 20 s step for a total time of 45 min. The upper panels show the typical appearance of RAD51 filaments. The middle panels show filaments formed after pre-incubation of RAD51 and the CTRD peptide. These filaments appear patchy as evidenced by stretches of bare DNA and less protein bound per DNA molecule. The lower panels show filaments formed after pre-incubation with the phosphorylated control peptide (P-CTRD). These filaments appear similar to the ones without peptide as they are not patchy.

SFM analysis of filament length in presence of the CTRD

To assess the effect of the CTRD on filament formation and structure, nucleoprotein filaments formed after pre-incubation of RAD51 and the CTRD, at a ratio of 5:1, on 3-kb dsDNA were analyzed by SFM (*27*). The images did not show a strong difference in appearance of the control filaments and those formed in the presence of the CTRD (data not shown). As RAD51 polymerization onto DNA stretches it up to 50% over regular B form length, we compared the contour lengths of RAD51 filaments without and with the CTRD (RAD51:CTRD = 5:1). The average elongation of filaments was not much decreased by the presence of the CTRD (1.4 ± 0.1 µm versus 1.29 ± 0.09 µm). However, the distribution of filament lengths was clearly skewed towards shorter filaments in the presence of the CTRD (Figure 5). A reduction in contour lengths could be attributed to reduced RAD51 polymerization onto DNA. Filament formation is a dynamic process consisting of nucleation and extension (growth) and the CTRD could specifically influence one or the other of these processes.
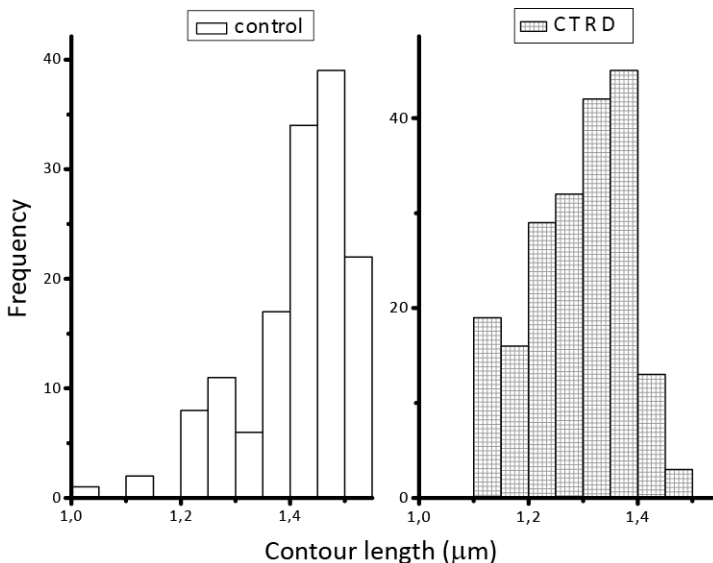
Figure 5. Contour length of RAD51 filaments formed in the presence and absence of the CTRD. The contour length of RAD51 filaments, from images obtained by SFM, were measured and plotted in histograms for control filaments (left) and filaments formed in the presence of the CTRD (right). The y-axis indicates the number of filaments, while the contour length in micrometer with a binning step of 50 nm is plotted along the x-axis. The left panel displays the histogram for the control filaments; the right panel for filaments formed after pre-incubation of RAD51 with CTRD at a ratio of 5:1.

The CTRD decreases RAD51 filament assembly rate in magnetic tweezers measurements

RAD51 filament assembly was followed on individual dsDNA molecules (7.3 kb) in magnetic tweezers (*13, 33*). The DNA molecules were tethered between a magnetic bead and the surface of a flow cell. A force of 7 ± 2 pN was applied by a pair of magnets and video microscopy was used to measure the end-to-end distance of the DNA tether. Due to the known extension of dsDNA upon RAD51 binding an increase in tether length can be directly correlated to the polymerization of RAD51 onto dsDNA. Assembly of a RAD51 filament in the absence of the CTRD resulted in a DNA tether length increase from 2.54 ± 0.04 µm to 3.76 ± 0.07 µm corresponding to a 1.48-fold extension (Figure 6, black curves), similar to previous observations (*13*). RAD51 filament assembly was however very sensitive to pre-incubation of RAD51 with the CTRD in a concentration dependent manner. At a ratio of RAD51:CTRD = 12.5:1 filament assembly was already markedly reduced (Figure 6, cyan curves).

The assembly profiles obtained by magnetic tweezers experiments were analyzed by fitting to Monte Carlo simulations, assuming a binding size of 3 bp per RAD51 monomer and filament nucleation and extension by RAD51 pentamers as described previously (*13, 29, 33*). Nucleation is the dominant step in filament formation. For the simulations the
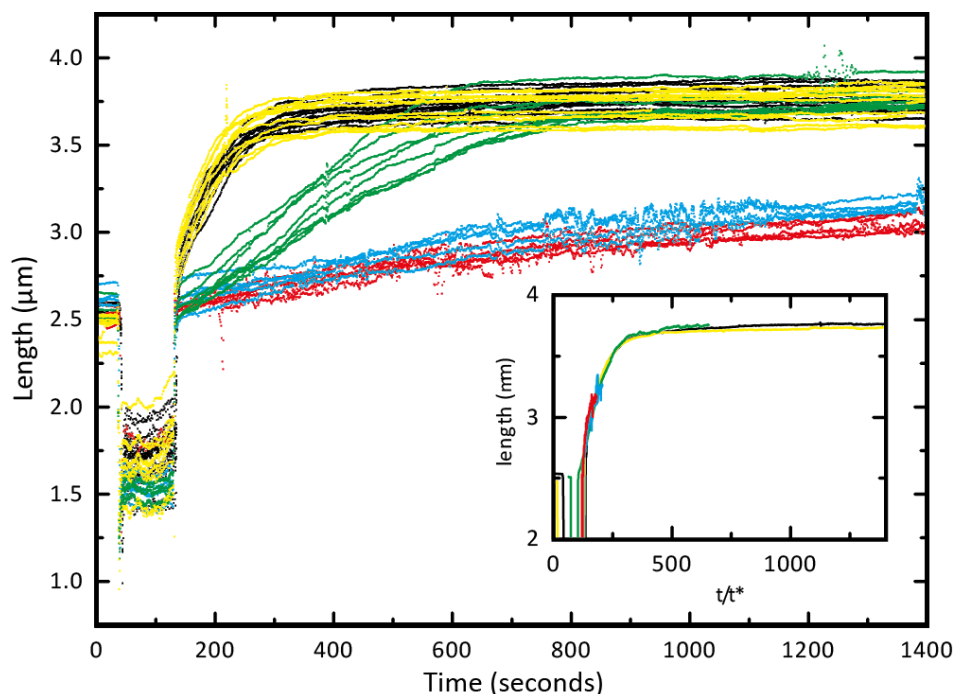
Figure 6. RAD51 filament assembly in real time. RAD51 filament assembly was measured as changes in the length of a DNA, tethered in magnetic tweezers, over time. Different CTRD concentrations are indicated by color: [CTRD] = 0 (black), [CTRD] = 2 nM (yellow), [CTRD] = 6nM (green), [CTRD] = 12 nM (cyan) and [CTRD] = 60 nM (red). Filament assembly was measured on several individual DNA molecules (n = 5–12) for each CTRD concentration. RAD51 and the CTRD were pre-incubated for 15 min at 37 °C. RAD51 concentration was constant at 150nM in all experiments. The inset shows the average growth profile for each concentration of the CTRD rescaled by t/t*, where t*=1/g and g is the nucleation rate determined from fitting to Monte Carlo simulations.

extension rate was linked to the nucleation rate by setting the cooperativity number ω to a value of 100 in line with results of fits with cooperativity as a free independent fit parameter and previous results (*29*). The Monte Carlo fitting procedure yielded nucleation rates of RAD51 at different CTRD concentrations (Figure 7). The validity of this approach for extracting filament assembly rates was demonstrated by plotting averaged assembly curves for each CTRD concentration against

a rescaled time axis (inset Figure 6). The time axis was normalized based on rates found after fitting to Monte Carlo simulations. After normalizing, the filament assembly profiles at different CTRD concentrations overlapped (inset Figure 6), confirming that the shape of the assembly curves is similar and that these curves differ in only one parameter, namely the assembly rate. Filament assembly was strongly decreased by the presence of the CTRD in a concentration dependent manner. The influence of the CTRD on filament assembly rates indicated that the amount of RAD51 available for filament assembly was decreased in the presence of the CTRD. When RAD51 nucleation rates are plotted against CTRD concentration (Figure 7), the power-law shape of the fit indicates that the CTRD interacts with multimeric RAD51, calculated to be on average 3-4 RAD51 monomers, (see Materials and Methods) consistent with previous observations (*23, 25*).
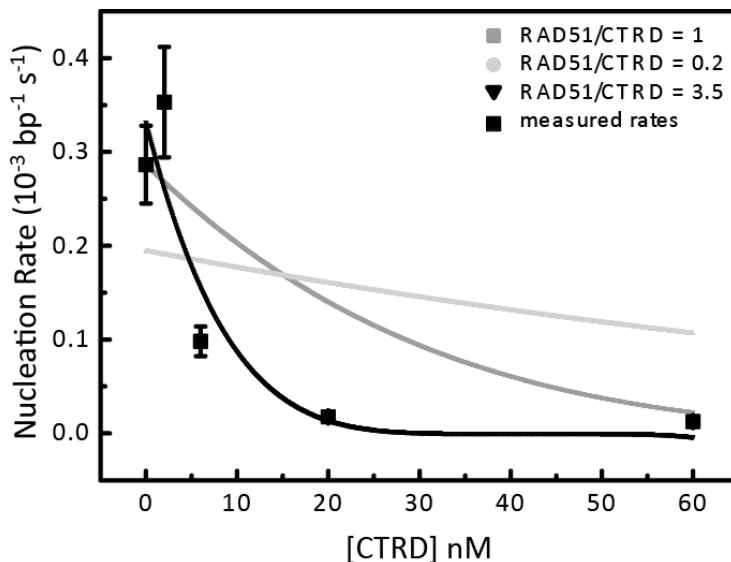
Figure 7. Effect of the CTRD on filament assembly rate. The nucleation rates of RAD51 filaments were extracted from fitting Monte Carlo simulations to the data from Figure 6 at a constant cooperativity number of $\omega=100$. Error bars indicate the standard deviations in the nucleation rates found by fitting the assembly profiles of Figure 6 at each CTRD concentration. A model used to fit nucleation rates (see 'Materials and Methods' section) resulted in a best fit for the number of RAD51 monomers interacting

with CTRD of 3.5 ± 0.4 (black trace). For comparison a model assuming a CTRD interaction with monomeric RAD51 (dark grey trace), and a model assuming an interaction of monomeric RAD51 with multiple CTRDs (light gray trace) is shown.

Discussion

Here we have addressed the effect of the CTRD domain of BRCA2 on the key entity in HR, the RAD51 filament. RAD51 nucleoprotein filaments are dynamic structures undergoing constant rearrangements coupled to ATP hydrolysis. Either suppressing ATP hydrolysis or mechanical protein-protein interactions could stabilize RAD51 filaments. The CTRD of BRCA2 was proposed to stabilize RAD51 filaments by stabilization of protein-protein interactions, acting as a bridge over the RAD51 monomer interface in one model (*23, 25*). In the context of full-length BRCA2 the CTRD domain is expected to have a role modulating RAD51 activity based on observations that phosphorylation of S3291 of CTRD by CDKs abolishes RAD51 binding (*21, 26*). However, we observe no effect of the isolated CTRD domain on filament disassembly rates by direct visualization of RAD51 dissociation from lambda phage dsDNA. Although this result suggests the model based on CTRD bridging RAD51 monomers in a filament to prevent access of BRC-repeats might not hold up it is not contradictory to previous work showing that RAD51 filament disassembly by BRC-repeat peptides is inhibited by the CTRD (*22-25*). That observation could also be due to CTRD induced RAD51 filament entanglement or aggregation as discussed below. Direct stabilization by altering inherent RAD51 dissociation was not previously tested (*22-25*). Since RAD51 dissociation in our set-up is dependent on ATP hydrolysis (*12, 14*), we can conclude that the presence of the CTRD (at a ratio of RAD51:CTRD = 15:1) does not suppress the ATPase activity of RAD51, nor is its interaction with the filament strong enough to slow dissociation in a flow cell set-up.

The absence of an effect of the CTRD peptide on RAD51 filament stability could have been due to absence of interaction with the filaments formed in our conditions. Although the amount of peptide available precluded adding it to the buffer flow during dissociation the persistence of CTRD-induced filament entanglement in the same flow conditions argues that the peptide does not simply dissociate. The EMSA experiments show that the CTRD interacts with RAD51-dsDNA complexes in a concentration-dependent manner in the same starting reaction conditions used in the flow cell i.e. Ca^{2+}/ATP. Because these gel assays required RAD51 at higher concentrations than in the flow cell, the concentration of the CTRD was also adjusted so that the ratio of RAD51:CTRD was 22:1, 11:1 and 7:1, encompassing the 15:1 ratio used in the flow cell. Thus, while the CTRD interacts with RAD51 filaments, it does not influence filament disassembly rates, suggesting that filament stability is not affected.

Several lines of evidence indicate that at higher concentration, or ratios to RAD51, CTRD causes entanglement of RAD51 filaments. Flow cell experiments were attempted at a higher protein concentration, such as required for the EMSA. At CTRD concentration of 45 nM, the lowest concentration showing an effect in the EMSA and corresponding to a final ratio of RAD51:CTRD of 1.5:1 in the flow cell, filaments could not be analyzed by flow stretching. The observation of round, intense, fluorescent signals, which sometimes untangled upon ATP hydrolysis, indicated that the long RAD51 filaments on lambda phage dsDNA may have aggregated in these conditions. Combined fluorescence and SFM imaging revealed that the large, brightly fluorescent objects are indeed CTRD-induced entangled RAD51 filaments that include stretches of naked DNA (Figure 3). This aggregation of RAD51-DNA complexes at higher CTRD concentration would have a detrimental effect on interactions of other proteins with the filament structure. Indeed, CTRD-induced filament aggregation has also been noted in other studies (23).

This could explain the previously observed protective effect of the CTRD on filaments exposed to high concentrations of BRC4 that will otherwise disrupt filaments (*23, 25*). The correlation between stronger CTRD:RAD51 interaction and longer persistence of local nuclear accumulations of RAD51 is also consistent with CTRD-induced filament aggregation or entanglement (*26*).

By contrast, the CTRD-RAD51 interaction did inhibit filament assembly. Interaction of RAD51 and the CTRD before adding dsDNA had a strong effect on filament appearance, even at a final CTRD concentration of approximately 5 nM (ratio RAD51:CTRD = 291:1). The nucleoprotein filament formed had more frequent and larger gaps of naked DNA between protein-bound patches (compare Figure 4 upper and lower panel), an appearance we refer to as "patchy". Furthermore, the concentrations used here were equivalent to the ones in the disassembly experiments, indicating that the lack of an effect on filament disassembly in the flow cell was not due to concentrations of the CTRD insufficient for interaction with RAD51. RAD51filaments, formed on 3 kbp-long dsDNA, in the presence of the CTRD are also somewhat shorter than control filaments (Figure 5). The average DNA extension by filament pre-incubated with the CTRD is only about 70% that of the control filaments (29% versus 40%). In the magnetic tweezers assay, RAD51 filament assembly was very sensitive to pre-incubation with the CTRD. Rates progressively decreased with increasing CTRD concentration (Figure 6). The shape of the assembly curves reflects the interplay between nucleation and extension events in RAD51 DNA-binding to assemble a filament (*13*). The average assembly curves for each CTRD concentration have the same shape, implying that the CTRD has not changed the way RAD51 extends dsDNA as reflected in the ratio of nucleation to extension. These data all support the idea that the CTRD inhibits RAD51 filament assembly by effectively reducing the active RAD51 concentration.

Alternatively, the CTRD could specifically cap nascent filament patches and block further extension. This would produce filaments with different appearance, shorter protein patches with a length correlating to the CTRD concentration, and would require more nucleation events to cover the DNA. However, filaments formed after pre-incubating RAD51 and the CTRD at a 5:1 ratio appeared mostly regular, without obvious gaps or multiple kinks that would indicate reduced extension events. Additionally, filament capping by the CTRD is expected to inhibit dissociation and to change the ratio of nucleation to extension in filament assembly kinetics. None of these effects were observed, thus the CTRD interaction with RAD51 apparently does not cap filaments.

The RAD51 assembly reactions show a power-law dependence of the nucleation rate on CTRD concentration. This was used to determine the stoichiometry of RAD51 affected by the CTRD. Assuming a nucleation unit of 5 RAD51 monomers (*13, 29*) the power-law fit had a minimum for least squares error i = 3.5 ± 0.4, indicating that one CTRD reacts on average with 3-4 RAD51 monomers. This is in accordance with the observation that the CTRD binds multimeric RAD51 in solution (*23, 25*) and suggests that the mode of the CTRD action in this experiment is to sequester RAD51 from filament assembly.

Inactivation of 3-4 RAD51 monomers for filament formation by CTRD binding can explain altered filament appearance as well as reduced assembly rates. The alternative model, that extending RAD51 filament patches are capped in RecX-like fashion is unlikely (*35-37*). Overall, our data are in accordance with recent work on the full-length BRCA2 (*38-40*) and previous studies with BRC peptides (*22-25, 41-43*). Those studies show that BRCA2 and its fragments interact with RAD51-dsDNA complexes and that BRCA2 modulates RAD51 DNA-binding such that filaments preferentially form on ssDNA over dsDNA. Here we show that not only BRC repeats (*23, 41-43*) but also the CTRD of BRCA2 interferes

with RAD51 filament formation on dsDNA. These two peptide portions of BRCA2 differ in details of how they affect RAD51 filaments. Stimulation of RAD51 binding to ssDNA specifically occurs when ATP hydrolysis is possible (*41, 42*). In contrast, the effect we report of the CTRD on RAD51 filaments does not require ATP hydrolysis, as reactions occur in conditions where RAD51's ATPase activity is suppressed. The interaction stoichiometry of the two domains is also different. The BRC repeat forms a complex with RAD51 at a 1:1 ratio (*24, 44, 45*). The CTRD interacts with RAD51 multimers (*23, 24*), and we show it affects filaments formation at substoichiometric amounts. How these different interaction phenomena are manifested in the context of full-length BRCA2 is an important question that can now be addressed. The CTRD domain could work in concert with the BRC domains modulating DNA binding towards ssDNA.

Acknowledgments

Funding

Materials & Methods

Protein production

Wild-type and variants of human RAD51 were purified by similar procedures, essentially as previously described (12). Briefly, RAD51 was expressed in bacteria, precipitated by ammonium sulfate, subsequently dialyzed and further purified by Heparin, gel filtration and anion exchange chromatography. The CTRD peptides were as described previously (21, 22).

Protein labeling

RAD51 was Alexa Fluor 488 labeled on a specific cysteine residue using maleimidine chemistry and checked for activity as previously described (*12*). The degree of labeling was 0.75 fluorophores per RAD51.

Surface tethering and visualization of fluorescent filaments in buffer

Flow cells, constructed from #1 glass cover slips (Menzel-Glaser) separated by a double-layer Parafilm in a custom holder, were prepared as follows: Neutravidin (Pierce) was introduced at 1 mg/ml and allowed to interact for 30 min. After removal of excess Neutravidin, the flow cell was washed and blocked with 2 mg/ml acetylated BSA, 2 mg/ml α-casein, 10 mM DTT, 50 mM Tris-HCl (pH 7.5), 30 mM KCl, and 10%

glycerol. Lambda phage dsDNA was biotinylated at one end and labeled with digoxygenin at the other by annealing biotinylated oligonucleotides to CosL (5'-P-AAG TCG CCG CCC dR-bio dR-bio-bioTEG-3') and 5'-P-GGG CGG CGdRDig CCT CGG CGC CCG GCC GCG dTDigAA ACG CGG CCG GGC GCC GG-3') to CosR as described (*30*). Filaments were assembled in a 20 µl reaction mixture containing 91 pM (molecules) of lambda phage dsDNA, 1.4 µM RAD51, 50 mM Tris-HCl (pH 7.5), 1 mM ATP, 2 mM $CaCl_2$, 1 mM DTT, and 60 mM KCl. Reaction mixtures were incubated at 37 ºC for 30 min. When indicated 4.8 nM CTRD peptide was added and the reaction mixtures incubated for another 15 min (RAD51:CTRD of 291:1). Alternatively, CTRD and RAD51 were incubated for 15 min before addition of the other reaction components. All reaction mixtures were diluted by addition of 380 µl $CaCl_2$/ATP buffer (50 mM Tris-HCl (pH 7.5), 1 mM ATP, 2 mM $CaCl_2$, 1 mM DTT, and 60 mM KCl), and injected into a flow cell. For the CTRD reactions the $CaCl_2$/ATP buffer also included 4.8 nM CTRD, changing the RAD51:CTRD ratio to 15:1. The flow was stopped for about 10 minutes to allow interaction of the biotynilated DNA with the Neutravidin surface. Unbound filaments were flushed by flow of $CaCl_2$/ATP buffer, including 4.8 nM CTRD if present in assembly reaction. Dissociation was triggered by switching to Mg^{2+}/ATP buffer (50 mM Tris-HCl (pH 7.5), 1 mM ATP, 10 mM $MgCl_2$, 1 mM DTT, and 60 mM KCl). Hydrodynamic flow was controlled with a precision pump (Harvard Apparatus). Dynamic visualization of filaments was performed with a Nikon 60 X or 100 X (NA 1.45) TIRF objective in a Nikon TE2000U inverted microscope equipped with a Cascade 512B CCD camera (Princeton Instruments) driven by Metamorph software (Molecular Devices). Excitation was performed with a mercury arc lamp. Intensity measurements were obtained defining regions of interest around the construct contour length in all planes, tracking them over time and correcting for background. The data were plotted using Origin software.

DNA constructs for magnetic tweezers

A 7.3-kb dsDNA construct was prepared as described previously (*33*).

Combined fluorescence and scanning force microscopy

RAD51 filaments were assembled as described above. After 30 min incubation at 37 ºC, the CTRD or a phosphorylated CTRD (P-CTRD) was added to a final concentration of 45 nM (RAD51:CTRD of 31:1). Reaction mixtures were diluted 10 fold in 50 mM Tris-HCl (pH 7.5), 1 mM ATP, 2 mM CaCl$_2$, 1 mM DTT, 60 mM KCl, and 45 nM CTRD for flow cell experiments, changing the RAD51:CTRD to 1.5:1. 10 µl aliquots of the dilution were supplemented with 3 pM red fluorescent (580/605) 40 nm diameter beads (FluoSpheres® microspheres from Invitrogen) and deposited on a freshly cleaved Mica. Fluorescent images were obtained with the set-up described above and correlated with topographic images obtained with a NanoWizard II scanner (JPK instruments) as described (*28*).

Electrophoretic mobility shift assays

Reactions were performed in a final volume of 20 µl containing 5'-end Alexa Fluor 532-labeled 66bp ds DNA (*31*) at 66 nM (nucleotides), 1 µM RAD51, 50 mM Tris-HCl (pH 7.5), 1 mM DTT, 60 mM KCl, 2 mM CaCl$_2$, and 1 mM ATP (*32*). After 5 min incubation at 37ºC, the CTRD peptide was added to the indicated concentrations in a 2 µl volume and incubations were continued for a further 15 min at 37 ºC. Reaction mixtures were then supplemented with 3 µl 30% glycerol and 24 µl were

fractionated by 0.8% agarose gel electrophoresis in 0.5X Tris-Borate for 2.5 hrs at 60 V at 4 ºC. Gels were analyzed using a T9600 typhoon scanner exciting the dye-coupled DNA with a 532 nm laser and detecting emission intensity using a the 555 nm BP 20 filter at 800 V PMT, 3 mm focal plane. Images obtained were analyzed with ImageQuant version 5.2 (Molecular Dynamics) or Image J.

Scanning force microscopy

Nucleoprotein filaments were formed in 10 µl reaction mixtures containing 7.5 µM 3-kb dsDNA (concentration in bp), 2.5 µM human RAD51, 25 mM HEPES–KOH (pH 7.5), 5 mM $CaCl_2$, 2 mM ATP and 30 mM KCl. Reaction mixtures were incubated at 37°C for 1 hr and then placed on ice. When indicated, 500 nM CTRD was added to RAD51 for 15 min at 37 °C before addition of the other components (RAD51:TR2 = 5:1). Aliquots of the reaction mixtures were then diluted 15-fold in 10 mM HEPES–KOH (pH 7.5) and 10 mM MgCl2 and deposited on freshly cleaved mica, scanned and analyzed as previously described (*27*).

Magnetic tweezers assay

The magnetic tweezers set-up used in these experiments was described previously (*34*). By using image processing, 10-nm position accuracy of the bead was obtained in all three dimensions. To exclude the effect of thermal drift, all positions were measured relative to beads fixed to the bottom of the flow cell. DNA constructs carrying a magnetic bead at one end were anchored to the bottom of a flow cell. Experiments were started by addition of RAD51 or RAD51 pre-incubated

with the CTRD at the indicated concentrations, in 50 mM NaCl, 50 mM Tris-HCl pH 7.5, 2 mM $CaCl_2$, 1 mM ATP. All measurements were carried out at 25 °C.

The nucleation rate dependence on the CTRD concentrations was fitted with a model that takes RAD51 nucleation into account. RAD51 nucleation requires multiple RAD51 monomers according to *nRAD51+DNA → (RAD51)n–DNA*, where values of n are reported between 2.7 and 4.3, indicating that nucleation requires 3 to 5 RAD51 monomers (*13, 15*). This model leads to a power-law dependence of the nucleation rate according to $R_{nuc} \propto [RAD51]^n$. We propose a model where the CTRD can interact with multiple RAD51 monomers to reduce the concentration of active RAD51 according to *[RAD51]$_{active}$ = [RAD51]-i[CTRD]*, where i is the number of RAD51 monomers that a CTRD peptide binds.

Supplementary Material
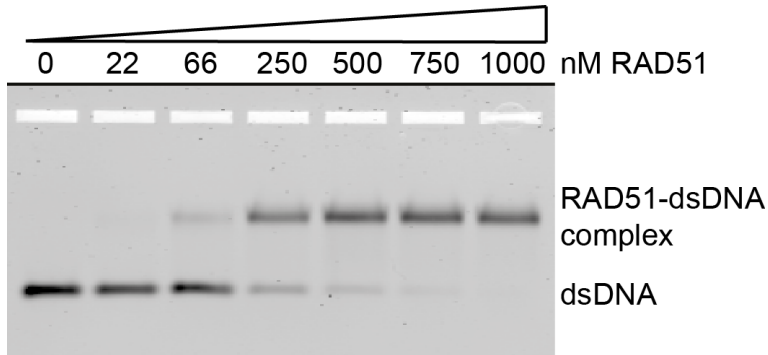
Figure S1. RAD51 interaction with dsDNA. Electrophoretic mobility shift assays (EMSA) were preformed with fluorescently end-labeled dsDNA (66 nM bp) and RAD51 at the indicated concentrations, using 0.8 % agarose gels to separate unbound from bound DNA. Reaction mixtures were in Ca^{2+}/ATP conditions that suppress RAD51 ATPase activity. RAD51-dsDNA complex formation is dependent RAD51 concentration. A complete shift is obtained at 1000 nM RAD51.
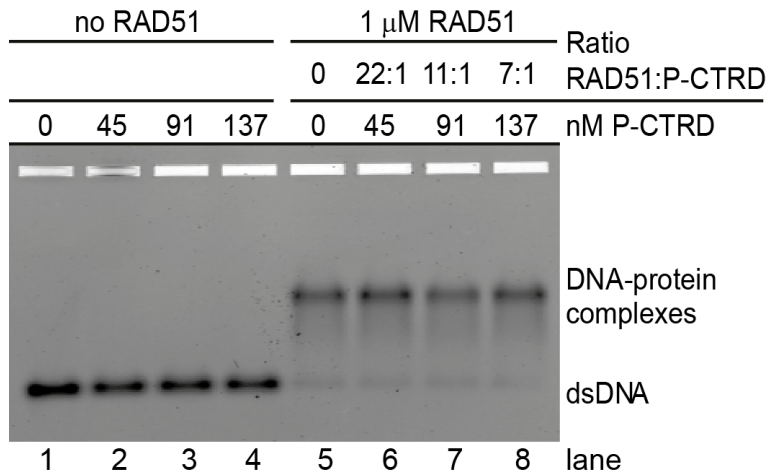
Figure S2. P-CTRD interaction with RAD51 filaments. Electrophoretic mobility shift assays (EMSA) were preformed with fluorescently end-labeled dsDNA and RAD51 (1 μM), P-CTRD or a combination of both using agarose gels to separate unbound from bound DNA. Reaction mixtures contained the indicated concentrations of the P-CTRD. Lanes 6-8 show that the P-CTRD does not interact with the RAD51-dsDNA complexes nor with dsDNA (lanes 2-4).

References

1.   J. H. Hoeijmakers, Genome maintenance mechanisms for preventing cancer. *Nature* **411**, 366 (May 17, 2001).

2.   S. C. West, Molecular views of recombination proteins and their control. *Nat Rev Mol Cell Biol* **4**, 435 (Jun, 2003).

3.   C. Wyman, R. Kanaar, DNA double-strand break repair: all's well that ends well. *Annu Rev Genet* **40**, 363 (2006).

4.   C. Wyman, D. Ristic, R. Kanaar, Homologous recombination-mediated double-strand break repair. *DNA Repair (Amst)* **3**, 827 (Aug-Sep, 2004).

5.   M. P. Longhese, D. Bonetti, N. Manfrini, M. Clerici, Mechanisms and regulation of DNA end resection. *EMBO J* **29**, 2864 (Sep 1, 2010).

6.   E. P. Mimitou, L. S. Symington, DNA end resection: many nucleases make light work. *DNA Repair (Amst)* **8**, 983 (Sep 2, 2009).

7.   U. Rass *et al.*, Mechanism of Holliday junction resolution by the human GEN1 protein. *Genes Dev* **24**, 1559 (Jul 15, 2010).

8.   J. M. Svendsen, J. W. Harper, GEN1/Yen1 and the SLX4 complex: Solutions to the problem of Holliday junction resolution. *Genes Dev* **24**, 521 (Mar 15, 2010).

9.   J. San Filippo, P. Sung, H. Klein, Mechanism of eukaryotic homologous recombination. *Annu Rev Biochem* **77**, 229 (2008).

10.   X. Li, W. D. Heyer, RAD54 controls access to the invading 3'-OH end after RAD51-mediated DNA strand invasion in homologous recombination in Saccharomyces cerevisiae. *Nucleic Acids Res* **37**, 638 (Feb, 2009).

11.   X. Li, C. M. Stith, P. M. Burgers, W. D. Heyer, PCNA is required for initiation of recombination-associated DNA synthesis by DNA polymerase delta. *Mol Cell* **36**, 704 (Nov 25, 2009).

12.   M. Modesti *et al.*, Fluorescent Human RAD51 Reveals Multiple Nucleation Sites and Filament Segments Tightly Associated along a Single DNA Molecule. *Structure* **15**, 599 (May, 2007).

13.   T. van der Heijden *et al.*, Real-time assembly and disassembly of human RAD51 filaments on individual DNA molecules. *Nucleic Acids Res* **35**, 5646 (2007).

14.   J. van Mameren *et al.*, Counting RAD51 proteins disassembling from nucleoprotein filaments under tension. *Nature* **457**, 745 (Feb 5, 2009).

15.   J. Hilario, I. Amitani, R. J. Baskin, S. C. Kowalczykowski, Direct imaging of human Rad51 nucleoprotein dynamics on individual DNA molecules. *Proc Natl Acad Sci U S A* **106**, 361 (Jan 13, 2009).

16.   S. S. Yuan *et al.*, BRCA2 is required for ionizing radiation-induced assembly of Rad51 complex in vivo. *Cancer Res* **59**, 3547 (Aug 1, 1999).

17.   M. E. Moynahan, A. J. Pierce, M. Jasin, BRCA2 is required for homology-directed repair of chromosomal breaks. *Mol Cell* **7**, 263 (Feb, 2001).

18.   V. P. Yu *et al.*, Gross chromosomal rearrangements and genetic exchange between nonhomologous chromosomes following BRCA2 inactivation. *Genes Dev* **14**, 1400 (Jun 1, 2000).

19.   A. R. Venkitaraman, Linking the cellular functions of BRCA genes to cancer pathogenesis and treatment. *Annu Rev Pathol* **4**, 461 (2009).

20.   T. Thorslund, S. C. West, BRCA2: a universal recombinase regulator. *Oncogene* **26**, 7720 (Dec 10, 2007).

21.   F. Esashi *et al.*, CDK-dependent phosphorylation of BRCA2 as a regulatory mechanism for recombinational repair. *Nature* **434**, 598 (Mar 31, 2005).

22.   V. E. Galkin *et al.*, BRCA2 BRC motifs bind RAD51-DNA filaments. *Proc Natl Acad Sci U S A* **102**, 8537 (Jun 14, 2005).

23.   F. Esashi, V. E. Galkin, X. Yu, E. H. Egelman, S. C. West, Stabilization of RAD51 nucleoprotein filaments by the C-terminal region of BRCA2. *Nat Struct Mol Biol* **14**, 468 (Jun, 2007).

24.   O. R. Davies, L. Pellegrini, Interaction with the BRCA C terminus protects RAD51-DNA filaments from disassembly by BRC repeats. *Nat Struct Mol Biol* **14**, 475 (Jun, 2007).

25.   M. I. Petalcorin, V. E. Galkin, X. Yu, E. H. Egelman, S. J. Boulton, Stabilization of RAD-51-DNA filaments via an interaction domain in Caenorhabditis elegans BRCA2. *Proc Natl Acad Sci U S A*, (May 2, 2007).

26.   N. Ayoub *et al.*, The carboxyl terminus of Brca2 links the disassembly of Rad51 complexes to mitotic entry. *Curr Biol* **19**, 1075 (Jul 14, 2009).

27.   D. Ristic *et al.*, Human Rad51 filaments on double- and single-stranded DNA: correlating regular and irregular forms with recombination function. *Nucleic Acids Res* **33**, 3292 (2005).

28.   H. Sanchez, R. Kanaar, C. Wyman, Molecular recognition of DNA-protein complexes: A straightforward method combining scanning force and fluorescence microscopy. *Ultramicroscopy* **110**, 844 (Jun, 2010).

29.   T. van der Heijden, C. Dekker, Monte carlo simulations of protein assembly, disassembly, and linear motion on DNA. *Biophys J* **95**, 4560 (Nov 15, 2008).

30.   A. Graneli, C. C. Yeykal, T. K. Prasad, E. C. Greene, Organized arrays of individual DNA molecules tethered to supported lipid bilayers. *Langmuir* **22**, 292 (Jan 3, 2006).

31.   E. van der Linden, H. Sanchez, E. Kinoshita, R. Kanaar, C. Wyman, RAD50 and NBS1 form a stable complex functional in DNA binding and tethering. *Nucleic Acids Res* **37**, 1580 (Apr, 2009).

32.   D. V. Bugreev, A. V. Mazin, Ca2+ activates human homologous recombination protein Rad51 by modulating its ATPase activity. *Proc Natl Acad Sci U S A* **101**, 9988 (Jul 6, 2004).

33.   M. T. van Loenhout, T. van der Heijden, R. Kanaar, C. Wyman, C. Dekker, Dynamics of RecA filaments on single-stranded DNA. *Nucleic Acids Res*, (May 8, 2009).

34.   T. R. Strick, J. F. Allemand, D. Bensimon, V. Croquette, Behavior of supercoiled DNA. *Biophys J* **74**, 2016 (Apr, 1998).

35.   M. M. Cox, Regulation of bacterial RecA protein function. *Critical reviews in biochemistry and molecular biology* **42**, 41 (Jan-Feb, 2007).

36.   J. C. Drees, S. L. Lusetti, S. Chitteni-Pattu, R. B. Inman, M. M. Cox, A RecA filament capping mechanism for RecX protein. *Mol Cell* **15**, 789 (Sep 10, 2004).

37.   S. Ragone, J. D. Maman, N. Furnham, L. Pellegrini, Structural basis for inhibition of homologous recombination by the RecX protein. *Embo J* **27**, 2259 (Aug 20, 2008).

38.   R. B. Jensen, A. Carreira, S. C. Kowalczykowski, Purified human BRCA2 stimulates RAD51-mediated recombination. *Nature*, (Aug 22, 2010).

39.   J. Liu, T. Doty, B. Gibson, W. D. Heyer, Human BRCA2 protein promotes RAD51 filament formation on RPA-covered single-stranded DNA. *Nat Struct Mol Biol*, (Aug 22, 2010).

40.   T. Thorslund *et al.*, The breast cancer tumor suppressor BRCA2 promotes the specific targeting of RAD51 to single-stranded DNA. *Nat Struct Mol Biol*, (Aug 22, 2010).

41.   A. Carreira *et al.*, The BRC repeats of BRCA2 modulate the DNA-binding selectivity of RAD51. *Cell* **136**, 1032 (Mar 20, 2009).

42.   M. K. Shivji *et al.*, A region of human BRCA2 containing multiple BRC repeats promotes RAD51-mediated strand exchange. *Nucleic Acids Res* **34**, 4000 (2006).

43.   M. K. Shivji *et al.*, The BRC repeats of human BRCA2 differentially regulate RAD51 binding on single- versus double-stranded DNA to stimulate strand exchange. *Proc Natl Acad Sci U S A* **106**, 13254 (Aug 11, 2009).

44.   L. Pellegrini *et al.*, Insights into DNA recombination from the structure of a RAD51-BRCA2 complex. *Nature* **420**, 287 (Nov 21, 2002).

45.   D. S. Shin *et al.*, Full-length archaeal Rad51 structure and mutants: mechanisms for RAD51 assembly and control by BRCA2. *EMBO J* **22**, 4566 (Sep 1, 2003).

Chapter 4:

Intercontinental comparison of fluorescent RAD51 filament disassembly by a set of single-molecule microscopes

J.T. Holthausen[1], J. Hilario[2,3], R. Kanaar[1,4], R.J. Baskin[3], S.C. Kowlaczykowski[2,3], C.Wyman[1,4]

[1]Department of Genetics and Department of [4]Radiation Oncology, Cancer Genomics Center, Erasmus Medical Center, P.O. Box 2040, 3000 CA Rotterdam, The Netherlands
[2]Departments of Microbiology and of [3] Molecular and Cellular Biology, University of California, Davis, CA 95616-8665, USA

Abstract

Genome maintenance by faithful repair of double-stranded DNA breaks is mediated by homologous recombination. At the core of recombination is the recombinase protein RAD51. It polymerizes around a newly generated single-stranded DNA at the site of the break and engages the homologous duplex DNA in search for the homologous site where it drives strand exchange. This results in the formation of a protein filament wound around the ensuing heteroduplex DNA. The invading strand needs to prime DNA synthesis spanning the site of the break to restore DNA lost at the break site. In order for the polymerase to be able to access the hydroxyl end of the invading strand, the RAD51 filament needs to disassemble. We employed fluorescence microscopy in combination with microfluidic systems to observe and evaluate RAD51 dissociation from double-stranded DNA. Here we compare dissociation results obtained from three different microscopes - identified by their location in Rotterdam, Amsterdam or Davis, California - and two distinctly labeled RAD51 proteins - Alexa-RAD51 from Rotterdam and FAM-RAD51 from Davis. This comparison should elucidate experimental details to explain a difference in outcomes. No disassembly of RAD51 nucleoprotein filaments was observed in the Davis setup and conditions. By contrast, in the buffer conditions used in Rotterdam and Amsterdam protein dissociation could be induced by a switch of buffers from one that suppressed to one that allowed RAD51 ATP hydrolysis. We show that independent of the microscope setup, both labeled proteins can give the same result in equal biochemical conditions. We also show that the disassembly rate can be controlled by divalent salt concentration.

Introduction

Homologous recombination is an essential DNA double-strand break repair pathway and is critical for generating genetic diversity in meiosis. Recombination is driven by a recombinase filament that forms on single-stranded DNA, engages duplex DNA in search for its complement, where it will recombine the single-stranded DNA with its complementary DNA while displacing the other strand. In the canonical recombination model the recombinase filament is bound to the product heteroduplex DNA after strand exchange. The filament protects the DNA within, effectively blocking access of polymerases to the 3' hydroxyl end of the invading strand. Therefore the filament needs to be removed for successful completion of recombination events (*1-3*). Although filaments are able to disassemble by themselves in *in vitro* biochemical and single molecule experiments (*4-7*) in a cellular environment the metastable nucleoprotein filament is acted upon by other proteins that can either promote or antagonize filament stability. Throughout recombination the arising intermediates are either reversible DNA structures or transient protein-DNA interactions. The control of recombination progression is what ensures the robustness of the process while acting as a quality control (*8, 9*).

One such control point is the regulation of recombinase filament stability. Factors that work towards removal of recombinase are helicases, e.g. RecQ family, and translocating proteins like RAD54 (*2, 10-14*). The initial filament forms on single-stranded DNA and undergoes constant rearrangements with proteins dissociating and associating (Figure 1A). The helicase Srs2 can tilt the balance towards dissociation from ssDNA by stimulation of Rad51 ATPase activity (Figure 1B) (*15*). This would contribute to recombination quality control by disrupting the process at inappropriate places. However, after successful strand exchange, the recombinase filament needs to be removed from double-

stranded DNA to allow access by polymerase. While RAD51 dissociates from double-stranded DNA by itself, it does so slower than from single-stranded DNA, and this is putatively a rate-limiting step (Figure 1D). There are many proteins that could facilitate filament disassembly mechanically, e.g. RAD54 by translocation along the heteroduplex DNA (Figure 1E) (*14*). Cell biology provides support for the importance of active/facilitated RAD51 filament disassembly. Cells expressing the RAD51 K133R mutant have defects in recombination. *In vitro* the mutant cannot hydrolyze ATP and does not spontaneously dissociate from DNA. In addition local nuclear accumulations of RAD51, known as foci, persist longer in cells expressing RAD51 K133R (*16, 17*). Similarly, the breast cancer susceptibility gene product (BRCA2), whose interaction with RAD51 is thought to stabilize RAD51 filaments, affects RAD51 foci persistence (*18-21*). High-affinity RAD51 binding mutants of BRCA2 cause RAD51 foci to persist longer and delay mitotic entry of avian cells (*22*).

The recombinase filaments assemble in such a way that a functional ATPase domain forms at the monomer-monomer interface. When ATP is bound, the filament stretches the DNA up to 50 % over its regular B-form length. The ATP bound filament is referred to as the active filament. ATP hydrolysis is not required for the assembly of filaments, homology search, strand invasion, joint molecule formation nor strand exchange (*1, 6, 23-26*). Instead all these reactions are promoted by keeping the filament in the ATP bound form. When ATP hydrolysis is permitted the *in vitro* efficiency of joint molecule formation is greatly reduced and in many studies the visualization of (stable) recombinase-DNA complexes by electrophoresis or scanning force microscopy (SFM) became difficult or not possible with oligonucleotides (*6, 20, 24, 27*). These data support the notion that the hydrolysis of ATP at the recombinase-recombinase interface results in destabilization of the protein interactions and subsequent filament disassembly. While

translocation of other proteins can mechanically remove RAD51 from DNA, this process may be impeded by the lack of ATP hydrolysis in the filament. The example of yeast Srs2 shows that alternatively, protein-protein interactions can stimulate RAD51 ATPase activity, which in turn increases its dissociation rate from ssDNA. The mechanical removal of RAD51 is facilitated and largely dependent on the rate of ATP hydrolysis within the filament.
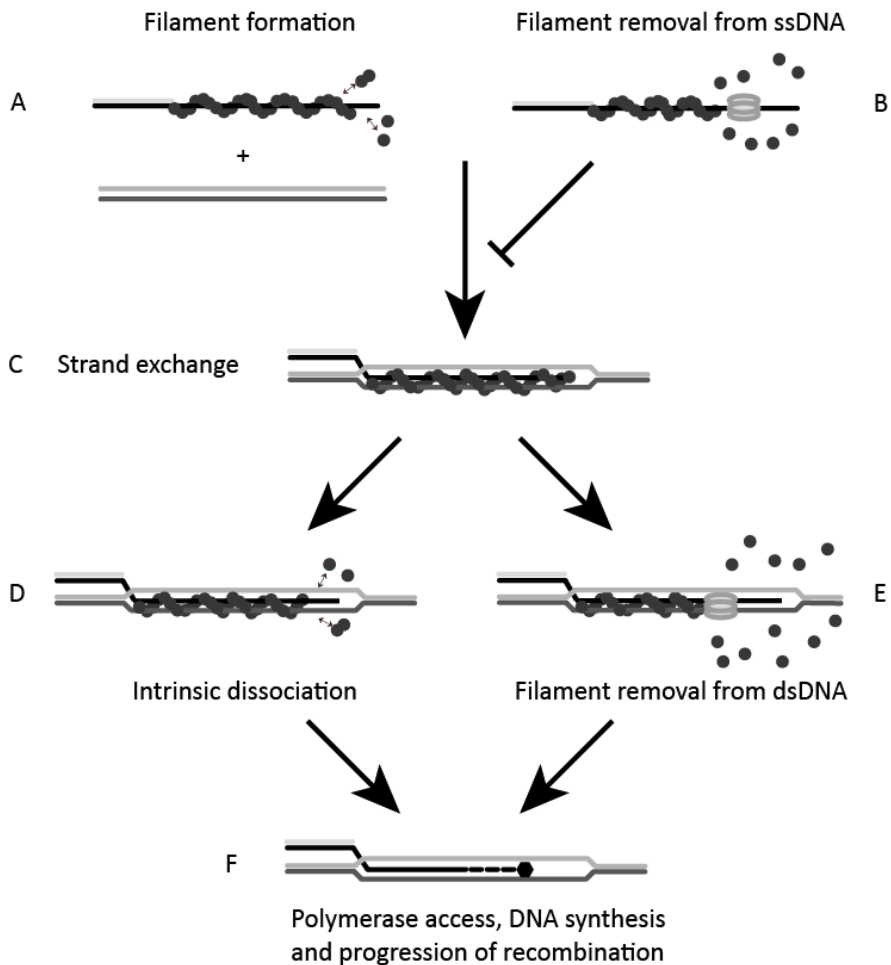
Figure 1: Illustrating the importance of RAD51 removal from DNA during recombination. Filament formation on ssDNA in presence of a homologous template

(A) will result in strand exchange (C). Removal of RAD51 from the ssDNA by a helicase (B) can block this step. After strand exchange either intrinsic dissociation (D) or filament disassembly facilitated by helicases (E) can give polymerases access to the 3' of the invading strand (F), followed by DNA synthesis and resolution of the resulting DNA structures.

The intrinsic dissociation of RAD51 recombinase from double-stranded DNA was followed using fluorescent protein interactions with individual DNA molecules. Three laboratories, in Rotterdam, Amsterdam and Davis, took this approach using different setups and protein preparations. The results from the Davis laboratory differed from the other two in that RAD51 did not dissociate from double-stranded DNA by itself. This chapter aims at comparing the setups, proteins and experimental conditions in order to understand the mechanistic importance of experimental parameters in explaining these different observations.

Results

In order to understand the difference in the approaches taken, the three setups are reviewed and their differences stated.

The experimental setups

The first laboratory of the three in this comparison, our laboratory in Rotterdam, used a Nikon TE2000U inverted microscope with a Nikon 603 (NA 1.45) objective and was fitted with a Cascade 512B EM-CCD camera (Figure 2). Excitation was mainly performed with a mercury

lamp; alternatively an argon laser could be used. The flow chamber had
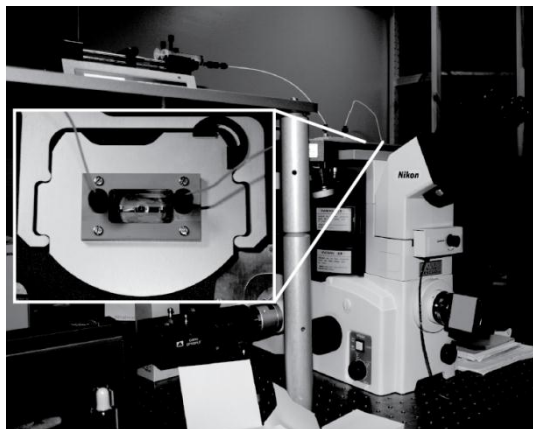
a single, several millimeters wide and about 120 μm deep channel, made from Parafilm sandwiched between two glass slides (Inset Figure 2). Filaments were attached to the surface and observed in epifluorescence mode as described in materials and methods.

Figure 2: Photograph of the setup in Rotterdam. The inset is an image of the flow-cell mounted on top of the microscope.

In collaboration with the group of Gijs Wuite and Erwin Peterman at the Vrije Universiteit (VU) in Amsterdam, we used a self-built microscope according to the scheme in the supplementary materials of van Mameren *et al* (*7*). This microscope had the same Cascade 512B EM-CCD camera providing single-molecule sensitivity. Molecules were excited in epifluorescence mode with lasers. The microscope was fitted with a three- or four-channel flow cell, also assembled from glass slides and a Parafilm mold. In this setup single DNA molecules are immobilized between dual optical traps. This enabled capture, manipulation and analysis of molecules in the center of the flow chamber.

At third laboratory, the group of Stephen Kowalczykowski in Davis (CA, USA), employed a self-built setup as described (*28-32*). Excitation in epifluorescence mode was achieved with a mercury lamp. The three-channel flow-chamber was assembled with an epoxy resin and could be used multiple times compared to the Parafilm assembled flow-cells that often were used only once. The data was acquired with an EB-CCD,

recorded on VHS and was digitized later. Single DNA molecules were immobilized by a single optical trap for observation in the center of the flow chamber. A more detailed perspective of the flow chambers can be found in Brewers *et al* (*33*).

As summarized in table 1 the three setups were distinct but also shared features. The major difference for experiments between the Rotterdam setup and the others was the way to trap molecules: In Rotterdam molecules were attached to the flow cell surface; in the other setups molecules where bound to beads that were then trapped in optical traps in the center of the flow cell.

	Rotterdam	Amsterdam	Davis
Excitation mode	Epi / TIRF	Epi	Epi
Excitation source	Mercury lamp/ lasers	Lasers	Mercury lamp
Detection	EM-CCD	EM-CCD	EB-CCD
Flow chamber	Single-channel	Multi-channel	Multi-channel
Optical trap	None	Dual	Single
Molecule location	Surface	Trapped bead	Trapped bead

Table 1 summarizes the main features of the three different setups used to study RAD51 dissociation from double-stranded DNA.

Alexa-RAD51 and FAM-RAD51

The three laboratories used two different versions of fluorescently labeled RAD51. For the experiments in Rotterdam and Amsterdam a variant of RAD51, RAD51 C319S, was generated that had cysteine 31 as the only surface-exposed cysteine. This protein was labeled at C31 with

Alexa fluorophore by thiol chemistry (Figure 3, Alexa 31). The labeling reaction and the removal of free dye with a sizing column were analyzed by SDS-PAGE by a combination of fluorescence signal and protein detection (Figure 4A). This protein, named Alexa-RAD51, hydrolyzed ATP and formed joint molecules with similar efficiency to the unlabeled version (Figure 5A and B).
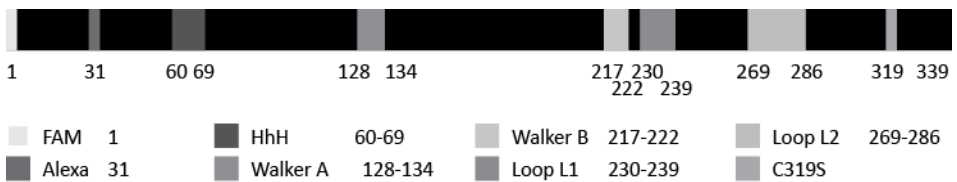
Figure 3: Schematic representation of RAD51 amino acid sequence derived from Shin et al (*34*). Name and position of the relevant motifs and modifications are indicated. FAM represents the amino-terminal labeling with fluorescein. Alexa represents Alexa fluorophore labeling of cysteine 31. HhH = helix – hairpin – helix. Walker A and Walker B domains constitute a functional ATPase domain; note that the Walker A domain of one monomer interacts with the Walker B of another monomer. Loop L1 and L2 have been implicated in DNA interactions. C319S indicates the amino acid change of the RAD51 variant used in Rotterdam and Amsterdam that leaves C31 as the only solvent accessible cysteine.
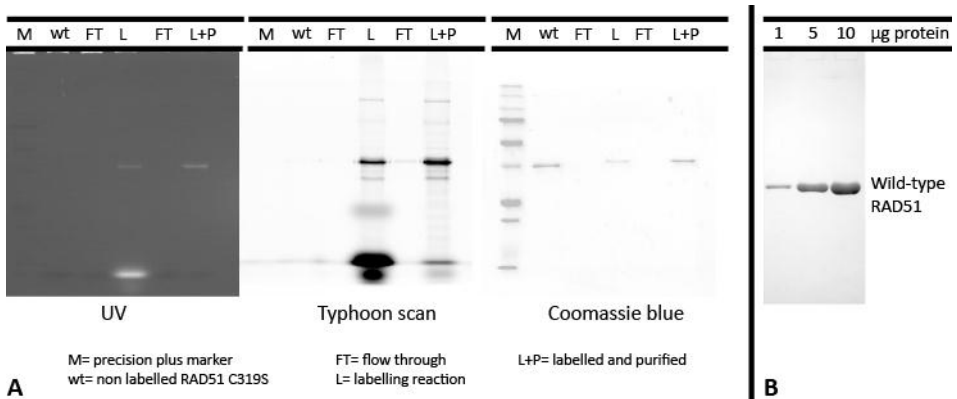
Figure 4: RAD51 analysis by gel electrophoresis. Panel A shows UV, Typhoon and Coomassie pictures of the steps of RAD51 labeling with Alexa 488. The left UV gel shows fluorescent signal from Alexa 488 in the labeling reaction lane (L) and after purification on a size exclusion column (L+P). The middle typhoon scan shows a more sensitive image of the Alexa 488 signal revealing some impurities and free dye. The right coomassie stain shows the slightly increased MW of the labeled RAD51 (lanes L and L+P) with respect to the unlabeled (wild-type). Panel B shows the Coomassie stain of the RAD51 to be labeled with fluorescein; adapted from supplementary material of Hilario *et al.* (*31*).
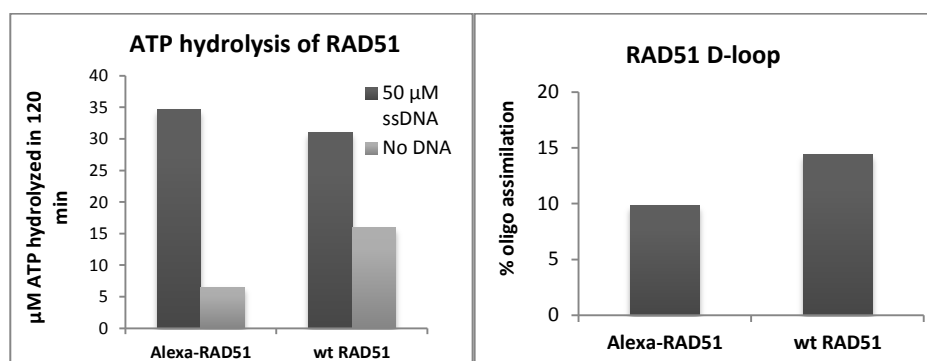
Figure 5: Biochemical activity of Alexa-RAD51 compared to unlabeled RAD51. The left panel shows a comparison of ssDNA dependent RAD51 ATPase activity. The right panel shows the ability the ability of Alexa-RAD51 to form D-loops with the unlabeled protein as control.

The study in Davis used wild-type RAD51 which was prepared and purified differently (Figure 4B). The protein was labeled at the N-terminus with fluorescein by ammine chemistry (Figure 3). As described in Hilario *et al.* the "FAM-RAD51" was proficient in ssDNA dependent ATP hydrolysis and joint molecule formation assays (*31*). The two fluorescent proteins, although prepared in different fashion, performed similarly in the biochemical assays.

Rotterdam buffers		Davis buffers			
CaRdam	MgRdam	CaDav	MgDav	CaDavMod	MgDavMod
50 mM Tris-HCl pH 7.5	50 mM Tris-HCl pH 7.5	50 mM TrisOAc pH 8.0	50 mM TrisOAc pH 8.0	50 mM TrisOAc pH 8.0	50 mM TrisOAc pH 8.0
2 mM $CaCl_2$	2 mM $MgCl_2$	2 mM $Ca(OAc)_2$	5 mM $Mg(OAc)_2$	2 mM $Ca(OAc)_2$	5 mM $Mg(OAc)_2$
1 mM DTT	1 mM DTT	30 mM DTT	30 mM DTT	30 mM DTT	30 mM DTT
1mM ATP	1mM ATP	1mM ATP		1mM ATP	
				30 mM KOAc	30 mM KOAc
		15 % sucrose	15 % sucrose		

Table 2 lists buffer compositions of the buffers used in flow cell experiments in Rotterdam and Davis.

Filament disassembly

Filament disassembly experiments performed in Davis and Rotterdam exhibited different outcomes with respect to RAD51 dissociation, and also used different approaches to evaluate the data. In Davis FAM-RAD51 did not dissociate from dsDNA. In Rotterdam Alexa-RAD51 readily dissociated from dsDNA.

In the Davis laboratory RAD51 dissociation was measured as a change in filament length based on the observed fluorescent signal. The duration of exposure was about 20 minutes and resulted in strong fluorescein bleaching (Figure 6A). In Rotterdam dissociation was measured as a loss of fluorescence intensity. Filaments were exposed for 200 ms every 30 seconds recording a time-lapse, which resulted in reduced bleaching and extended experiment times of 45 minutes (*4, 5*). When filaments were exposed continuously in Rotterdam, the time-frame of the disassembly experiment matched that of the ones in Davis

(Figure 6B). However, independent of the exposure method Alexa-RAD51 dissociated from dsDNA. Compared to a bleaching control, where filaments are maintained in CaRdam buffer, the filaments in MgRdam buffer disassembled readily within 20 minutes as measured by loss of fluorescent signal (Figure 6B; see Table 2 for buffers).

The difference in behavior became more evident when comparing kymographs of the two disassembly experiments. The FAM-RAD51 filament lost fluorescence intensity but did not become shorter, as seen by the horizontal distribution of the fluorescence signal in the kymograph (Figure 7A). Since disassembly was measured as changes in DNA length no disassembly was recorded. The loss of fluorescence signal could also be attributed to bleaching of the fluorophore. The Alexa-RAD51 not only lost fluorescence intensity, but also became shorter (Figure 7B). The reduction in filament (patch) length together with the quick loss of fluorescence signal indicated substantial RAD51 dissociation.
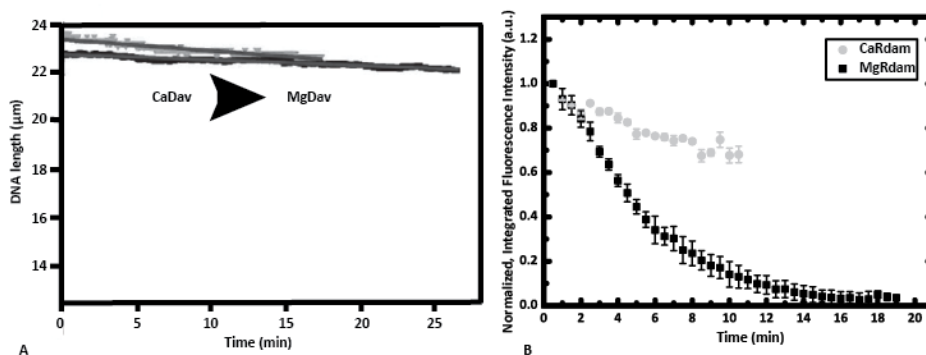
Figure 6: RAD51 dissociation. The left panel, adapted from Figure 2, Panel A of Hilario *et al.* (*31*), shows trajectories of DNA length changes over time of FAM-RAD51 filaments. Experiments using CaDav to MgDav buffer switch are in light grey. The longer, dark grey trajectory represents the CaDav bleaching control. The right panel shows a plot of Alexa-RAD51 dissociation under continuous exposure after a switch from CaRdam buffer to MgRdam buffer (black squares) and a CaRdam bleaching control (light grey circles).

The experiments in Amsterdam, done with Alexa-RAD51, gave similar results to those done in Rotterdam. Since the DNA was trapped on both ends and kept under tension, the reduction in total filament length was not as evident as in the kymographs obtained in Rotterdam, but the patches did shrink together with a loss in fluorescence intensity. This confirmed that RAD51 filaments dissociate intrinsically from dsDNA and it was further established that the filament disassembly was tension-dependent (*7*). See Figure 1b in van Mameren *et al.* for an example kymograph (*7*).
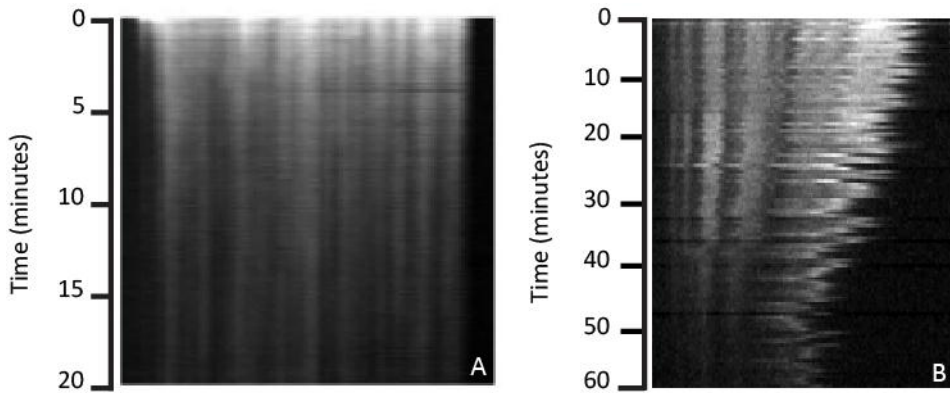
Figure 7: Kymographs of fluorescent RAD51 dissociation experiments. The filament anchor point is on the left. Each pixel row represents an image of the filament with time progressing as indicated. 7A shows a representative FAM-RAD51 filament dissociation in MgDav buffer from Davis. Frames of a video of the filament under continuous exposure were averaged to obtain the kymograph. The kymograph was adapted from Figure 7, Panel A in Hilario *et al.* (*31*). 7B shows a representative dissociation of Alexa-RAD51 in MgRdam buffer in Rotterdam. The kymograph was made from a time-lapse exposure - the standard in this laboratory.

The two sets of experiments with the Alexa-labeled RAD51 resulted in filament disassembly while FAM-RAD51 experiments did not. A possible reason could be the difference between surface attachment of filaments

in Rotterdam and trapping in Davis. However, the experiments in Amsterdam use filament trapping, indicating that the molecule trapping is not responsible for the different outcome. Microscope components other than those affecting the flow-chamber environment are unlikely to contribute to these experiment differences. Another explanation could be the different fluorescently labeled proteins, Alexa-RAD51 and FAM-RAD51.

Comparison of fluorescent RAD51

A straight forward explanation for impaired FAM-RAD51 dissociation would be an ATPase deficiency. However, FAM-RAD51 ATP hydrolysis is not impaired by the protein labeling. To address the discrepancy in dissociation results, further investigation was necessary. A collaborative exchange to test Alexa-RAD51 in the Davis setup was arranged.

First Alexa-RAD51 filaments were assembled in CaDav buffer inside the flow-cell or a reaction tube, to account for that difference, and then tested for dissociation by a switch to MgDav buffer. Even after an extensive exposure over 45 minutes the filaments did not shrink and hence did not disassemble (Figure 8A). Alexa-RAD51 behaved like the FAM-RAD51 in the Davis experiment conditions (CaDav to MgDav switch; compare Figure 7A with Figure 8A). This experiment further revealed a striking difference in the quality of the two fluorophores used. The Alexa fluorophore was much brighter and bleached much slower than fluorescein.

Next, Alexa-RAD51 and FAM-RAD51 filaments were tested in the Davis setup with the Rotterdam buffers; assembly in CaRdam buffer and observation/dissociation in the MgRdam buffer channel. The buffer switch triggered shrinking and rapid loss of fluorescence of both Alexa-

RAD51 and FAM-RAD51 filaments (Figure 8B and 8C, respectively). The result corresponded to those previously obtained in Rotterdam or Amsterdam (compare Figure 8B with Figure 7B). Further the results indicated that the difference in microscope setup was irrelevant and that the protein was not the cause for the different results. Instead the data suggested that the ability of RAD51 to dissociate depended on the Rotterdam buffer composition.
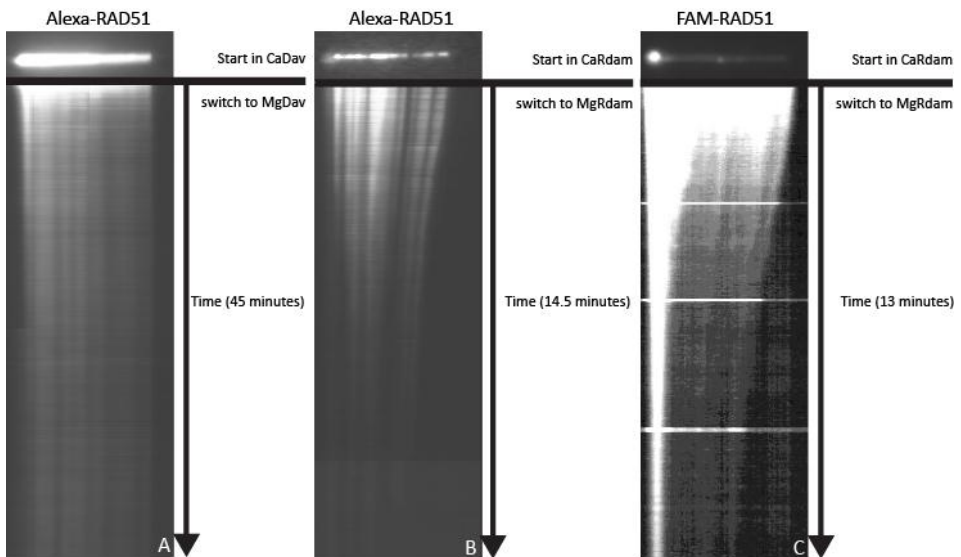

Figure 8: Kymographs of fluorescent RAD51 dissociation experiments done in the Davis laboratory. A shows an Alexa-RAD51 filament dissociation in MgDav buffer. B shows Alexa-RAD51 filament dissociation in MgRdam buffer. C shows a FAM-RAD51 filament dissociation in MgRdam buffer.

As summarized in Table 2 the buffers differed mainly in the choice of the counter ion, chloride vs. acetate, the pH, 7.5 vs. 8.0, DTT concentration and the presence of sucrose, which only the Davis buffers

contained. In the presence of 30 mM DTT the ATPase activity of labeled RecA, the bacterial homolog of RAD51, was not affected (data not shown). Therefore, the DTT concentration was not expected to affect RAD51 ATPase. The difference in pH between 7.5 and 8.0 was previously shown not to affect RAD51 ATPase and not considered further (*35*). Based on these considerations we focused on the sucrose, and the counter ions as distinctions between the Rotterdam and Davis buffers. Therefore an experiment was done without sucrose in the CaDav buffer. In the Davis setup this caused less efficient bead trapping, but filaments still did not disassembly (data not shown). However, as bead trapping was inefficient, not many molecules could be observed. Due to limited time and available material in the Davis lab the experiment was not repeated. This experiment suggested that the filaments in the Rotterdam buffer disassemble because there are Cl⁻ counterions instead of acetate as in the Davis buffers.

In Rotterdam the issue of buffers containing sucrose was addressed again in a converse experiment. Alexa-RAD51 filaments were assembled in CaDav buffer inside a reaction tube, attached to the flow cell surface and then analyzed. In the sucrose containing CaDav buffer, individual filaments could not be observed, instead they appeared aggregated. In time, flowing of MgDav buffer revealed disentanglement of individual Alexa-RAD51 filaments (data not shown). As the increased viscosity of the sucrose containing CaDav buffer interfered with the surface attachment approach, the buffer was modified: sucrose was left out and KOAc was added to the buffer, now named CaDavMod buffer. Filaments assembled in CaDavMod buffer yielded individually attached filaments that appeared to fully cover the DNA (data not shown). A switch to identically modified MgDav bufer, MgDavMod, triggered filament disassembly (Figure 9, 5 mM MgOAc). The filaments disassembled in a similar fashion to those in MgRdam buffer (Figure 10, 2 mM $MgCl_2$).
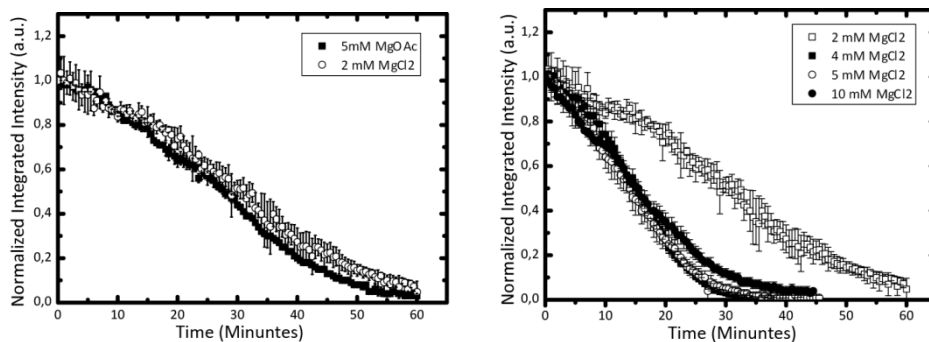
Figure 9: Comparison of Alexa-RAD51 dissociation in MgDav buffer, without sucrose and supplemented with 30 mM KOAc (black squares), with the one in MgRdam buffer (hollow squares).

Figure 10: Dependence of Alexa-RAD51 dissociation from dsDNA on the MgCl2 concentration.

The disassembly data with the MgDavMod buffer showed, that neither pH, DTT concentration nor the anion choice was responsible for the previous observation that RAD51 filaments did not disassemble in MgDav buffer. The new data suggested that the presence of sucrose made the difference in filament disassembly. However, the addition of monovalent salt, here KOAc, could have contributed to the successful disassembly in the MgDavMod buffer as well. Addition of KCl to the MgRdam buffer did not affect Alexa-RAD51 filaments disassembly. Therefore, we conclude that the presence of sucrose is responsible for different dissociation behavior. Anyways, monovalent salt was subsequently added to all experiments. Discussion about salt concentrations led to the investigation of the effect of the divalent salt concentration. Filament dissociation experiments were done with the Rotterdam protocol including KCl in all buffers and $MgCl_2$ was titrated in a range from 2 mM to 10 mM. From a 4 mM $MgCl_2$ concentration filaments disassembled quicker than at 2 mM $MgCl_2$ (Figure 10). There

appeared to be a threshold between 2 mM and 4 mM $MgCl_2$ that changed the shape of the disassembly curves form linear at 2mM to an exponential one at higher $MgCl_2$ concentrations. This implied that RAD51 dissociation was governed by single kinetic step, which was influenced by the $MgCl_2$ concentration.

Discussion

The dissociation experiments with both Alexa-RAD51 and FAM-RAD51 highlighted the importance of experimental conditions and the strength of biochemical assays. Initially the FAM-RAD51 used in the Davis laboratory appeared not to be able to dissociate from DNA by itself (*31*). However, previous data showed that RAD51 does dissociate (*4, 5, 7*). While the lack of intrinsic dissociation is in accordance with the notion that other proteins disassemble RAD51 filaments *in vivo*, the discrepancy in results was confusing. In a direct comparison of the two different proteins in the same microscope setup, we showed that the two proteins behave the same way using identical conditions. I.e. both FAM-RAD51 and Alexa-RAD51 do not disassemble in the buffer conditions used in Davis, but both do so in the buffer conditions used in Rotterdam (compare Figure 7A with Figure 8A and Figure 8C with Figure 8B, respectively). That the proteins behave in a similar fashion under equivalent experiment conditions is in accordance with their similar behavior in the ATPase and D-loop assays. Further this similarity indicates that the observed behavior is intrinsic to RAD51 and not due to different protein preparations.

The different microscope/flow cell setups were excluded as a reason for the different disassembly results. However, the presence of sucrose in the buffer differed in the experiments and impacted RAD51's ability to

dissociate. While sucrose facilitated bead trapping in the Davis setup and consequently enhanced the experiment efficiency, it had an adverse effect on the surface attachment approach, as filaments started to entangle and were not suitable for analysis. Comparison and modification of the buffers resulted in the addition a defined monovalent salt concentration. In retrospect, it was hard to understand that this was not done from the very beginning. In the Rotterdam buffer conditions, addition of 30 mM KCl did not affect RAD51 filament disassembly. This suggests that the presence of sucrose is the reason that filaments do not disassemble in the Davis buffer conditions. The experiments highlighted that biochemical activity depends on defined conditions, and that biochemical experiments need to be validated by correlation to cell biological and genetics experiments. Finally, the experiments in Davis and Rotterdam did not give a different result on intrinsic RAD51 filament disassembly, but were two biochemically distinct experimental conditions, which were internally consistent independent of the protein used.

Materials & Methods

Protein Production

Rotterdam: Wild-type human RAD51 and the C319S variant were purified by similar procedures. RAD51 C319S is a fully functional variant that has only one surface-exposed cysteine (C31) (*5*). It was generated to label RAD51 with a single fluorophore per monomer using thiol chemistry. The human RAD51 open reading frame with a NcoI site encompassing the ATG and a BamHI site just after the stop codon was subcloned between the NcoI and BamHI sites of pET11d (Novagen). The

cysteine-to-serine variants were generated by the QuikChange Site-Directed Mutagenesis method using the wild-type RAD51 pET11d subclone as template (Stratagene). Overexpression was performed in 12 l (cysteine variant) batches in Rosetta/pLysS (Novagen) by pre-growth at 37 ºC until the OD_{600nm} reached 0.5 followed by induction at the same temperature for 4 hours after addition of IPTG to 0.5 mM. Cells were collected by centrifugation and resuspended with 36 ml of PBS giving ~80 ml of cell paste that was frozen at -80 ºC. Lysis was performed by addition of one volume of 3M NaCl, 100 mM Tris-HCl (pH 7.5), 4 mM EDTA, 20 mM β-mercaptoethanol, 2 mM PMSF/ isopropanol (or α-complete tablets without EDTA) to the thawed cell paste.

The lysate was briefly sonicated and clarified by centrifugation at 20,000 rpm at 4 ºC in a Sorval SS34 rotor. Polyethylenimine (10% stock [pH 7.5] with HCl) was added to the decanted supernatant drop by drop while mixing to a final concentration of 0.1% and incubated on ice for > 1 hr. After clarification as described above, one volume of 4 M $(NH4)_2SO_4$ was slowly added to the decanted supernatant while mixing and incubation was continued for >1 hour on ice. The precipitate containing RAD51 was collected by centrifugation at 10,000 rpm in a GSA Sorval rotor for 30 min at 4 ºC, resuspended in 0.5 M KCl, 50 mM Tris-HCl (pH 7.5), 1 mM EDTA, 2 mM DTT, 10% glycerol and clarified by centrifugation at 20,000 rpm at 4 ºC in a Sorval SS34 rotor. After dialysis against 0.05 M KCl, 50 mM Tris-HCl (pH 7.5), 1 mM EDTA, 2 mM DTT, and 10% glycerol, the sample was loaded on a 5 ml heparin sepharose column (GE Healthcare) equilibrated in the same buffer. A KCl gradient from 0.15 to 0.6 M was applied to the column. RAD51 eluted around 400 mM KCl. Peak fractions were pooled, diluted 3-fold with 50 mM Tris-HCl (pH 7.5), 1 mM EDTA, 2 mM DTT, and 10% glycerol, and loaded on a 1 ml Resource Q column equilibrated with 0.15 M KCl, 50 mM Tris-HCl (pH 7.5), 1 mM EDTA, 2 mM DTT, and 10% glycerol. RAD51 eluted around

300 mM KCl in a gradient from 0.15 to 0.6 M KCl. Pooled peak fractions were aliquoted and stored at -80 ºC.

Davis: Wild-type human RAD51 for labeling with fluorescein was purified in Davis as described in the supporting information of Hilario *et al.* (*31*).

Protein Labeling

Rotterdam: The concentration of DTT was adjusted to 20 mM in the purified RAD51 C319S samples (at 1–2 mg/ml of RAD51) and incubated for 30 min on ice. The sample was buffer exchanged (EconoPac 10DG, BIORAD) into labeling buffer (50 mM MOPS-HCl [pH 7.0], 300 mM KCl, 1 mM EDTA, 10% glycerol). The maleimide-coupled dye (Invitrogen) was resuspended in labeling buffer just prior to use and immediately added to the protein sample at a 10-fold molar excess (dye/protein) while mixing. The reaction was incubated on ice for 30 minutes and quenched by addition of DTT to 20 mM with further 30 minutes incubation on ice. Excess dye was removed by buffer exchange into 0.3 M KCl, 50 mM Tris-HCl (pH 7.5), 1 mM EDTA, 2 mM DTT, 10% glycerol as described above and dialyzed against the same buffer before storage at -80 ºC. Proteins were labeled with Alexa 488, mainly used in Rotterdam or Alexa 555, which was used in Amsterdam.

The degree of labeling (D.O.L.) was determined by spectrophotometric quantification of the fluorophore and protein. RAD51 had 0.75 dye molecules per monomer on average.

Davis: Wild-type RAD51 was labeled with 5(6)-carboxyfluorescein succinimidyl ester (Invitrogen) at the amino-terminus as described in the supporting information of Hilario et al. (*31*). Ammine chemistry allows

preferential labeling of the amino-terminus, but also primary ammines exposed on the protein's surface may be labeled.

ATPase assay

Rotterdam: Reactions (20 µl) contained 50 µM virion φX174 DNA (NEB), 2.5 µM recombinase in 50 mM Tris (pH 7.5), 1 mM DTT, 2 mM $MgCl_2$, 100 mg/ml acetylated BSA, 0.1 µM ATP spiked with $[\gamma^{32}\text{-P}]ATP$ (6000 Ci/mmole, 10 mCi/ml; 2µl $[\gamma^{32}\text{-P}]ATP$ in 200 µl 1mM ATP). Incubation was at 37 ºC, and at the indicated times, 5 µl aliquots were removed, stopped by addition of 5 µl of 0.5M EDTA, shock freezing on dry ice, and analyzed by thin-layer chromatography (PEI-cellulose-F) with 0.4 M LiCl and 1 M formic acid as running buffer. Plates were air-dried, exposed for Phosphorimaging, detected by a Typhoon scanner and quantified with ImageQuant version 5.2 (Molecular Dynamics).

Davis: An ATPase assay for FAM-RAD51 were not described in the publication of Hilario *et al.*, but was performed similar to the ones in Rotterdam (personal communication with Joe Hilario). The ability of FAM-RAD51 to hydrolyze ATP is implied form the findings in Hilario *et al*. (*31*)

Strand exchange activity measured by D-Loop assays

Rotterdam: Reactions were performed in a final volume of 20 µl containing 5'-end radiolabeled SK3 oligonucleotide (*36*) at 3.6 µM (nucleotides), 1 µM RAD51, 50 mM Tris-HCl (pH 7.5), 1 mM DTT, 0.1 mg/ml acetylated BSA, 60 mM KCl, 2 mM $CaCl_2$, and 1 mM ATP (*23*). After 5 min incubation at 37 ºC, 2 µl of supercoiled pUC19 plasmid DNA

at 0.429 mg/ml (prepared by detergent lysis and purified twice by CsCl gradient equilibrium sedimentation) was added and further incubated for 20 min at 37 ºC. Reactions were stopped by addition of 5 µl of 0.5% SDS, 50 mM EDTA, and 30% glycerol and deproteinized by incubation for 15 min at 37 ºC with 1 mg/ml final of Proteinase K. Reaction mixtures were fractionated by 0.6% agarose gel electrophoresis in Tris-Borate buffer for 1 hour at 120 V. Gels were dried on DEAE paper, and signals were captured by Phosphorimaging with a Typhoon scanner and quantified with ImageQuant version 5.2 (Molecular Dynamics).

Alternatively, RAD51 D-loop reactions were performed in a in a final volume of 20 µl containing ALEXA 555 5'-end labeled SK3 oligonucleotide (*34*) at 4.5 µM (nucleotides), 1.5 µM RAD51, 50 mM Tris-HCl (pH 7.5), 1 mM DTT, 0.1 mg/ml acetylated BSA, 50 mM KCl, 2 mM Ca(OAc)$_2$, and 1 mM ATP (*23*). After 5 min incubation at 37 ºC, 3 µl of supercoiled pUC19 plasmid DNA at 0.29 mg/ml (prepared by detergent lysis and purified by CsCl gradient equilibrium sedimentation) was added and further incubated for 20 min at 37 ºC. Reactions were stopped by addition of 5 µl of 0.5% SDS, 50 mM EDTA, and 30% glycerol and deproteinized by incubation for 15 min at 37 ºC with 1 mg/ml final of Proteinase K. Reaction mixtures were fractionated by 0.6% agarose gel electrophoresis in Tris-Borate buffer for 1 hour at 120 V. Signals were captured with a Typhoon scanner (green 532 nm laser, 555BP 20 filter, normal sensitivity, 500 V PMT) and quantified with ImageQuant version 5.2 (Molecular Dynamics).

Davis: D-loop experiments, similar to those in Rotterdam, were as described in the supporting information of Hilario *et al.* (*31*).

Surface Tethering and Visualization of Fluorescent Filaments in Rotterdam

Flow cells, constructed from #1 glass cover slips (Menzel-Glaser) separated by a double-layer Parafilm in a custom holder, were prepared as follows: Neutravidin (Pierce) was introduced at 1 mg/ml and allowed to interact for 30 min. After removal of excess Neutravidin, the flow cell was washed and blocked with 2 mg/ml acetylated BSA, 2 mg/ml α-casein, 10 mM DTT, 50 mM Tris-HCl (pH 7.5), 30 mM KCl, and 10% glycerol. Lambda phage dsDNA was biotinylated at one end and labeled with digoxygenin at the other by annealing biotinylated oligonucleotides to CosL (5'-P-AAG TCG CCG CCC dR-bio dR-bio-bioTEG-3') and 5'-P-GGG CGG CGdRDig CCT CGG CGC CCG GCC GCG dTDigAA ACG CGG CCG GGC GCC GG-3') to CosR as described (*37*). Filaments were assembled in a 20 µl reaction mixture containing 91 pM (molecules) of lambda phage dsDNA and 1.4 µM RAD51 in CaRdam buffer (50 mM Tris-HCl (pH 7.5), 1 mM ATP, 2 mM $CaCl_2$, 1 mM DTT, and 60 mM KCl) or CaSMB* (50 mM TrisOAc pH 8.0, 2 mM $Ca(OAc)_2$, 1 mM ATP, 30 mM DTT, and 60 mM KOAc). After incubation at 37 ºC for 30 min, the reaction mixtures were diluted by addition of 380 µl CaRdam buffer, or CaSMB* , and injected into a flow cell. The flow was stopped for about 10 minutes to allow interaction of the biotinylated DNA with the Neutravidin surface. Unbound filaments were flushed by flow of the corresponding Ca^{2+} buffer. Dissociation was triggered by switching to Mg^{2+}/ATP buffer (50 mM Tris-HCl (pH 7.5), 1 mM ATP, 2 mM to 10 mM $MgCl_2$ as indicated, 1 mM DTT, and 60 mM KCl) or MgSMB* (50 mM TrisOAc pH 8.0, 5 mM $Mg(OAc)_2$, 30 mM DTT, and 60 mM KOAc). Hydrodynamic flow was controlled with a precision pump (Harvard Apparatus). Dynamic visualization of filaments was performed with a Nikon 60 X or 100 X (NA 1.45) TIRF objective in a Nikon TE2000U inverted microscope equipped with a Cascade 512B CCD camera (Princeton Instruments) driven by Metamorph software (Molecular Devices). Excitation was performed

with a mercury arc lamp. Intensity measurements were obtained by defining regions of interest around the construct contour length in all planes, tracking them over time and correcting for background. The data were plotted using Origin software.

Single-molecule fluorescence microscopy

Davis: Experiments were as described in the supporting information of Hilario *et al.* (*31*). A variation was the assembly of RAD51 filaments in reaction tubes as described in the above section. The filaments were then bound to streptavidin-coated beads as and subsequently flushed into the flow cell. Trapped filaments could directly be analyzed increasing experiment efficiency.

Amsterdam: Experiments were as described as in the supporting online material of van Mameren *et al.* (*7*).

References

1. J. San Filippo, P. Sung, H. Klein, Mechanism of eukaryotic homologous recombination. *Annu Rev Biochem* **77**, 229 (2008).
2. X. Li, W. D. Heyer, RAD54 controls access to the invading 3'-OH end after RAD51-mediated DNA strand invasion in homologous recombination in Saccharomyces cerevisiae. *Nucleic acids research* **37**, 638 (Feb, 2009).
3. X. Li, C. M. Stith, P. M. Burgers, W. D. Heyer, PCNA is required for initiation of recombination-associated DNA synthesis by DNA polymerase delta. *Molecular cell* **36**, 704 (Nov 25, 2009).
4. J. T. Holthausen *et al.*, Effect of the BRCA2 CTRD domain on RAD51 filaments analyzed by an ensemble of single molecule techniques. *Nucleic acids research*, (May 16, 2011).
5. M. Modesti *et al.*, Fluorescent Human RAD51 Reveals Multiple Nucleation Sites and Filament Segments Tightly Associated along a Single DNA Molecule. *Structure* **15**, 599 (May, 2007).
6. D. Ristic *et al.*, Human Rad51 filaments on double- and single-stranded DNA: correlating regular and irregular forms with recombination function. *Nucleic acids research* **33**, 3292 (2005).
7. J. van Mameren *et al.*, Counting RAD51 proteins disassembling from nucleoprotein filaments under tension. *Nature* **457**, 745 (Feb 5, 2009).
8. R. Kanaar, C. Wyman, R. Rothstein, Quality control of DNA break metabolism: in the 'end', it's a good thing. *Embo J* **27**, 581 (Feb 20, 2008).
9. J. T. Holthausen, C. Wyman, R. Kanaar, Regulation of DNA strand exchange in homologous recombination. *DNA repair* **9**, 1264 (Dec 10, 2010).
10. D. K. Singh, A. K. Ghosh, D. L. Croteau, V. A. Bohr, RecQ helicases in DNA double strand break repair and telomere maintenance. *Mutat Res*, (Jun 13, 2011).
11. K. A. Bernstein, S. Gangloff, R. Rothstein, The RecQ DNA helicases in DNA repair. *Annual review of genetics* **44**, 393 (2010).
12. N. Hunter, The RecQ DNA helicases: Jacks-of-all-trades or master-tradesmen? *Cell Res* **18**, 328 (Mar, 2008).
13. C. Z. Bachrati, I. D. Hickson, RecQ helicases: guardian angels of the DNA replication fork. *Chromosoma* **117**, 219 (Jun, 2008).
14. D. V. Bugreev, F. Hanaoka, A. V. Mazin, Rad54 dissociates homologous recombination intermediates by branch migration. *Nat Struct Mol Biol* **14**, 746 (Aug, 2007).
15. E. Antony *et al.*, Srs2 disassembles Rad51 filaments by a protein-protein interaction triggering ATP turnover and dissociation of Rad51 from DNA. *Molecular cell* **35**, 105 (Jul 10, 2009).
16. J. M. Stark *et al.*, ATP hydrolysis by mammalian RAD51 has a key role during homology-directed DNA repair. *J Biol Chem* **277**, 20185 (Jun 7, 2002).
17. A. L. Forget, M. S. Loftus, D. A. McGrew, B. T. Bennett, K. L. Knight, The human Rad51 K133A mutant is functional for DNA double-strand break repair in human cells. *Biochemistry* **46**, 3566 (Mar 20, 2007).
18. A. Carreira *et al.*, The BRC repeats of BRCA2 modulate the DNA-binding selectivity of RAD51. *Cell* **136**, 1032 (Mar 20, 2009).
19. A. A. Davies *et al.*, Role of BRCA2 in control of the RAD51 recombination and DNA repair protein. *Molecular cell* **7**, 273 (Feb, 2001).
20. F. Esashi, V. E. Galkin, X. Yu, E. H. Egelman, S. C. West, Stabilization of RAD51 nucleoprotein filaments by the C-terminal region of BRCA2. *Nat Struct Mol Biol* **14**, 468 (Jun, 2007).
21. R. B. Jensen, A. Carreira, S. C. Kowalczykowski, Purified human BRCA2 stimulates RAD51-mediated recombination. *Nature*, (Aug 22, 2010).
22. N. Ayoub *et al.*, The carboxyl terminus of Brca2 links the disassembly of Rad51 complexes to mitotic entry. *Curr Biol* **19**, 1075 (Jul 14, 2009).
23. D. V. Bugreev, A. V. Mazin, Ca2+ activates human homologous recombination protein Rad51 by modulating its ATPase activity. *Proc Natl Acad Sci U S A* **101**, 9988 (Jul 6, 2004).
24. P. Chi, S. Van Komen, M. G. Sehorn, S. Sigurdsson, P. Sung, Roles of ATP binding and ATP hydrolysis in human Rad51 recombinase function. *DNA repair* **5**, 381 (Mar 7, 2006).

25.   K. S. Shim *et al.*, Magnesium influences the discrimination and release of ADP by human RAD51. *DNA repair* **5**, 704 (Jun 10, 2006).

26.   Y. Liu *et al.*, Conformational changes modulate the activity of human RAD51 protein. *Journal of molecular biology* **337**, 817 (Apr 2, 2004).

27.   E. H. Egelman, A robust algorithm for the reconstruction of helical filaments using single-particle methods. *Ultramicroscopy* **85**, 225 (Dec, 2000).

28.   P. R. Bianco *et al.*, Processive translocation and DNA unwinding by individual RecBCD enzyme molecules. *Nature* **409**, 374 (Jan 18, 2001).

29.   R. Galletto, I. Amitani, R. J. Baskin, S. C. Kowalczykowski, Direct observation of individual RecA filaments assembling on single DNA molecules. *Nature* **443**, 875 (Oct, 2006).

30.   I. Amitani, R. J. Baskin, S. C. Kowalczykowski, Visualization of Rad54, a chromatin remodeling protein, translocating on single DNA molecules. *Molecular cell* **23**, 143 (Jul 7, 2006).

31.   J. Hilario, I. Amitani, R. J. Baskin, S. C. Kowalczykowski, Direct imaging of human Rad51 nucleoprotein dynamics on individual DNA molecules. *Proc Natl Acad Sci U S A* **106**, 361 (Jan 13, 2009).

32.   M. Spies *et al.*, A molecular throttle: the recombination hotspot chi controls DNA translocation by the RecBCD helicase. *Cell* **114**, 647 (Sep 5, 2003).

33.   L. R. Brewer, P. R. Bianco, Laminar flow cells for single-molecule studies of DNA-protein interactions. *Nat. Methods* **5**, 517 (Jun, 2008).

34.   D. S. Shin *et al.*, Full-length archaeal Rad51 structure and mutants: mechanisms for RAD51 assembly and control by BRCA2. *Embo J* **22**, 4566 (Sep 1, 2003).

35.   G. Tombline, R. Fishel, Biochemical characterization of the human RAD51 protein. I. ATP hydrolysis. *J Biol Chem* **277**, 14417 (Apr 26, 2002).

36.   A. V. Mazin, E. Zaitseva, P. Sung, S. C. Kowalczykowski, Tailed duplex DNA is the preferred substrate for Rad51 protein-mediated homologous pairing. *Embo J* **19**, 1148 (Mar 1, 2000).

37.   A. Graneli, C. C. Yeykal, T. K. Prasad, E. C. Greene, Organized arrays of individual DNA molecules tethered to supported lipid bilayers. *Langmuir* **22**, 292 (Jan 3, 2006).

Chapter 5:

Assembly of RAD51-ssDNA filaments at the single molecule level

J.T. Holthausen[2]*, A. Candelli[1]*, M. Modesti[4], R. Kanaar[2,3], C. Wyman[2,3], G.J.L. Wuite[1] and E.J.G. Peterman[1]

[1]LaserLaB Amsterdam and Department of Physics and Astronomy, VU University, De Boelelaan 1081, 1081 HV, Amsterdam, The Netherlands
[2]Department of Cell Biology & Genetics, Cancer Genomics Center, [3]Department of Radiation
Oncology, Erasmus Medical Center, PO Box 2040, 3000 CA Rotterdam, The Netherlands
[4]CNRS, Unité Propre de Recherche 3081, Genome Instability and Carcinogenesis Conventionné par l'Université d'Aix-Marseille 2, 13402 Marseille Cedex 20, France.
*These authors contributed equally to the work.

Manuscript in preparation

Abstract

Homologous recombination is an essential DNA-repair pathway ubiquitous across all kingdoms of life. The core-molecular machinery that catalyzes the DNA strand-exchange step of homologous recombination in humans is RAD51, bound as a helical filament on single-stranded DNA (ssDNA). Defining the intrinsic rate and mechanism of RAD51 interaction with ssDNA is required to understand the mechanism of homologous recombination and to reveal steps where control by mediator proteins would be needed. Here we directly visualize and quantify RAD51 nucleoprotein filament formation with single-monomer resolution on individual molecules of ssDNA held in defined conformation using dual optical tweezes. We confirm that the rates of RAD51 nucleation and extension of RAD51 nuclei depend on protein and monovalent salt concentration. We show that the size of the nucleation unit is dependent on the protein state in solution and by counting fluorescent RAD51 molecules contained in nuclei we determine a nucleation unit of on average 4 - 5 and minimally 3 RAD51 monomers. Importantly, we demonstrate that RAD51 nucleation and extension of RAD51 nuclei is 2 - 3 orders of magnitude faster on ssDNA than on dsDNA, thereby revealing part of the mechanism that targets RAD51 to DNA damage.

Introduction

Double-stranded DNA breaks (DSB) are a deleterious type of lesion that can lead to apoptosis, cancer and chromosome instability (*1-3*). Homologous recombination is a multi-step DNA-repair pathway which occurs across all kingdoms of life and is capable of restoring chromosome integrity without loss of genetic information (*4, 5*). At the core of homologous recombination is the RAD51 nucleoprotein filament- RAD51 assembled into a helical filament around ssDNA. The structure and catalytic activity of the filament are dependent on the nucleotide bound at the monomer-monomer interface, which constitutes a functional ATPase domain (*6, 7*). The ATP-bound RAD51 nucleoprotein filament drives homology search, homology recognition, and strand exchange (*4, 5*). RAD51 filament formation on ssDNA is therefore a crucial step. Furthermore, *in vivo*, RAD51 filament formation is controlled by the tumor suppressor protein BRCA2, arguing in favor of a pivotal role of the filament assembly step in avoiding carcinogenesis (*2, 3, 8, 9*). Defining the intrinsic rates and mechanism of RAD51 filament formation on ssDNA is an essential step towards the quantitative description of the complex protein machinery responsible for catalyzing DNA strand exchange *in vivo* and possibly for understanding how recombination mediators or accessory factors act on RAD51.

A substantial body of results points at a two-step filament formation mechanism composed of nucleation and extension *(10-13)*. Nucleation, the minimal form of stable protein binding, represents the control and most critical step of filament formation (*3*). RAD51 filaments can form on both ssDNA and dsDNA. Filaments on dsDNA are only desirable as an intermediate during DNA repair. Random RAD51 binding to dsDNA is detrimental to efficient recombination repair and a system directing RAD51 toward ssDNA must be in place

(*14, 15*). An intrinsic RAD51 DNA substrate selection mechanism was unknown, but the recombinase mediator BRCA2 modulates RAD51 binding to favor ssDNA (*9, 16-18*). In several biochemical assays and microscopy experiments RAD51 seemed to display similar affinity for ssDNA and dsDNA (*19-23*). This is in contrast with the structural properties of RAD51 filaments: RAD51 in an ATP bound state extends DNA from 40% to 65% of its ds B form (*10, 11, 24, 25*). Since ssDNA has no defined form or length, this implies that for the formation of RAD51 filaments on ssDNA there will be no energy penalty derived from the lengthening of the DNA. Instead, the unwinding of dsDNA induced by RAD51 binding has profound consequences for the energetic landscape of the assembly reaction. The energy barrier associated with the unwinding and extension of the double helix may hinder RAD51 binding to dsDNA with respect to ssDNA, and provide the molecular basis for RAD51 DNA substrate selection mechanism. However, neither biochemical assays, electron microcopy nor magnetic tweezers experiments have detected a differential RAD51 nucleation rate on ssDNA versus dsDNA (*11, 16, 20, 21, 23*).

Extension of RAD51 nuclei is the other crucial step in the formation of the nucleoprotein filament. Whether the structure of the invading nucleoprotein filament consists of long and continuous or short and frequent RAD51 patches is determined by the ratio between nucleation and extension rates. The functional structure of the filament may have important consequences concerning the efficiency of homology search and of the strand exchange reaction. Having quantitative insights into filament extension dynamics together with nucleation rates is therefore a prerequisite to formulate predictions regarding the functional structure of the nucleoprotein filament.

Past single-molecule studies addressing these questions detected filament formation as changes in length of DNA molecules (*11, 26*).

This read out is thus indirect in quantifying the actual local interaction between RAD51 and ssDNA and requires mathematical modeling to distinguish the contributions of nucleation and extension. This lack of information limits the quantitative assessment of intrinsic RAD51 binding. Modeling with RAD51 protomers of 1 - 15 yielded a best fit of a protomer in the range of 4-6 (*11, 26*). The direct visualization and quantification of individual RAD51 filaments on ssDNA has remained elusive, mostly due to technical limitations of the available approaches.

To overcome these limitations we used a custom-developed single-molecule assay combining optical tweezers, single-molecule fluorescence microscopy, micro-fluidics, and force-induced DNA melting. This allowed us to directly visualize and compare the assembly of a fluorescent variant of RAD51 on ssDNA and dsDNA *(27-29).* Nucleation and extension kinetics, i.e. their rate, probability, and the protomer size, together with their interplay with mechanical tension on both ssDNA and dsDNA were investigated. Our experiments provide a detailed characterization of the filament formation that can be mechanistically interpreted.

Results

To investigate the mechanism of RAD51 filament formation we used a biochemically active Alexa-labeled RAD51 with a defined level of fluorescence per monomer (*29*); Chapter 4). The single-molecule assay was assembled in situ using a multi-channel, laminar flow-cell system (*30*) (Figure 1 A). Optical tweezers were used to manipulate and control the position of small streptavidin-coated polystyrene microspheres (4.26 µm diameter). DNA molecules labeled with biotin at both ends of one strand (see materials and methods) were

captured between beads by flow-stretching. Force-induced melting of the tethered DNA produced ssDNA (Supplementary Figure 01) (*28*). RAD51 filament formation was directly initiated by exposing the DNA molecule, held under a defined tension, to a buffer containing fluorescent RAD51. Combining a computer-controlled microscope-stage and the properties of laminar flow (virtually separated buffer channels), the interaction time of DNA with the protein (inside a dedicated channel) could be controlled with a precision of 1 to 2 seconds. The resulting DNA-RAD51 complex was visualized in the imaging buffer channel, in the absence of free RAD51 protein, to avoid fluorescent background and obtain single-molecule sensitivity. Depending on the experimental goal, fluorescence was visualized in different ways; either by continuous exposure resulting in complete photobleaching or as single short exposure snapshots. Continuous exposure bleaching traces were used for the quantification of fluorescent RAD51 at the single-molecule level. Single short exposure snapshots were used to follow RAD51 assembly in time.

RAD51-ssDNA nucleoprotein filament formation: nucleation and extension kinetics in absence of ATP hydrolysis

The approach employed for characterizing the properties of RAD51 binding to ssDNA consisted of exposing a ssDNA molecule, held under defined tension between two optically trapped beads, to fluorescent RAD51 in a buffer allowing ATP binding but suppressing ATP-hydrolysis (1 mM Ca^{2+}, 0.5 mM ATP) (*31*). The fluorescent signal resulting from the ssDNA-RAD51 interaction was used to quantify RAD51 binding events. We expected individual RAD51 binding events to appear as sparse, diffraction limited spots along the ssDNA molecule. Figure 1 B shows an example where two bright fluorescent spots were observed after

incubation of a single ssDNA molecule in 25 nM of RAD51 for 15 seconds. The size of these spots was close to the diffraction limit (width ≈ 300 nm), indicating the presence of individual or patches of RAD51 bound to the ssDNA molecule. In the low-coverage regime (less than 10 spots per DNA molecule) we were able to count individual spots and unambiguously measure the nucleation rate of RAD51 on ssDNA. At a protein concentration of 50 nM and in 100 mM KCl the nucleation rate was 3.5 x10^{-6} nucleation events s^{-1} nt^{-1}.
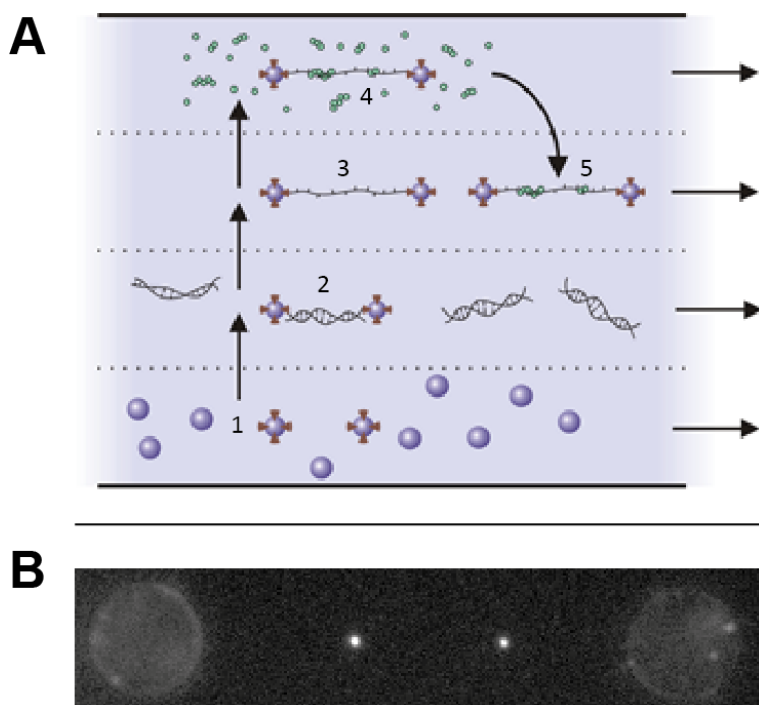
Figure 1: Combined dual optical trapping, fluorescence microscopy and micro-fluidics for studying RAD51 binding to ssDNA and dsDNA. **A)** A 4-channel micro-fluidics device is used as a platform for the assembly of the single molecule assay. The typical experiment is composed of six distinct steps: (1) catching of two streptavidin-coated beads in the optical traps; (2) tethering of a single dsDNA molecule between the beads; (3) optional force-induced dsDNA melting to produce a ssDNA template (DNA force-

stretching curves are acquired in order to verify the integrity of the molecules); (4) controlled incubation with fluorescent RAD51; (5) visualization of the RAD51-DNA complex in a background free environment (complete photo-bleaching of the fluorescent signal is used to quantify RAD51); **B)** Snapshot of 2 RAD51 patches on ssDNA.

RAD51 nucleation rates were analyzed over a range of different monovalent salt and RAD51 concentrations, as well as in conditions suppressing or permitting RAD51 mediated ATP hydrolysis (Ca^{2+} and Mg^{2+}). When the RAD51 ATPase activity was not suppressed the (apparent) nucleation rate was approximately two-fold decreased (supplementary figure 2). As expected for DNA-protein interactions involving electrostatic effects, RAD51 nucleation rate depended on monovalent salt concentration (supplementary Figure 3). In a regime from 50 mM to 400 mM KCl the RAD51 nucleation rate on ssDNA was reduced up to about 10 fold in a concentration dependent manner. A more moderate effect compared to that previously observed for dsDNA (*10*). When the RAD51 concentration was varied from 7.5 nM to 100 nM, nucleation rates varied from 10^{-7} to 10^{-5} events s^{-1} nt^{-1} (Figure 2 B). The dependence of the nucleation rate on concentration can be described by the power-law relationship $k_{nucl} = k_0[RAD51]^n$, where the fitted value of n represents the minimum number of monomers required for nucleation (*10, 32*). The fit yielded a nucleation rate of $k_0 = (3 \pm 4) \times 10^{-9}$ s^{-1} nt^{-1} and nucleation unit $n = 1.9 \pm 0.4$ for RAD51 concentrations ranging from 7.5 nM to 50 nM. According to this interpretation, a RAD51 dimer constitutes a functional nucleus. For RAD51 concentrations from 50 to 100 nM a different fit of $k_0 = (5.2 \pm 0.1) \times 10^{-14}$ s^{-1} nt^{-1} and $n = 4.5 \pm 0.5$ was obtained. This suggests that at higher protein concentrations nucleation involves 4 - 5 RAD51 monomers.
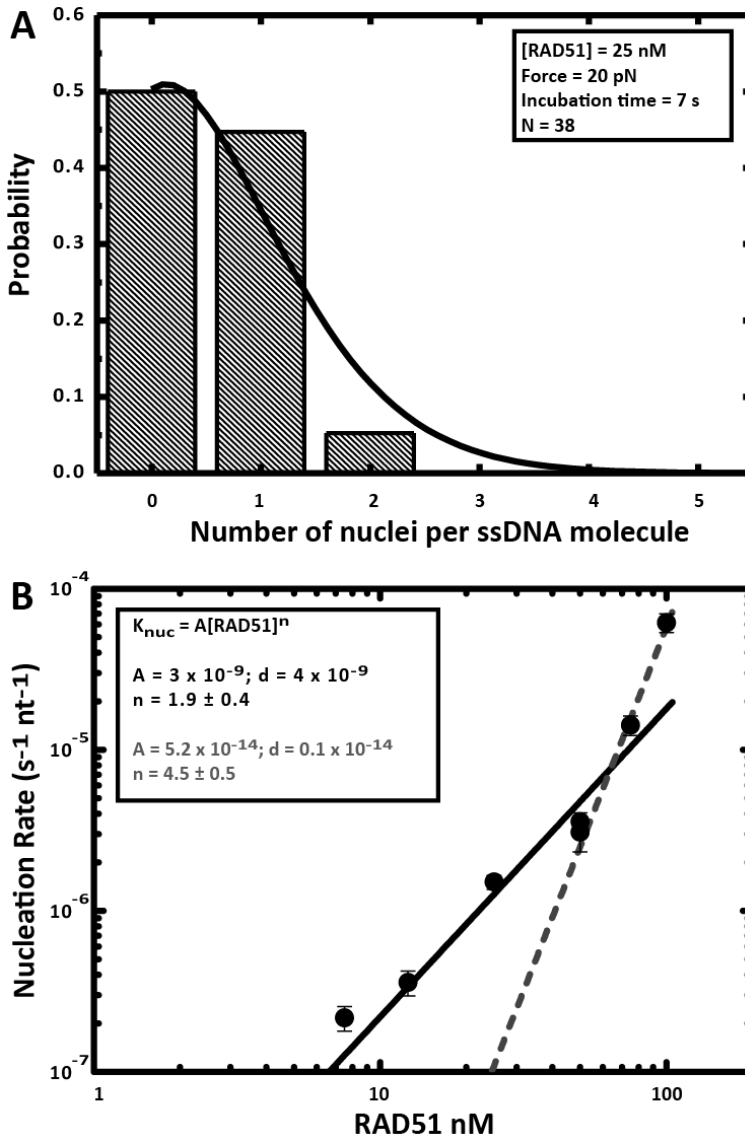
Figure 2: Quantification of RAD51 nucleation on ssDNA. **A)** Distribution of nucleation events on individual ssDNA molecules. During incubation cycles of 7 s in the presence of 25 nM protein, nucleation of RAD51 displays a Poisson-distribution (black line; average r = 0.68 ± 0.07), indicating that it occurs in a single-step. **B)** Dependence of RAD51 nucleation rate on protein concentration. The nucleation data were fit with 2 independent power law functions. The dashed grey line is a fit to experiments at 50 nM, 75 nM and 100 nM RAD51. The solid black line is the fit to experiments performed

at 7.5 nM, 12.5 nM, 25 nM and 50 nM. The vertical error bars are the standard error of the mean. The inset shows the nucleation rates to the corresponding fits and the exponent (n) indicating the average binding unit size.

The size of the nucleation unit was also analyzed by another, more direct method. Fluorescence intensity of the nucleation patches was used to determine the number of RAD51 monomers contained in it. First the fluorescence intensity arising from individual Alexa fluorophores was characterized. Fluorophore intensities and characteristics varied with different microscope setting and buffer compositions. For each condition multiple single-step bleaching traces were recorded and the single-molecule fluorescence calibrated (see supplementary Figure 4 for an example). The intensity variation was low enough to allow the absolute number of fluorophores per fluorescent RAD51 patch to be determined. Given the degree of labeling (1.3 fluorophores per RAD51) the protein quantity for a given fluorescent intensity was computed and a distribution of RAD51 proteins per detected patch was obtained. The histogram in Figure 3 shows the distribution of RAD51 patch composition from experiments performed at 75 nM RAD51.

Interestingly, a heterogeneous distribution of nucleation events ranging from single monomers to up to 10 RAD51 proteins was observed. A Gaussian fit over this distribution suggested an average of 4 ± 2 RAD51 monomers (mean ± SD). This average is in accordance with data from magnetic tweezers measurements from which a pentameric binding unit for nucleation was determined by mathematical modeling of data obtained at 187 nM RAD51 (*11*).
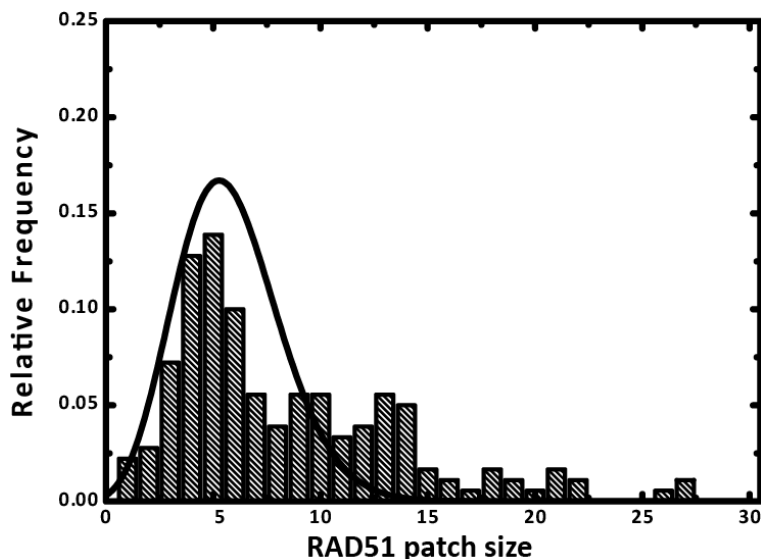
Figure 3: Distribution of RAD51 nucleation patch sizes at 75 nM RAD51 and 15 second incubations (n = 57). The relative frequency of different sizes of RAD51 patches reveals that nucleation occurs in multimers of varying sizes. The Gaussian fit (black line) suggests an average nucleation unit size of 4 ± 2 RAD51 monomers (mean ± SD).

The amount of RAD51 in the higher intensity patches could be due to extension of an initial nucleation event. To discern nucleation from filament extension, short incubation cycles at low protein concentration (12.5 nM RAD51) were analyzed (supplementary Figure 4). The results suggested that only 10% of the observed patches were a result of combined nucleation and extension. Therefore, it is likely that initial RAD51 binding occurs by a variety of oligomeric forms. The data for the nucleation rates at different protein concentrations (Figure 2 B) suggested that nucleation units are on average 2 RAD51 molecules at concentrations below 50 nM, while above 50 nM the average nucleation unit was 4-5 RAD51 monomers. Together with the data from the fluorophore quantification, this implies that the size of the RAD51 nucleation unit depends on the oligomerization state of

the protein in solution. Therefore, the oligomerization state of RAD51 was tested by chemical cross-linking of 7.5 nM, 25 nM and 75 nM Alexa-labeled RAD51 followed by gel electrophoresis (Figure 4). Indeed, the amount of protein in defined oligomers increased with RAD51 protein concentrations.
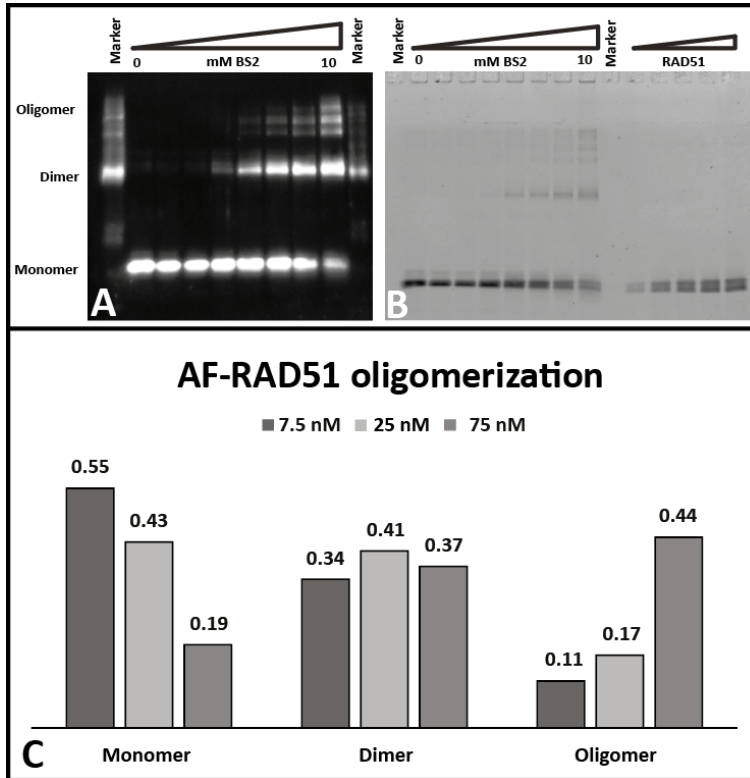
Figure 4: Alexa-RAD51 cross-linking in solution with BS2. RAD51 containing complexes were resolved by polyacrylamide gel electrophoresis. Detection of RAD51 by anti-RAD51 antibodies using immunoblotting (**A**) and typhoon scan of the Alexa fluorescence signal (**B**) show that with increasing cross-linker concentration more multimeric species of RAD51 are cross-linked. The example shows cross-linking at 75 nM RAD51. **C)** The percentage of different forms of RAD51 determined from densitometry scanning of protein cross-linked at 7.5 nM, 25 nM and 75 nM RAD51 and separated by gel electrophoresis. Increasing protein concentration reveals a decrease in monomeric RAD51 and an increase in oligomeric forms.

We also determined the relationship between nucleation patch size and persistance of RAD51 on the ssDNA. The RAD51 nucleation patches were categorized based on the number of fluorophores and the average persitence of each class was determined (Figure 5). Patches consisting of up to three fluorophores remained bound to DNA for maximally 30 - 60 seconds, the minimal time-frame of the measurement. Patches having four fluorophores, on the other hand, were bound on average for longer than two minutes, up to a maximum measurement time of 20 minutes. The experiment showed a clear difference in persistence from three to four fluorophores. Considering the degree of labeling of 1.3 fluorophores per RAD51, there are less RAD51 than fluorophores detected. Therefore, we propose a minimal productive nucleation unit of three RAD51.
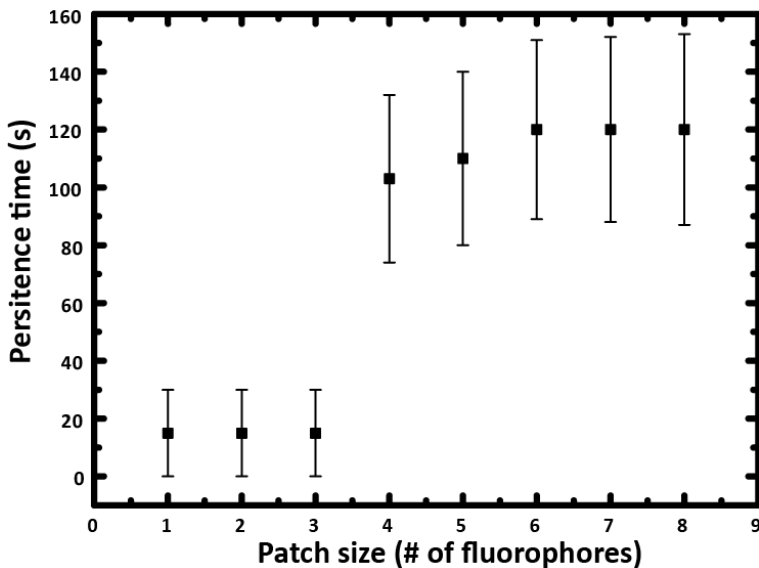
Figure 5: RAD51 patch stability as a function patch sizes. The time a RAD51 patch could be observed is plotted against patch size. Conditions were adjusted to reduce photobleaching and observe over a maximum period of 20 minutes. Of the 48 patches only 4 were observed to have 1-3 fluorophores. Others may have dissociated within the minimal experimental time frame of 30 seconds. Patches containing more than three fluorophores persist for at least two minutes.

The ability to observe individual RAD51 patches bound to DNA also allowed us to observe extension of RAD51 patches. In order to achieve maximum sensitivity in detecting individual extension events, nucleation patches were completely photo-bleached after each incubation cycle. Extension events were detected and quantified by superimposing images resulting from consecutive incubation cycles and counting the new fluorescent patches that co-localized with previous fluorescent signals at the sub-pixel level (Figure 6). This assay allowed to estimate the probability of filament extension and to quantify the number of RAD51 monomers in individual extension events. The probability of extension of RAD51 patches was calculated as the fraction of the filaments exhibiting extension at different RAD51 concentrations, normalized for the incubation time (Figure 7).
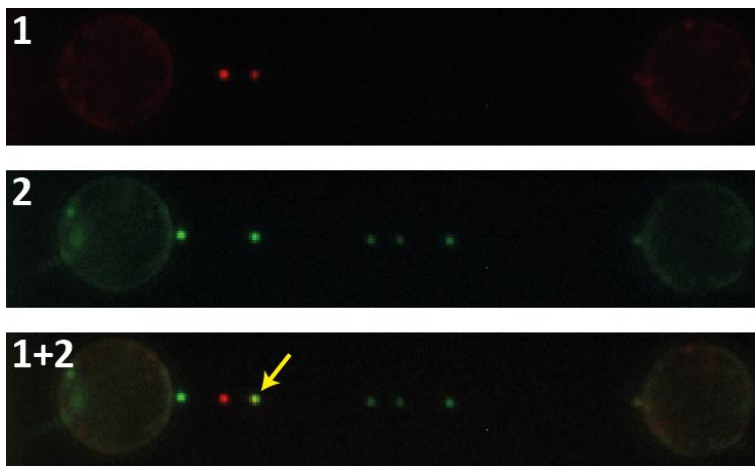
Figure 6: Discriminating RAD51 nucleation and extension at the single molecule level. The DNA was exposed to RAD51 containing buffer for a defined time and RAD51 patches were counted (Panel 1). The fluorescence signal was completely bleached to quantify the number of RAD51 molecules per patch. Subsequently, the same DNA molecule was incubated again in the channel containing fluorescence labeled RAD51, and the newly formed RAD51 patches were quantified (Panel 2). To distinguish RAD51 from the different incubation cycles, fluorescent RAD51 from the second incubation cycle was false colored in green. The images of consecutive RAD51 incubation cycles

were superimposed extension events scored by the occurrence of colocalization (accuracy < 20 nm) of isolated fluorescent patches along the ssDNA molecule (yellow arrow, panel 1+2).

Fitting a power-law dependence ($P_{ext} = A[RAD51]^n$) yielded an extension rate of $A = (1.1 \pm 0.1) \times 10^{-4} \, s^{-1}$ filament^{-1} and an extension unit of $n = 1 \pm 0.3$. The linear slope and power-dependence suggest that there is no requirement for a multimeric species of RAD51 for filament extension, which therefore most likely involves the binding of RAD51 monomers to existing patches. The amount of RAD51 added in each extension event was quantified by analysis of the photo-bleaching traces, as described above for nucleation. Care was taken to perform the measurements in conditions such that consecutive, multiple RAD51 extension events could be statistically ruled out.
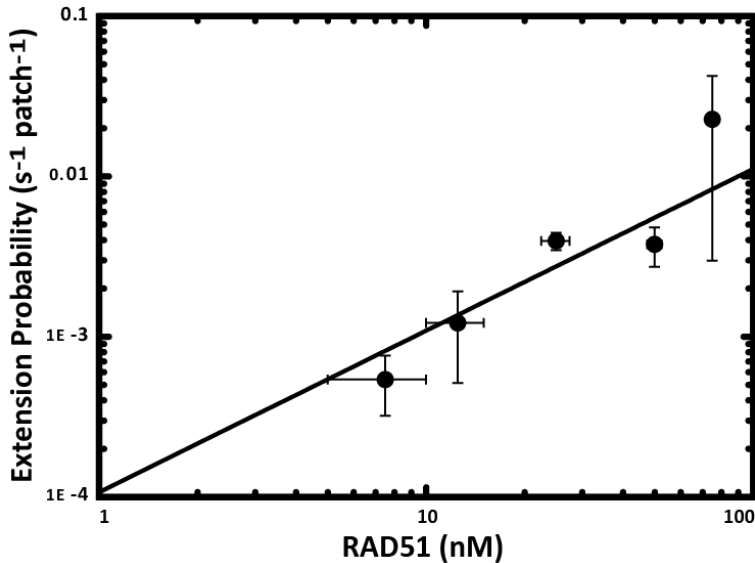
Figure 7: Probability of extension of a RAD51 nucleus plotted against RAD51 concentration. The direct quantification of the extension probability reveals a linear behavior. The error bars are standard error of the mean.
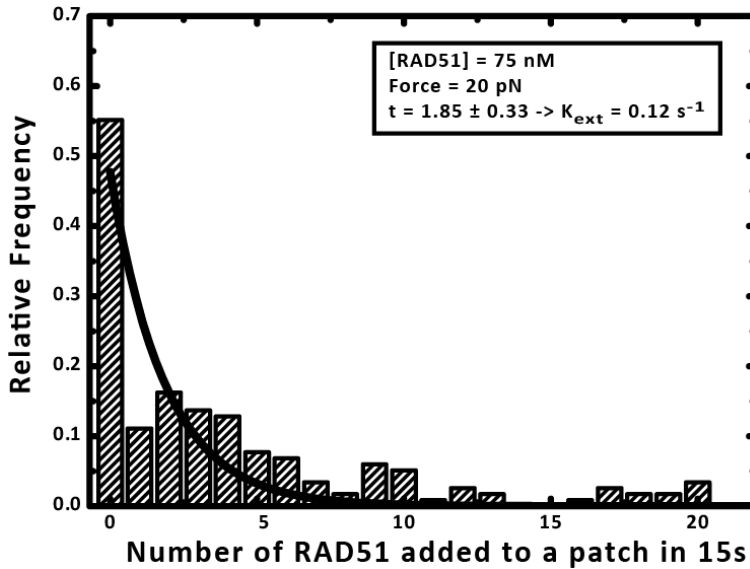
Figure 8: Relative frequency of different size extension events on ssDNA at 75 nM RAD51 (n = 86). Extension of RAD51 nuclei occurs without a defined multimeric binding unit as shown by the heterogeneous distribution. The exponential fit (black line) suggests an extension rate of nucleation patches of 0.12 RAD51 molecules s^{-1}.

Similar to nucleation, extension of RAD51 patches revealed a heterogeneous distribution of the amount of RAD51 binding to patches (Figure 8). The lack of a clear peak implies that extension does not occur by multimeric units of RAD51. Only half of the available nuclei were extended in our observation conditions.

DNA mechanics regulate RAD51 filament assembly and substrate specificity

A previous single-molecule study showed that the mechanical tension stored in the RAD51-dsDNA filament plays an important role in filament disassembly, supplying a driving force during the disassembly process (*33*). Therefore the influence of the mechanical

tension on both ssDNA and dsDNA on RAD51 assembly rates was investigated. The accurate control of both ssDNA and dsDNA within the same experimental set-up offered a straightforward way to compare the binding behaviors in a controlled environment.

The affinity of RAD51 for different DNA substrates was compared by alternately incubating ssDNA and dsDNA; at the same tension (Force=20 pN) and in the same incubation conditions. The results demonstrated that RAD51 nucleated more effectively on ssDNA compared to dsDNA. Qualitatively, there was an obvious difference in the amount of fluorescent patches on ssDNA and dsDNA molecules incubated with RAD51 for 15 and 480 seconds, respectively (Figure 9 A, B). To quantify this differential behavior, nucleation and extension rates were characterized at different forces on ssDNA and dsDNA (Figure 10 A and B). The results revealed two important aspects of RAD51 filament assembly. First, RAD51 filament nucleation and extension were systematically faster on ssDNA compared to dsDNA throughout the explored force regime. In the low force regime filament formation on ssDNA was up to 3 orders of magnitudes faster than on dsDNA. The rates measured for dsDNA were in the same order of magnitude (10^{-7} bp^{-1} s^{-1}) as previously reported (*10*). Second, the applied tension strongly influenced RAD51 filament nucleation and extension on dsDNA but not on ssDNA. Both facts are consistent with the notion that RAD51 filament formation on dsDNA required the transition of an energy barrier deriving from the unwinding of dsDNA. RAD51 binding to ssDNA does not have the same energetic consequences or cost.
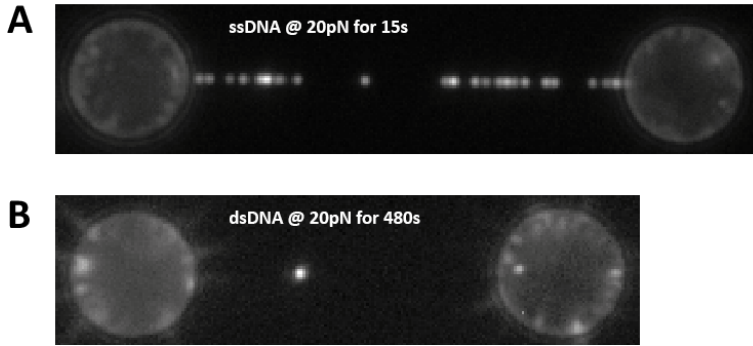
Figure 9: Nucleation efficiency of RAD51 on ssDNA and dsDNA. **(A)** RAD51 patches on ssDNA after 15 second incubation with 75 nM protein. (B) As in panel A, except the DNA was ds and the incubation time was 480 seconds.

To further describe the energy barrier RAD51 has to overcome when binding dsDNA, the force-dependence of both nucleation and filament extension rates of RAD51 on dsDNA were fit with the following functions based on the Arrhenius law:

$$k_{nuc/ext}(F) = k_{nuc/ext}(0)\text{Exp}[-x^*_{nuc/ext}F/k_BT],$$

where k_BT is the thermal energy, F the mechanical force (tension) applied across the dsDNA molecule and x^* is the distance to the transition state along the reaction coordinate. For the nucleation rate $x^*_{nuc} = 0.45 \pm 0.08$ nm and $k_{nuc}(0) = (4 \pm 3) \times 10^{-9}$ s^{-1} bp^{-1} was computed (Figure 10 A). For the extension rate the function resulted in $x^*_{ext} = 0.24 \pm 0.06$ nm and $k_{ext}(0) = (3 \pm 2) \times 10^{-3}$ s^{-1} $nucleus^{-1}$ (Figure 10 B). The obtained value for x^*_{nuc} of 0.45 nm corresponds to the relative amount dsDNA is stretched upon RAD51 in conditions suppressing RAD51 ATP hydrolysis. The lower energy barrier for extension probably derives from favorable protein-protein interactions.

RAD51 dissociation from ssDNA

Disassembly of RAD51 patches can be triggered by permitting ATP hydrolysis. Dissociation from ssDNA was analyzed by incubating it for a defined time with fluorescent RAD51, in buffer that allowed ATP hydrolysis (Mg^{2+} and ATP). Then the DNA molecule was quickly moved into an observation channel, where RAD51 nuclei were observed and dissociation of individual RAD51 patches visualized in real-time. The fluorescence illumination and the camera exposure were tuned in order to minimize photobleaching and to retain single molecule sensitivity. The recorded behavior closely resembled previous observations of RAD51 dissociating from dsDNA in that disassembly occurred in bursts of different sizes and was characterized by the presence of long pauses (33). Disassembly traces from many individual RAD51 filaments were characterized for pause duration and dissociation rate.
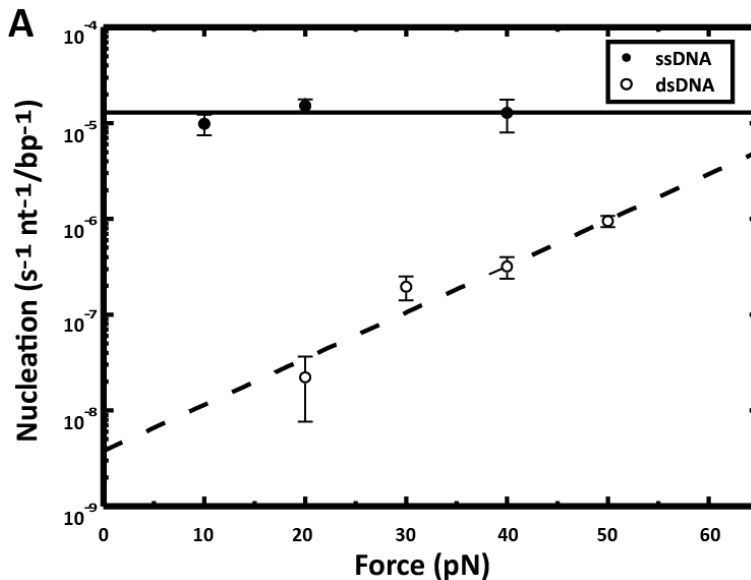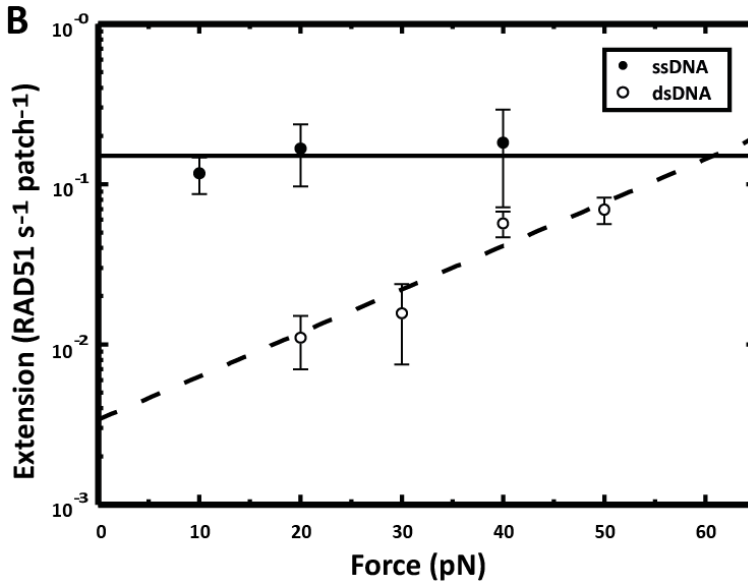
Figure 10: Effect of DNA tension on RAD51 nucleation and extension rates. **A)** Comparison between ssDNA and dsDNA of the effect of DNA tension on RAD51 nucleation rates. Nucleation rates are plotted as a function of force applied to the DNA. The horizontal solid line fitted to the ssDNA data shows no force dependence of nucleation rate on ssDNA. The dotted line fitted to the dsDNA data reveals a strong force dependence of nucleation rates on dsDNA. **B)** Comparison between ssDNA and dsDNA of the effect of DNA tension on the extension rate of RAD51 patches. Extension rates are plotted as a function of force applied to the DNA. The horizontal solid line fitted to the ssDNA data shows no force dependence on extension rate on ssDNA. The dotted line fitted to the dsDNA data reveals a strong force dependence of nucleation rates on dsDNA.

A histogram of measured pauses showed an exponential behavior with a characteristic decay constant of 55 ± 3 seconds (supplementary Figure 6), about three fold faster compared to that previously observed for dsDNA (*33*). The pauses are suggested to reflect ATP hydrolysis occurring within the filament, with disassembly requiring hydrolysis at the terminal monomer interface. Based on this interpretation, the ATP hydrolysis rate could be extracted from the reciprocal of the pause duration. The deduced k_{hydr} for ssDNA in our

conditions was 1.8×10^{-2} s^{-1}. This rate of ATP hydrolysis during dissociation from ssDNA is three fold faster than during dissociation from dsDNA. This correlated well with biochemical data on the stimulation of ATP hydrolysis by ssDNA and dsDNA, where the hydrolysis rate was three fold higher in the presence of ssDNA with respect to dsDNA (*34*). Consequently, disassembly of RAD51 from ssDNA was substantially faster than disassembly from dsDNA. Dissociation rates, extracted from the burst sizes, were on the order of 0.6 ± 0.3 RAD51 s^{-1}.

Discussion

In this study we have used dual optical tweezers, fluorescence microscopy and micro-fluidics to dissect the molecular details of the assembly and disassembly of RAD51 filaments on ssDNA and dsDNA. We find that RAD51 nucleation occurred as a single kinetic step involving a heterogeneous distribution of RAD51 protomers ranging from individual monomers to higher oligomeric forms. Fitting RAD51 nucleation rates as a function of RAD51 concentration yielded two distinct values for the average size of a nucleation unit. The fit of the experiment series below 50 nM RAD51 suggests a nucleation unit of 1.9 ± 0.4 RAD51, while the fit to the experiment series from 50 nM to 100 nM suggests a stable nucleation unit of 4.5 ± 0.5 RAD51 (Figure 2 B). This variation can be explained by the different oligomerization state of RAD51 at different protein concentrations. Indeed, cross-linking experiments show higher degrees of RAD51 multimerization at concentrations above 50 nM RAD51 (Figure 4). Cross-linking experiments with unlabeled protein at 20 μM showed a similar amount of defined oligomeric states as those at 75 nM (data not shown). This suggests that above a certain concentration RAD51

forms distinct oligomers, presumable in a range up to octamers, encompassing the measured unit of pentamers. This is also consistent with the pentameric nucleation unit proposed from magnetic tweezers studies where RAD51 was 187 nM, in the range where multimers are prevalent in solution (*11*). The monte carlo simulations used to model the size of the nucleation unit, in the tweezers studies, have an inherent error of 30% (*26*). The average size of the RAD51 nucleation unit by fluorophores quantification is 4 - 5 RAD51 per nucleation event, supporting the data from other single-molecule experiments (*11*). We show that RAD51 patches made of more than three monomers are bound for over two minutes. Therefore, it is likely that a stable or functional nucleation unit consist of three or more RAD51 molecules (Figure 5). Further, we demonstrate in a direct and quantitative manner that RAD51 nucleation on ssDNA represents the limiting step of filament formation; filament nucleation and extension rates differs by approximately three to four orders of magnitude, confirming that filament assembly is characterized by an intrinsic high degree of cooperativity (*21, 23, 26, 35, 36*). Defining the nucleation process is important for understanding the role of recombinase mediators or accessory factors like BRCA2 and RPA.

Knowing the nucleation rate and size of nucleation patches and the rate and probability of filament extension, we can formulate a prediction for the structure of the functional RAD51-ssDNA nucleoprotein filament. Taking into account the obtained nucleation and extension rates, as well as the average size of nucleation events and monomeric extension, the filament structure on a ssDNA would consists of frequent short protein patches encompassing between 10 and 30 RAD51, separated by segments of 3 to 20 nucleotides of bare ssDNA. This is similar to the previously proposed structure that was obtained by measuring changes in DNA length rather than direct

observation of the protein. Here, the average patch size was proposed to be 35 ± 45 RAD51 and a gap size of up to 14 nucleotides (*11*). We support the notion that this configuration can serve the purpose of maximizing the efficiency of homology search. In fact, the frequent and short filaments can act in parallel as target finders, with the short ssDNA segments providing the necessary structural flexibility rendering the homology search process fast and efficient (*11, 15, 37*).

By direct comparison in the same experimental set up we find a striking difference between the behavior of RAD51 filament formation on ssDNA and dsDNA. Nucleation and filament extension on ssDNA are 2 - 3 orders of magnitude faster compared to dsDNA. Preferential nucleoprotein filament formation on ssDNA compared to dsDNA is of vital biological importance for RAD51 function. The strong preference of RAD51 for ssDNA substrates can be understood by taking into account the different elasticity of the two substrates and the energy cost associated with extension of dsDNA. RAD51 filament formation on dsDNA is heavily influenced by the mechanical tension applied on the substrate, with increasing external tension facilitating RAD51 binding. On the other hand, nucleation and filament extension rates on ssDNA are independent of the mechanical tension. Our result is important because it helps to explain how RAD51 is targeted to its correct initial substrate DNA. Given the large excess of dsDNA in mammalian cells it is imperative that the recombinase is directed towards ssDNA. Up to this represented an open question because a strong preference for ssDNA was previously not detected in ensemble experiments or magnetic tweezers studies (*11, 19-21, 23*). Although RAD51 disassembly rates from ssDNA are also higher with respect to dsDNA, as also seen in a magnetic tweezers study, the increase in disassembly rate might not balance out the much higher nucleation rate on ssDNA (*11*). We argue that the difference in substrate

specificity was occluded in gel-shift assays or electron microscopy, because they lacked the time resolution for RAD51-DNA interaction. RAD51 is incubated for several minutes with either ssDNA or dsDNA in gel shift experiments allowing the formation of an equilibrium or simply saturation of DNA binding. The higher protein concentration (187 nM) used in the magnetic tweezers study arguably is also high enough to occlude detection of differential filament assembly rates for ssDNA and dsDNA. To date, the similar binding affinity of RAD51 to ssDNA and dsDNA has been one of the main arguments for the requirements of mediator (*2, 3, 9, 15*). However, based on the results presented here we propose that in addition to effects of mediator proteins, there is also an intrinsic mechanism for RAD51 DNA substrate selectivity. The 2 - 3 orders of magnitude increased binding preference for ssDNA with respect to dsDNA is not large enough to account for the large excess of dsDNA, certainly not in the presence of RPA, but we propose that at low or limiting RAD51 concentrations it poses and important contribution to filament formation on ssDNA. Concluding, these findings can serve as a reference platform for understanding the role of mediators and accessory factors in modulating rate limiting steps of RAD51 filament dynamics.

Materials & Methods

Combined optical tweezers, fluorescence microscopy and microfluidics setup

The experimental setup has been described elsewhere in detail. A scheme is presented in supplementary figure 7. In brief, our combined dual optical trapping and single-molecule fluorescence

setup is built around an inverted microscope (Nikon Eclipse TE2000-U). Optical traps are generated by a powerful near-IR laser (Ventus 1064 nm, 3W, Laser Quantum, Cheshire, UK). An optical isolator (Newport 1030-1080 ISO-FRDY-OPT) is placed directly in front of the laser output to prevent coupling of back-reflections into the laser cavity. A combination of a zero order half-wave plate (WPH10M-1064, Thorlabs) and a polarizing beam splitter (10BC16PC.9, Newport, Irvine, CA) is used as a power regulator. A second zero order half-wave plate (WPH10M-1064, Thorlabs) and polarizing beam splitter (10BC16PC.9, Newport, Irvine, CA) are used to set the linear polarization and split the laser into two independent beams. After splitting, a Galilean telescope (1:2.67) is used to obtain the desired beam diameter (approximately 8 mm) and to steer the trap position. In one path, computer-controlled steering is achieved by displacing the first telescope lens with motorized actuators (T-LA28, Zaber Technologies Inc., Richmond, BC, Canada). The two beams are recombined using a second polarizing beam splitter (10BC16PC.9, Newport, Irvine, CA) and coupled into a high-NA water-immersion objective (PlanApo 60X, NA 1.2, Nikon) via a dichroic mirror (950 dcsp, Chroma Tech Corp, Rockingham, VT). The focusing power of the objective produces a three-dimensional optical trap where individual beads can be trapped and manipulated. Force detection is achieved by collecting the transmitted trapping light via a high NA oil-immersion condenser (Achromat/Aplanat, NA 1.4, Nikon) and imaged on a position-sensitive diode (DL100-7PCBA3 - Pacific Silicon Sensor) using a single achromatic single. Rejection of the unwanted polarization is achieved by a polarizing beam splitter (10BC16PC.9, Newport, Irvine, CA).

The end-to-end distance of the DNA is monitored by acquiring bright-field images of the trapped beads. Illumination of the sample is performed by a blue LED (LXHL-NB98 Luxeon Star/O, Lumileds) a

single lens and a dichroic mirror and images are recorded using a CCD camera (CCD-902K, Watec) and digitized by a frame grabber.

Fluorescence excitation is performed in an epi-, wide-field strategy. Alexa-Fluor 555 fluorophore is excited by a 532 nm laser (GCL-0.25L, 25 mW, Crystal laser, Reno, NV). The fluorescence excitation beam is first expanded and then coupled into the microscope via a dichroic mirror (z532rdc, Chroma Technology Corp.) and a lens. The emitted fluorescence signal is passed through a band-pass filter (hq575/50m, Chroma Technology Corp.) and imaged on an EMCCD camera (Cascade 512B, Princeton instruments, Monmouth Junction, NJ) and read using the Winview software.

A glass, custom-fabricated, multi-channel laminar flow-system is used to obtain parallel flow and to rapidly exchange buffer during the experiment. Image analysis is performed using a custom-written program in Labview (National Instruments).

DNA constructs

To produce a 38.412 Kbp construct having biotin labels on the same strand, Phage lambda dsDNA (0.25 mg/mL) was digested with ApaI for 30 minutes at 37°C. This reaction yielded a 10 kbp and a 38.4 kbp dsDNA fragments. One overhang resulting from restriction digest was filled-in with biotin-coupled nucleotides by addition of Klenow buffer (final concentration 0.28x), nucleotides (dGTP, dTTP, final concentration 67 µM), biotin-coupled nucleotides (biotin-14-dACTP and biotin-14-dCTP, final concentration 43 µM) and Klenow DNA polymerase exo- (final concentration 0.07 U/µL) for 30 minutes at 37°C. The Klenow reaction was heat-inactivated for 10 minutes at 75°C and ethanol precipitated. The pellet was resuspended in 50 µL of 10 mM Tris pH 7.5. The other overhang was biotinylated by annealing 1 µM primer containing 4 biotin d-TTP (5'-cTcTcTcTctcttccttctcttggcc-3') for 15 minutes at 65°C. The

primer was ligated by T4 DNA Ligase for 45 minutes at RT, T4 DNA The ligation was heat-inactivated for 5 minutes at 65°C, followed by ethanol precipitation.

Protein production

Wild-type and variants of human RAD51 were purified by similar procedures, essentially as previously described (*11*). Briefly, RAD51 was expressed in bacteria, precipitated by ammonium sulfate, subsequently dialyzed and further purified by Heparin, gel filtration and anion exchange chromatography.

Protein labeling

RAD51 was Alexa Fluor 555 or 488 labeled on a specific cysteine residue using maleimidine chemistry and checked for activity as previously described (*29*). The degree of labeling was 1.3 fluorophores per RAD51 and 1 fluorophores per RAD51 for Alexa 555 and Alexa 488 labeled RAD51 respectively.

Experimental conditions

Beads catching, DNA tethering and overstretching, as well as RAD51 incubation are performed in the following conditions (unless otherwise mentioned): 25 mM Tris-HCl pH 7.5, 100 mM KCl, 1 mM $CaCl_2$, 0.5 mM ATP and 10 mM DTT.

Protein cross-linking

The protocol was adapted from Davies *et. al* (*38*). Briefly, RAD51 was buffer exchanged into 20 mM HEPES (pH 8.0), 300 mM KCl, 1mM EDTA, 2mM DTT and 10% glycerol. Protein (9 µl) was cross-linked by incubation with 1 µl of 0, 0.002, 0.02, 0.2, 1, 2, 5 or 10 mM BS2 (Sigma-Aldrich; dilutions in 20 mM HEPES pH 8.0) at room

temperature for 30 min. Cross-linking was terminated by adding 2 µl 80 mM Tris-HCl (pH 8.0) for 15 min at room temperature, and products were analyzed by SDS-PAGE. Alexa-RAD51 was cross-linked at 7.5 nM, 25 nM and 75 nM. The complexes were resolved by 8% SDS. Alexa488-RAD51 was detected by Typhoon scan of the Alexa fluorescent signal and by Western blot (ECL) against RAD51 as previously described (*39*).

Supplementary Material
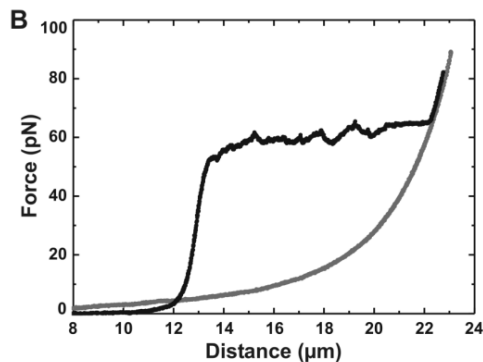
Supplementary Figure 1: Force-induced melting of a dsDNA molecule produces ssDNA templates for RAD51 binding experiments. A single DNA molecule is labeled with biotins at the ends of the same strand and tethered between two optically trapped streptavidin-coated beads. A force stretching curve can be obtained by moving the optically trapped beads away from each other (black trace). When the molecule is pulled beyond the overstretching plateau and high tensions are applied (F>85 pN) we observe the complete melting of the strand without biotin. By slowly moving the beads towards each other (light grey trace) the force-stretching curve indicates the presence of a single ssDNA molecule between the beads.
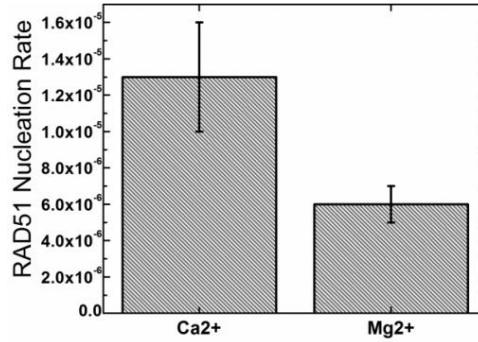
Supplementary Figure 2: Nucleation of RAD51 nucleation rate in absence of presence of ATP hydrolysis. Replacing $CaCl_2$ with $MgCl_2$ in the assembly buffer permits RAD51 mediated ATP hydrolysis and triggered its dissociation from ssDNA. Both experiments are performed in 20 mM Tris, 100 mM KCl, 0.5 mM ATP, 10 mM DTT and 75 nM RAD51 with the indicated divalent metal ion. Since dissociation can occur in the time the DNA molecule needs to travel to the observation channel, the nucleation rate with $MgCl_2$ is apparently two fold lower than with suppressed ATPase activity ($CaCl_2$).
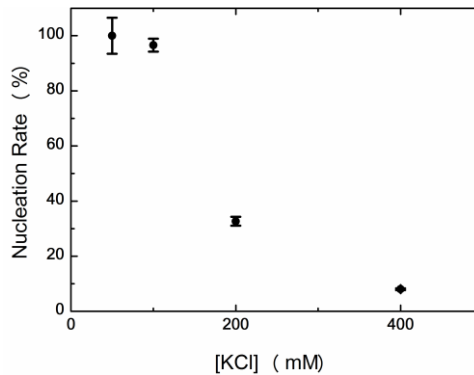
Supplementary Figure 3: RAD51 nucleation rate is modulated by the concentration of monovalent salt (KCl). Increasing the KCl concentration reduced the nucleation rate of RAD51 on ssDNA. This indicates that the electrostatic interaction between RAD51 and the DNA backbone are relevant for modulating the RAD51 binding rate. Experiments were performed in the following conditions: 75 nM Alexa488-RAD51, 1 mM $CaCl_2$, 0.5 mM ATP, 10 mM DTT, and the indicated KCl concentration.
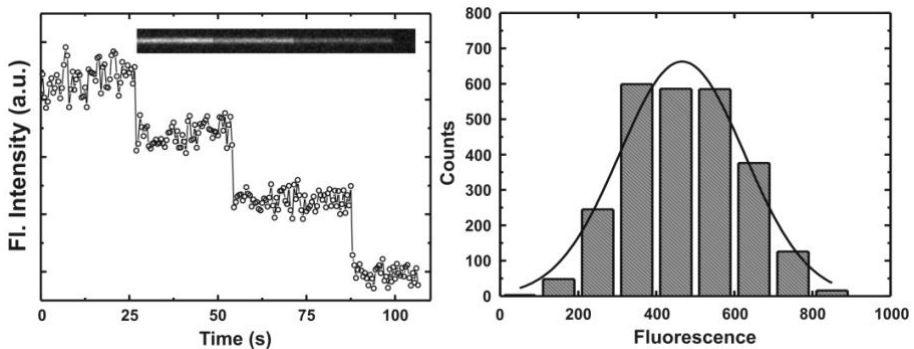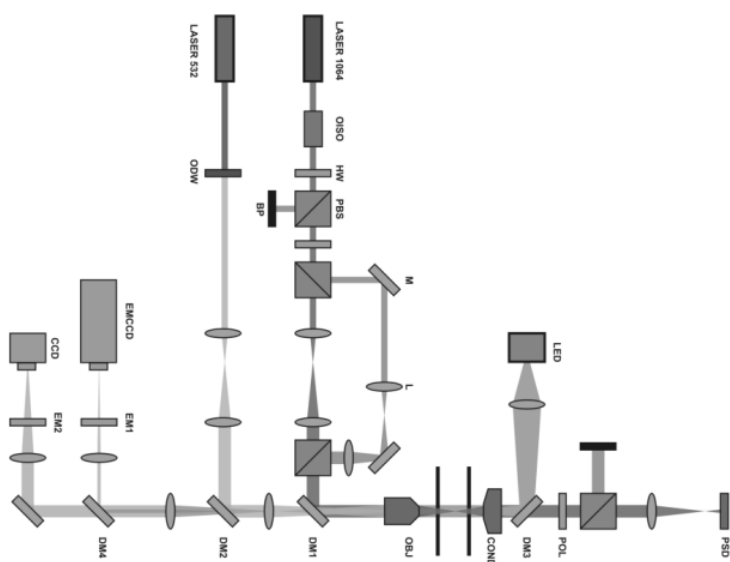
Supplementary Figure 4: Fluorescence intensity can be used to determine the composition of individual RAD51 filaments. A) Example of a photobleaching trace showing a staircase pattern due to the consecutive bleaching of individual fluorophores; the inset shows the fluorescence signal over time. **B)** The histogram shows a distribution of the fluorescence intensity values of the last bleaching step of multiple photobleaching traces. The black line is a Gaussian fit with a center value at Xc=460 and a standard deviation σ=160. The low intensity variation allows the quantification of the number of fluorophores contained in each fluorescent spot. Fluorophore were characterized for each microscope setting and buffer conditions.

RAD51 filament growth statistic
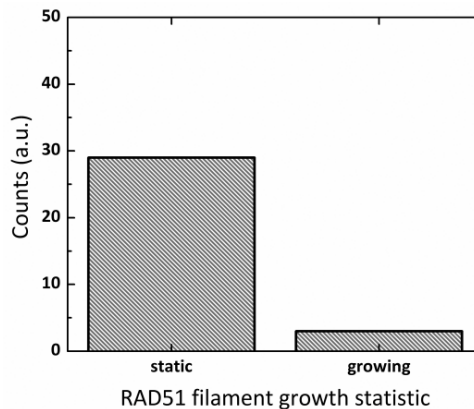
Supplementary Figure 5: Statistics of growth kinetics at 12.5 nM RAD51 and incubation time of 60 s. The histogram shows the result of an experiment aimed at characterizing the growth probability of 15 incubations of individual RAD51 patches. According to this result, the frequency of growth is approximately 10%. This indicates that in this regime the binding events we observed should be attributed almost entirely to the nucleation.

The fit data shown in the plot:

Model	ExpDec1	
Equation	y = A1*exp(-x/t1) + y0	
Reduced Ch	0.1623	
Adj. R-Squar	0.99071	
	Value	Standard E
Counts y0	0	0
A1	22.54	1.13865
t1	55.12	2.91937
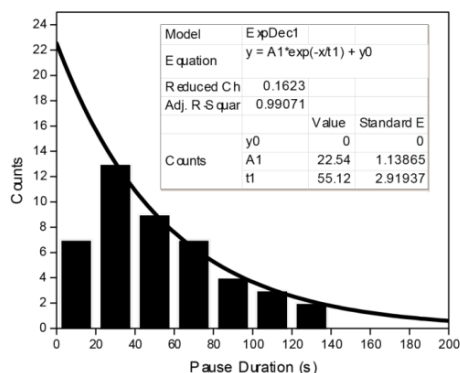
Supplementary Figure 6: Pause duration histogram during RAD51 disassembly from ssDNA. The fit (black line) indicates that pause durations during disassembly are exponentially distributed with a average time of 55 ± 3 seconds. Pause durations below 20 seconds cannot be detected due to the limited time resolution.

Supplementary Figure 7: Schematic representation of the setup combining Dual optical trapping and fluorescence microscopy. OISO: Faraday Optical Isolator; HW: Half-wave plate; PBS: Polarizing Beam splitter; BP: beam block; DM: dichroic mirror; OBJ: objective; COND: condenser; POL: polarizer; PSD: position sensitive detector; LED: light emitting diode; ODW: optical density filter wheel; EM: Emission filter for fluorescence imaging; EMCCD: Electron-multiplying CCD Camera; CCD: CCD camera.

References

1. J. H. Hoeijmakers, Genome maintenance mechanisms for preventing cancer. *Nature* **411**, 366 (May 17, 2001).
2. J. San Filippo, P. Sung, H. Klein, Mechanism of eukaryotic homologous recombination. *Annu Rev Biochem* **77**, 229 (2008).
3. P. Sung, H. Klein, Mechanism of homologous recombination: mediators and helicases take on regulatory functions. *Nat. Rev. Mol. Cell Biol.* **7**, 739 (Oct, 2006).
4. C. Wyman, R. Kanaar, DNA double-strand break repair: all's well that ends well. *Annu Rev Genet* **40**, 363 (2006).
5. C. Wyman, R. Kanaar, Homologous recombination: down to the wire. *Curr Biol* **14**, R629 (Aug 10, 2004).
6. Y. Wu, Y. He, I. A. Moya, X. Qian, Y. Luo, Crystal structure of archaeal recombinase RADA: a snapshot of its extended conformation. *Mol Cell* **15**, 423 (Aug 13, 2004).
7. A. B. Conway *et al.*, Crystal structure of a Rad51 filament. *Nat Struct Mol Biol* **11**, 791 (Aug, 2004).
8. A. R. Venkitaraman, Linking the cellular functions of BRCA genes to cancer pathogenesis and treatment. *Annu Rev Pathol* **4**, 461 (2009).
9. R. B. Jensen, A. Carreira, S. C. Kowalczykowski, Purified human BRCA2 stimulates RAD51-mediated recombination. *Nature*, (Aug 22, 2010).
10. J. Hilario, I. Amitani, R. J. Baskin, S. C. Kowalczykowski, Direct imaging of human Rad51 nucleoprotein dynamics on individual DNA molecules. *Proc. Natl. Acad. Sci. U. S. A.* **106**, 361 (Jan, 2009).
11. T. van der Heijden *et al.*, Real-time assembly and disassembly of human RAD51 filaments on individual DNA molecules. *Nucleic Acids Res.* **35**, 5646 (Sep, 2007).
12. H. Arata *et al.*, Direct observation of twisting steps during Rad51 polymerization on DNA. *Proc. Natl. Acad. Sci. U. S. A.* **106**, 19239 (Nov, 2009).
13. J. Mine *et al.*, Real-time measurements of the nucleation, growth and dissociation of single Rad51-DNA nucleoprotein filaments. *Nucleic Acids Res.* **35**, 7171 (Dec, 2007).
14. R. Kanaar, C. Wyman, R. Rothstein, Quality control of DNA break metabolism: in the 'end', it's a good thing. *Embo J* **27**, 581 (Feb 20, 2008).
15. J. T. Holthausen, C. Wyman, R. Kanaar, Regulation of DNA strand exchange in homologous recombination. *DNA Repair (Amst)* **9**, 1264 (Dec 10, 2010).
16. A. Carreira *et al.*, The BRC Repeats of BRCA2 Modulate the DNA-Binding Selectivity of RAD51. *Cell* **136**, 1032 (Mar, 2009).
17. J. T. Holthausen *et al.*, Effect of the BRCA2 CTRD domain on RAD51 filaments analyzed by an ensemble of single molecule techniques. *Nucleic Acids Res.*, (May 16, 2011).
18. M. K. Shivji *et al.*, The BRC repeats of human BRCA2 differentially regulate RAD51 binding on single- versus double-stranded DNA to stimulate strand exchange. *Proc Natl Acad Sci U S A* **106**, 13254 (Aug 11, 2009).
19. P. Baumann, S. C. West, Role of the human RAD51 protein in homologous recombination and double-stranded-break repair. *Trends Biochem Sci* **23**, 247 (Jul, 1998).
20. P. Chi, S. Van Komen, M. G. Sehorn, S. Sigurdsson, P. Sung, Roles of ATP binding and ATP hydrolysis in human Rad51 recombinase function. *DNA Repair (Amst)* **5**, 381 (Mar 7, 2006).
21. F. E. Benson, A. Stasiak, S. C. West, Purification and characterization of the human Rad51 protein, an analogue of E. coli RecA. *Embo J* **13**, 5764 (Dec 1, 1994).
22. P. Baumann, S. C. West, The human Rad51 protein: polarity of strand transfer and stimulation by hRP-A. *Embo J* **16**, 5198 (Sep 1, 1997).
23. P. Baumann, F. E. Benson, S. C. West, Human Rad51 protein promotes ATP-dependent homologous pairing and strand transfer reactions in vitro. *Cell* **87**, 757 (Nov 15, 1996).
24. E. H. Egelman, Does a stretched DNA structure dictate the helical geometry of RecA-like filaments? *J Mol Biol* **309**, 539 (Jun 8, 2001).

25. E. H. Egelman, A robust algorithm for the reconstruction of helical filaments using single-particle methods. *Ultramicroscopy* **85**, 225 (Dec, 2000).

26. T. van der Heijden, C. Dekker, Monte carlo simulations of protein assembly, disassembly, and linear motion on DNA. *Biophys J* **95**, 4560 (Nov 15, 2008).

27. A. Candelli, G. J. L. Wuite, E. J. G. Peterman, Combining optical trapping, fluorescence microscopy and micro-fluidics for single molecule studies of DNA-protein interactions. *Phys. Chem. Chem. Phys.* **13**, 7263.

28. J. van Mameren *et al.*, Unraveling the structure of DNA during overstretching by using multicolor, single-molecule fluorescence imaging. *Proc. Natl. Acad. Sci. U. S. A.* **106**, 18231 (Oct, 2009).

29. M. Modesti *et al.*, Fluorescent human RAD51 reveals multiple nucleation sites and filament segments tightly associated along a single DNA molecule. *Structure* **15**, 599 (May, 2007).

30. L. R. Brewer, P. R. Bianco, Laminar flow cells for single-molecule studies of DNA-protein interactions. *Nat. Methods* **5**, 517 (Jun, 2008).

31. D. V. Bugreev, A. V. Mazin, Ca2+ activates human homologous recombination protein Rad51 by modulating its ATPase activity. *Proc. Natl. Acad. Sci. U. S. A.* **101**, 9988 (Jul, 2004).

32. R. Galletto, I. Amitani, R. J. Baskin, S. C. Kowalczykowski, Direct observation of individual RecA filaments assembling on single DNA molecules. *Nature* **443**, 875 (Oct, 2006).

33. J. van Mameren *et al.*, Counting RAD51 proteins disassembling from nucleoprotein filaments under tension. *Nature* **457**, 745 (Feb, 2008).

34. G. Tombline, R. Fishel, Biochemical characterization of the human RAD51 protein. I. ATP hydrolysis. *J Biol Chem* **277**, 14417 (Apr 26, 2002).

35. X. Yu, E. H. Egelman, DNA conformation induced by the bacteriophage T4 UvsX protein appears identical to the conformation induced by the Escherichia coli RecA protein. *J Mol Biol* **232**, 1 (Jul 5, 1993).

36. T. Ogawa, X. Yu, A. Shinohara, E. H. Egelman, Similarity of the yeast RAD51 filament to the bacterial RecA filament. *Science* **259**, 1896 (Mar 26, 1993).

37. S. L. Lusetti, M. M. Cox, The bacterial RecA protein and the recombinational DNA repair of stalled replication forks. *Annu Rev Biochem* **71**, 71 (2002).

38. O. R. Davies, L. Pellegrini, Interaction with the BRCA2 C terminus protects RAD51-DNA filaments from disassembly by BRC repeats. *Nat Struct Mol Biol* **14**, 475 (Jun, 2007).

39. P. M. Krawczyk *et al.*, Mild hyperthermia inhibits homologous recombination, induces BRCA2 degradation, and sensitizes cancer cells to poly (ADP-ribose) polymerase-1 inhibition. *Proc. Natl. Acad. Sci. U. S. A.* **108**, 9851 (Jun 14, 2011).

Summary

The DNA in our cells is constantly exposed to agents that damage it. A particularly severe type of lesions are double-strand breaks. Under normal circumstances they derive mainly from endogenous sources, e.g. other unrepaired lesions that are encountered by replication forks and result in the formation of double-strand breaks. On the other hand the deleterious effects of double-strand breaks on cells are exploited in radiotherapy by the exogenous application of ionizing radiation. There are distinct ways of repairing double-strand breaks, of which non-homologous end-joining and homologous recombination are the most commonly used pathways.

Chapter 1 describes homologous recombination as a repair pathway divided in three stages: pre-synapsis, synapsis and post-synapsis. It discusses the main proteins involved and their functions during the different steps of recombination. Briefly, detection of breaks by the MRN-complex; the DNA end resection involving MRE11, CtIP, EXOI, DNA2, BLM; in detail the RAD51 filament assembly on ssDNA, its structure and its disassembly from dsDNA; a proposal for homology search and strand exchange; the dissolution of DNA structures resulting from recombination (Holliday junctions) by BLM, TOPO IIIα, RMI1, RMI2 and by structure-specific endonucleases are described. Further the chapter discusses the effect on RAD51 or on strand exchange of recombination mediators, BRCA2, RAD51AP1, RAD54, and of the RAD51 paralogues, RAD51B, RAD51C, and RAD51D.

Chapter 2 is a review on the regulation of strand exchange, the central step in homologous recombination. It is proposed that there are many meta-stable structures in recombination that provide control

points and/or quality control steps. RAD51 filament formation is one example. The constant association of RAD51 to DNA-bound protein patches and the simultaneous dissociation of RAD51 from DNA after ATP hydrolysis infer that there is an intrinsic meta-stability to the filament that requires a delicate balance between association and dissociation. This balance can be easily be tilted by proteins promoting assembly, stabilizing filaments or by proteins de-stabilizing and disrupting filaments.

Chapter 3 analyzes the effect of the BRCA2 C-terminal RAD51 interaction domain (CTRD) on RAD51 filaments. The CTRD was suggested to have a role in stabilizing RAD51 filaments. That could be by suppressing the RAD51 ATPase or by protein-interactions that involve several RAD51 monomers bound per CTRD. The studies reported here confirm that RAD51 dissociates from dsDNA when ATP hydrolysis is triggered, and show that CTRD does not change RAD51 dissociation kinetics, and hence does not stabilize filaments as expected from suggestions in the literature. On the other hand the presence of CTRD can aggregate filaments and change their appearance (they have less protein bound). Interestingly, CTRD reduces the rate of filament formation on dsDNA in a concentration dependent manner, putatively by sequestration of 3 – 4 RAD51 monomers per CTRD.

Chapter 4 discusses RAD51 dissociation from dsDNA, studied by single-molecule methods. The Kowalczykowski laboratory in Davis obtained RAD51 dissociation results different from ours in Rotterdam and those from the Wuite/Peterman laboratory in Amsterdam. In the Davis setup and conditions no disassembly of RAD51 nucleoprotein filaments was observed. By contrast, in the buffer conditions used in Rotterdam and Amsterdam protein dissociation could be induced by a switch of buffers from one that suppressed to one that allowed RAD51 ATP hydrolysis. In Chapter 4 the three different microscopes and two

distinctly labeled RAD51 proteins - Alexa-RAD51 from Rotterdam and FAM-RAD51 from Davis - are compared. The work showed that independent of the microscope setup, both labeled proteins can give the same result in equal biochemical conditions. I.e. in same the microscope setup in Davis, the Alexa-RAD51 filaments also did not disassemble from dsDNA in the biochemical conditions used in Davis. Conversely, FAM-RAD51 filaments did disassemble from dsDNA in the biochemical conditions used in Rotterdam. Further the disassembly rate could be controlled by divalent salt concentration.

   Chapter 5 focuses on the assembly of RAD51 on ssDNA – the molecular machine driving homology search/recognition and strand exchange. This chapter describes the first application of a novel technique to study the assembly of a macromolecular machine. The generation of, and ability to perform fluorescence microscopy experiments with, individual single-stranded DNA molecules of several kilobases in length was a limitation for many years. The laboratory of Wuite and Peterman in Amsterdam overcame this limitation by integrating dual-optical traps in their fluorescence microscope setup. The traps allowed the generation ssDNA by force-induced melting of DNA. This tool, together with a well-defined fluorescent RAD51, allowed analyzing RAD51 assembly on ssDNA and directly comparing it to dsDNA. The data show that RAD51 nucleation and extension rates depend on RAD51 and KCl concentration. The size of the nucleation unit is dependent on the protein state in solution, which in turn is dependent on protein concentration. Counting fluorescent RAD51 contained in nuclei we determine an average nucleus size of 4 - 5 and with a minimal size of three RAD51 monomers. Further, RAD51 nucleation and extension on dsDNA are DNA tension dependent, while tension on ssDNA does not affect nucleation and extension rates. Extension is 3 - 4 orders of magnitude faster than nucleation on ssDNA, confirming that RAD51 filament assembly is highly cooperative. Importantly, the data

reveal that RAD51 nucleation and extension are 2 - 3 orders of magnitude faster on ssDNA than on dsDNA, which solves a long-standing conundrum in the field. To date such a preference for ssDNA by RAD51 had not been detected. It is important since RAD51 needs to assemble into a filament on the newly generated single-stranded DNA at the site of the double-strand break to drive strand exchange. But there is much more double-stranded DNA available to be bound by RAD51. Without an intrinsic binding preference for ssDNA, filament formation on single-stranded DNA would solely dependent on the aid of recombination mediators.

Nederlandse Samenvatting

Het DNA in onze cellen wordt voortdurend blootgesteld aan stoffen die het beschadigen. Een bijzonder ernstige vorm van DNA-schade zijn de dubbelstrengs breuken. Onder normale omstandigheden vloeien zij voornamelijk voort uit lichaamseigen bronnen, zoals andere niet gerepareerde laesies die door replicatie vorken ondervonden worden en in de vorming van dubbelstrengs breuken resulteren. Aan de andere kant worden de schadelijke gevolgen van dubbelstrengs breuken op cellen uitgebuit in de radiotherapie door de toepassing van ioniserende straling. Er zijn verschillende manieren om dubbelstrengs breuken te herstellen, waarvan niet-homologe end-joining en homologe recombinatie de meest gebruikte routes zijn.

Hoofdstuk 1 beschrijft homologe recombinatie als een reparatie pad verdeeld in drie fases: pre-synapsis, synapsis en post-synapsis. Het bespreekt de belangrijkste eiwitten die betrokken zijn bij homologe recombinatie en hun functie tijdens de verschillende stappen. Allereerst de detectie van een dubbelstrengs breuk door het MRN-complex, vervolgens de DNA-end resectie door MRE11, CtIP, EXOI, DNA2 en BLM. Daarnaast worden in detail de RAD51 filament formatie op het enkelstrengs DNA, de structuur en de demontage van dubbelstrengs DNA, een voorstel voor homologie zoeken en strengs uitwisseling en de ontbinding van de DNA-structuren als gevolg van recombinatie (Holliday junctions) door BLM, TOPO IIIα, RMI1, RMI2 en door structuur-specifieke endonucleasen beschreven. Verder wordt in het hoofdstuk het effect van RAD51 op strengs uitwisseling van recombinatie bemiddelaars, BRCA2, RAD51AP1, RAD54, en van de RAD51 paralogen, RAD51B, RAD51C, en RAD51D besproken.

Hoofdstuk 2 is een review over de regulering van de DNA strenguitwisseling, de centrale stap tijdens homologe recombinatie. Voorgesteld wordt dat er veel metastabiele structuren gedurende recombinatie zijn, welke controle punten en/of kwaliteitscontrole stappen bieden. Een van die controle punten is de RAD51 filament formatie. De constante associatie van RAD51 aan DNA-gebonden eiwit patches en de gelijktijdige dissociatie van RAD51 van DNA na ATP hydrolyse laten zien dat er een intrinsieke metastabiliteit van het filament is, welke een delicate balans tussen associatie en dissociatie vereisen. Dit evenwicht kan gemakkelijk worden gekanteld door de eiwitten die de montage bevorderen en daardoor de filamenten stabiliseren of door deze eiwitten te destabiliseren en dus de filamenten te verstoren.

Hoofdstuk 3 analyseert het effect van de BRCA2 C-terminus, het RAD51 interactie domein (CTRD), op de RAD51 filamenten. Van origine dacht men dat de CTRD een rol heeft in het stabiliseren van RAD51 filamenten. Dit zou kunnen doormiddel van het onderdrukken van de RAD51 ATPase activiteit of door eiwit-eiwit interacties tussen een aantal RAD51 monomeren per CTRD. Onze resultaten bevestigen dat RAD51 zich distantieert van dubbelstrengs DNA als ATP hydrolyse geactiveerd wordt, en dat de CTRD RAD51 dissociatie kinetiek niet veranderd waardoor de filamenten zich niet stabiliseren zoals voorgesteld in de literatuur. Aan de andere kant kan de aanwezigheid van CTRD RAD51 filamenten aggregeren en van vorm veranderen (ze hebben minder gebonden eiwit). Belangrijk is ook dat CTRD de snelheid van filament vorming op dsDNA vermindert in een concentratie afhankelijke manier, vermeende door beslaglegging van 3 - 4 RAD51 monomeren per CTRD.

Hoofdstuk 4 bespreekt enkel-molekuul methoden om RAD51 dissociatie van dubbelstrengs DNA te bestuderen. Het Kowalczykowski laboratorium in Davis behaalde RAD51 dissociatie resultaten die

verschillend zijn van de onze in Rotterdam en die van het Wuite / Peterman laboratorium in Amsterdam. In de Davis setup werd geen demontage van RAD51 nucleoproteïne filamenten waargenomen. Daarentegen kan in de buffer omstandigheden zoals gebruikt in Rotterdam en Amsterdam, eiwit dissociatie veroorzaakt worden door een switch van buffers van een die RAD51 ATP hydrolyse onderdrukt naar een die het toestaat. In hoofdstuk 4 worden drie verschillende microscopen en twee verschillende gelabelde RAD51 eiwitten - Alexa-RAD51 uit Rotterdam en de FAM-RAD51 uit Davis - vergeleken. Uit dit werk bleek dat onafhankelijk van de microscoop setup, beide gelabelde eiwitten hetzelfde resultaat in gelijke biochemische omstandigheden kunnen geven. Dat wil zeggen in dezelfde microscoop opstelling in Davis kunnen de Rotterdamse Alexa-RAD51 filamenten in de biochemische omstandigheden van Davis ook niet van dubbelstrengs DNA demonteren. Omgekeerd demonteren FAM-RAD51 filamenten van dubbelstrengs DNA in de biochemische omstandigheden van Rotterdam. Verder zou de demontage snelheid door tweewaardig zoutconcentratie gecontroleerd worden kunnen.

Hoofdstuk 5 richt zich op de opbouw van RAD51 filamenten op enkelstrengs DNA, de moleculaire aandrijfmechanisme voor homologie zoeken en streng uitwisseling. Dit hoofdstuk beschrijft de eerste toepassing van een nieuwe techniek om de opbouw van een macromoleculaire machine te bestuderen. Het genereren van en het vermogen om fluorescentie microscopie experimenten uit te voeren met individuele enkelstrengs DNA-moleculen van verschillende kilobasen in lengte was een jarenlange beperking. Het laboratorium van Wuite en Peterman in Amsterdam overwon deze beperking door de integratie van dual-optische vallen in hun fluorescentie microscoop setup. De vallen staan de generatie van enkelstrengs DNA door kracht-geïnduceerde smelten van DNA toe. Deze tool, samen met een goed gedefinieerde fluorescerende RAD51, laat het analyseren van RAD51 montage op

enkelstrengs DNA en de directe vergelijk met dubbelstrengs DNA toe. De gegevens tonen aan dat de snelheden van RAD51 nucleatie en extensie afhankelijk van de RAD51 en Kalium Chloride concentratie zijn. De grootte van de nucleatie eenheid is afhankelijk van het eiwitstaat in oplossing, die op zijn beurt afhankelijk van eiwit concentratie is. Door het tellen van fluorescerende RAD51 in kernen bepalen we een gemiddelde kern grootte van 4 – 5, met een minimale grootte van drie RAD51 moleculen. Verder is RAD51 nucleatie en extensie op dubbelstrengs DNA afhankelijk van de spanning op DNA, terwijl de spanning op enkelstrengs DNA geen invloed op nucleatie en extensie heeft. Extensie is 3 - 4 ordes van grootte sneller dan nucleatie op enkelstrengs DNA, wat bevestigt dat RAD51 filament montage zeer coöperatief is. Belangrijk is dat uit de gegevens blijkt dat RAD51 nucleatie en extensie op enkelstrengs DNA 2 - 3 orden van grootte sneller is dan op dubbelstrengs DNA, wat een langdurige raadsel in het veld oplost. Tot op heden was zo'n voorkeur voor enkelstrengs DNA door RAD51 niet gedetecteerd. Het is belangrijk, omdat RAD51 een filament op de nieuw gegenereerde enkelstrengs DNA op de plaats van het dubbelstrengs breuken monteren moet voor streng uitwisseling. Maar er is veel meer dubbelstrengs DNA beschikbaar om te worden gebonden door RAD51. Zonder een intrinsieke voorkeur voor enkelstrengs DNA binding, zou filament formatie op enkelstrengs DNA alleen afhankelijk van de hulp van recombinatie mediators zijn.

Portfolio

Name:	Jan Thomas Holthausen
Microsection number:	355800
Cluster:	Medical Genetics (15)
Department:	Genetics
Position:	PhD student
Period:	April 2007 – September 2011
Promotors:	Prof.dr. R. Kanaar, Prof.dr. C. Wyman
Co-promotor:	Prof.dr. J.H.J. Hoeijmakers

PhD training   *Year*

Courses / classes

	2007
Safely working in the laboratory	2008
Molecular and Cell Biology class	2008
Reading and discussing literature class	2011
Illustrator CS5 Workshop for PhD-student and other researchers	2011
InDesign CS5 Workshop for PhD-student and other researchers	2011

Permits / Experience

	2006/07
Radiation worker 5B	2007
ML-1 (Work permit for GMOs)	2006
ML-2 (Biosafety level II work experience; Adeno- and Lentivirus)	

Seminars and workshops

	2007 – 2011
Department journal club	2007 – 2010
MGC symposia	2007 – 2011
	2011

MGC graduate student workshop	2011
Life science Post-doc retreat (PCDI)	2011
Seminar at Marie Curie, Orsay, France	2011
Seminar at Harvard Medical, Boston, MA, USA	2011
Seminar atUC Davis, Davis, CA, USA	

International conferences

DNA repair meeting; Rotterdam, The Netherlands	2008
DNA Damage Response and Repair Mechanisms; Creete, Greece;	2009
Responses to DNA damage: from molecular mechanism to human disease; Egmond aan Zee, The Netherlands	2011

Presentations

Holthausen J.T., Modesti M., Kanaar R., and Wyman C. *Single-molecule analysis of RAD51 filament dissociation from double strand DNA.*
Dutch Meeting on Molecular and Cellular Biophysics, September 2008, Veldhoven, The Netherlands

Holthausen J.T., Sanchez H., Modesti M., Thorslund T., West S.C, Kanaar R., and Wyman C. *Fluorescent RAD51 nucleoprotein filament dissociation from double strand DNA: Real-time single-molecule visualization and analysis.*
NWO Studiegroepbijeenkomst Eiwitten, Nucleïnezuren en Lipiden & Biomembranen, December 2008, Veldhoven, The Netherlands

Holthausen J.T., van Loenhout M.T.J., Sanchez H., Ristic D., Modesti M., Thorslund T., West S. C., Dekker C., Kanaer R. and Wyman C. *Single-molecule analysis of RAD51 filament dissociation from double strand DNA.*
16th MGC graduate student workshop, June 2009, Bruges, Belgium

Holthausen J.T., Candelli A., Modesti M., Kanaar R., Wyman C., Wuite G.J.L., and Peterman E.J.G. *Counting RAD51 assembly on ssDNA.*
17th MGC graduate student workshop, June 2010, Cologne, Germany

Holthausen J.T., Candelli A., Modesti M., Kanaar R., Wyman C., Wuite G.J.L., and Peterman E.J.G. *RAD51 nucleoprotein filament assembly and disassembly.*
Dutch Meeting on Molecular and Cellular Biophysics, September 2010, Veldhoven, The Netherlands

Holthausen J.T., van Loenhout M.T.J., Sanchez H., Ristic D., Modesti M., Thorslund T., West S. C., Dekker C., Kanaer R. and Wyman C. *Single-molecule analysis of the effect of BRCA2 C-terminal fragment TR2 on RAD51 filaments.*
MGC meeting, September 2010, Leiden, The Netherlands

Holthausen J.T., Candelli A., Modesti M., Kanaar R., Wyman C., Wuite G.J.L., and Peterman E.J.G. *RAD51 nucleoprotein filament assembly on ssDNA.*
NWO Studiegroepbijeenkomst Eiwitten, Nucleïnezuren en Lipiden & Biomembranen, December 2010, Veldhoven, The Netherlands

Holthausen J.T., Candelli A., Modesti M., Kanaar R., Wyman C., Wuite G.J.L., and Peterman E.J.G. *Assembly of RAD51 filaments on ssDNA.*
DNA Repair meeting Egmond aan Zee, April 2011, Egmond aan Zee, The Netherlands

Holthausen J.T., Candelli A., Modesti M., Kanaar R., Wyman C., Wuite G.J.L., and Peterman E.J.G. *Unraveling the dynamics of RAD51 nucleoprotein assembly and disassembly by an ensemble of single-molecule methods.*
Seminar at Marie Curie, July 2011, Orsay, France

Holthausen J.T. *et al. Mechanism of genome protection by homologous recombination repair. A single molecule RAD51-DNA interaction study.*
Seminar at Harvard Medical, November 2011, Boston, MA, USA

Holthausen J.T. *et al. Mechanism of genome protection by homologous recombination repair. A single molecule RAD51-DNA interaction study.*
Seminar at UC DAvis, December 2011, Davis, CA, USA

Publications

Holthausen J.T., Wyman C., Kanaar R. (2010) *Regulation of DNA strand exchange in homologous recombination.* DNA Repair 9, 1264 - 72.

Holthausen J.T., van Loenhout M.T.J., Sanchez H., Ristic D., van Rossum-Fikkert S., Modesti M., Dekker C., Kanaar R., and Wyman C. (2001). *Effect of the BRCA2 CTRD domain on RAD51 filaments analyzed by an ensemble of single molecule techniques.* Nucleic Acid Research 39(15), 6558 – 6567

Holthausen J.T., Candelli A., Modesti M., Franker M., Depken M., Kanaar R., Wyman C., Wuite G.J.L.,and Peterman E.J.G. *Molecular insights into the heterogeneity, size-dependent stability and selectivity of the RAD51 nucleation process.* Manuscript in preparation

Curriculum Vitae

Personal information:

Name: Holthausen

Given names: Jan Thomas

Date of birth: October, 5th 1980

Nationalities: German, Italian

Work Address: Erasmus MC, Dept. Genetics, Ee600

P.O. box 2040, 3000CA

Rotterdam, The Netherlands

Work Email: j.holthausen@erasmusmc.nl

Private Email: tommyholthausen@yahoo.com

Education:

1991 – 2000   Abitur at Nicolaus Cusanus Gymnasium, Bergisch Gladbach, Germany

1997 – 1998   Junior year at Walden High School, Louisville, KY, USA

2001 – 2004   B.Sc. in Job Creation Oriented Biotechnology (JCOB) at Università degli Studi di Perugia, Italy

2005 – 2007   M.Sc. in Medical biotechnology at Wageningen University and Research Center, The Netherlands.

2007 – 2012   PhD at department of Genetics at the Erasmus MC, Rotterdam, The Netherlands.

Work experience:

Internship (June – August 2002)

Dept. Of Molecular Neurobiology, Rheinische Friedrich-Wilhelms-Universität, Bonn, Germany. Introduction into all techniques required to generate transgenic mice. The context of the research was the sensation of pain and addictive behavior.

B.Sc. thesis (June – August 2003; January – June.2004)

Vaccines lab (HCV/HIV), Instituto di ricerca di biologia moleculare (IRBM; MSD), Pomezia, Italy. Functional Characterization Of Human Scavenger Receptor Class B Type I (SR-BI): A Putative HCV Receptor. Thesis available on request.

Minor M.Sc. thesis (January – April.2006).

Virology Department, Wageningen University and Research Centre, Wageningen, The Netherlands. Biochemical analysis of viral RNA silencing suppressors NS1 of Influenza Virus A and NSs of Tomato Spotted Wilt Virus. Thesis available on request.

Major M.Sc. thesis (May – November 2006)

Dept. of Viral Vectors and Cell Biology (MCB), Leiden University Medical Center (LUMC), Leiden, The Netherlands. Analysis of cathepsin cleavage sites in pIX.FLAG.75.13R4.MYC.HIS Human Adenovirus type 5 retargeting construct to enhance transgene delivery. Thesis available on request.

PhD thesis (April 2007 – September 2012)

Department of Genetics at the Erasmus MC, Rotterdam, The Netherlands. Mechanism of genome protection by homologous recombination repair - a single molecule DNA-protein interaction study. Defense date: February 10th, 2012

Skills:

Adaptability	Independence
Learning (quick) capability	Integrity
Networking	Discipline
Teamwork	Goal-oriented
Social	Self-education
Perseverance	

Other:

Spoken languages include as native languages German and Spanish and further English, Italian and Dutch. Studied languages also include Latin and classic Greek.

Military service with the German Airforce (2000 – 2001). Combat training with the 1. Company of the Luftwaffenausbildungsregiment I. Later stationed at Fliegerhorst Wahn working at the Ausbildungskommando of the Luftwaffenamt. My duties can be described as administrative duties for the officers in command of pilot education. Certificates qualifying for office work available. Two promotions.

President and representative of the biotechnology students at Perugia University (2002-2004). Activities involved setting up a laboratory for 40 people on site, a free library and internet access for the students in the class room, and attending board meetings for the organization of the JCOB curriculum.

2009 Member of the organization committee of the16th MGC graduate student workshop. The workshop was a meeting attended by approximately 100 PhD students. The program consisted of three key-note lectures by international speakers, presentations of participants and poster sessions. Further we organized activities aiming at improving group-work and communication skills.

International drivers licenses for motorbikes, cars and trucks up to 7.5 tons including trailers (European code A, BE, CE1,ML), and for motor yachts inside countries and the sea.

Acknowledgements

To all those to read this after actually reading the thesis: thanks for doing that. To all others: it like starts on the other end of the book like thing you are holding. You might actually learn something about recombination that you should know anyways if working on it, or in a laboratory working on double strand DNA breaks.

After beginning with such a non-fun statement, I want to turn to actually thank some people. Foremost I want to thank those that have supervised me in the past. People that have prepared me well for doing a PhD and who have inspired me to work in science by their motivation and skill in each of their subjects. Chronologically, Meliha Karsak and Andreas Zimmer; Helenia Ansuini, Alessandra Vitelli and Alfredo Nicosia; Hans Hemmes and Rob Goldbach; Jort Vellinga and Rob Hoeben. Along the way I have also met many great scientists and people who I did not get to acknowledge officially. You all know why. Thanks to Giuseppe Cecere and Nicola Iovino, Mirko Arcuri, Agostino Cirillo, Bruno Bruniercole, Andrea Sbardelli. The best! All you guys at Wagenignen and Leiden made each an unforgettable experience.

I want to thank Jan Hoeijmakers for giving me the opportunity to do a PhD in the Genetics Department, Roland Kanaar for accepting me in his group, and mostly Claire Wyman for her support and the scientific discussions. Thanks for all the effort put in correcting my manuscripts.

Thanks to Peter Verrijzer, Erwin Peterman and Tizia Sima for reading and approving the thesis.

All those that contributed to the actual work presented here are acknowledged in the corresponding chapters. I think it is redundant to mention you all here. In some way everybody in the lab contributed at some point. Anyways,

I want to thank my collaborators in Delft at Cees' lab, especially Marijn van Loenhout, who suffered to some intriguing tweezers experiments while I

So I guess this part here is for personal thanks, which of course I extend to all in the lab and those that made me have better times at work. Don't be upset if I do not mention you separately.

I do want to do so though for Humberto Sanchez Gonzales. Thanks for listening to me all these year. I guess it kept me from going insane and enabled me to finish my PhD. What about that Whikey Marcin left us? Hope you are planning on drinking that today ;)

Everybody I know at EMC in some way made me have some good times at the EMC and I really hope I do not miss anyone. Thanks: Ricardo, Cintia, Herve, Özge, Maikel, Kris, Eddy, Ekim, Diana, Magda, Juergen, Hans, Daniel, Edward, Devashish, Ashok, Elena, Olaf, Jan, Francesca, Jeffrey, Eskeatnaf, Akiko, Dan, Iris, Nilhan, Alex, Thiago, Wendy, meine Deutschen Kollegen, Gosia, Filippo, Paula, Nicole, Nicole, Natasja, Anja, Michele, Eri, Aryandi, Indriati, Sophia, Khek Chien, Klaas, Iztok, Kostas, Marcel, Dianwen, Jeroen, Joyce, Pauline, Davide, and Gaston.

My other Dutch colleagues Aude, Mark, Sjoerd, Dwi Dwi, Arnoud, Francoise, Jeroen, Taco, Martijn,

The guys at Tuesday's soccer. Thanks for playing with me: Erik, Pim, Ron, Gerard, Jan, Francesco, Johan, Diederick, Youri, Marcin, Rodrigo, Gao, Rui, Valdo, Christof, Herve, Ricardo, Tim, Laurens, Martijn, all the sporadic guests, and Christian "Zidane" Bertholle.

At last I want to thank my family, especially my mom, for supporting me during the time of the PhD. You all know exactly why I thank you.